Tailoring Materials for Biological Applications

Nathan Westcott

A dissertation submitted to the faculty of the University of North Carolina at Chapel Hill in partial fulfillment of the requirements for the degree of doctor of philosophy in the Department of Chemistry.

Chapel Hill
2011

Approved by
Advisor: Professor Muhammad Yousaf
Chair: Professor Wei You
Professor Nancy Allbritton
Professor Marcy Waters
Professor Mark Schoenfisch

Abstract

Nathan Westcott: Tailoring Materials for Biological Applications
(Under the Direction of Muhammad Yousaf)

The ECM is a very complex, heterogeneous mixture of proteins, peptides, and

hormones, which has proven difficult to model in vitro. Currently, a number of model substrates

and systems have been developed utilizing polymers, layer-by-layer methods, and self-

assembled monolayers (SAMs). SAMs of alkanethiolates on gold in particular, have proven to

be useful model substrates with a number of key advantages; SAMs are chemically well defined,

synthetically flexible, conductive, compatible with live-cell high resolution fluorescence

microscopy techniques, can be patterned at the micro- and nanoscale, and most importantly,

they can be made to resist non-specific protein adsorption. These advantages allow for

fabrication of complex, flexible substrates for studies of cell phenomena at the molecular level.

To tailor SAMs on gold with precise spatial control and quantification of ligand density,

smart SAM surfaces have been developed to immobilize a variety of ligands using the

hydroquinone. By installing the peptide ligand sequence RGD (an epitope for the ECM protein

fibronectin), cells have been biospecifially adhered to SAMs to study cell behavior based on

specific ligand-receptor interactions. During the course of my thesis, I have combined analytical

techniques with the unique capabilities of surface chemistry to study cell biology problems

regarding ligand-receptor and small molecule-protein interactions. I have fabricated flexible

biological substrates capable of binding different cellular ligands based on SAMs and hydrogels

to observe their effects on cell behavior.

In chapter 1, I review the relevant literature on SAMs and cell adhesion and migration. In chapter 2 and 3, two methods combining microfluidics and SAMs are described. In chapter 4, alcohol oxidation was used to functionalize simple SAMs. In chapter 5, this method was extended to create protein affinity platforms. In chapter 6, cell adhesion was monitored at the nanoscale using DPN and evaporative lithography. In chapter 7, hydrogels were created to monitor cell adhesion in 3D. Chapter 8 is dissertation conclusions and future directions. These interactions and substrates were characterized by a variety of techniques including XPS, fluorescence microscopy, electrochemistry, and mass spectrometry.

Acknowledgements

I would like to acknowledge my advisor and mentor Muhammad Yousaf for the guidance and help in growing as a scientist. I would also like to thank my family, friends, and labmates for their support and advice during my graduate studies.

Table of Contents

List of Figures

List of Schemes and Tables

List of Symbols and Abbreviations

μm	micrometer
AFM	atomic force microscopy
$CDCl_3$	deuterated chloroform
$C_{16}SH$	hexadecane thiol
d	day(s)
Da	dalton
DI	deionized
DPN	dip-pen nanolithography
ECM	extracellular matrix
EG	ethylene glycol
$EG_4C_{11}SH$	tetra (ethylene glycol) undecane thiol
EtOH	ethanol
h	hours
HDT	hexadecane thiol
$HQEG_4C_{11}SH$	hydroquinone butyl tetra (ethylene glycol) undecane thiol
$HQC_{11}SH$	hydroquinone undecane thiol
mM	millimolar
nm	nanometer
PEG	poly (ethylene glycol)
PDMS	poly (dimethyl siloxane)
RGD	arginine-glycine-aspartic acid
SAM	self-assembled monolayer
SEM	scanning electron microscopy

TEG   tetra (ethylene glycol) undecane thiol

THF   tetrahydrofuran

w/w   weight/weight ratio

XPS   x-ray photoelectron spectroscopy

PCC   pyridinium chlorochromate

Chapter I: Literature Review of SAMs on Gold and Cell-ECM Interactions
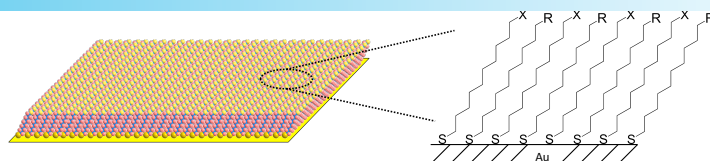
1.1 Introduction

The majority of this thesis is concerned with smart surfaces that are generated with self-assembled monolayers (SAMs) of alkanethiolates on gold. These surfaces respond to external stimuli to switch from unreactive to reactive. To create these smart surfaces, I used multiple molecule functionalities that respond to electrochemical, chemical, and light inputs. These materials were used to study a variety of cell behaviors, such as cell polarity, division, migration, and adhesion. In the following chapter, I will review the literature on the relevant cell behaviors as well as SAMs.

1.2 The Interaction of Cells and the Extracellular Matrix

The extracellular matrix (ECM) is a complex mixture of proteins, signaling molecules, and other soluble factors that provide a scaffold for cell adhesion and migration. The constituent cells maintain the ECM, and fibroblasts in particular serve in this role. Fibroblasts secrete proteins and enzymes that not only add to the matrix, but also destroy other proteins. This constant remolding creates a dynamic environment wherein the cells are constantly experiencing ligand conformational changes and orientations. In fact, these orientations affect cell adhesion and migration rates. Typically, the ECM is composed of fibronectin, collagen, fibrinogen, and laminin. Collagen forms the structural backbone of the ECM and defines two

structural regions.[1-3] The first region is a condensed region and is adjacent to epithelial cells with covering sheeting of muscle cells and the like. The second regions comprises the interstitial matrix.[4] Collagen can form many different structures depending on the structure of the tissue and is typically synthesize by ECM caretaker cells, including fibroblasts and osteoblasts.[5] Laminin is another important component of the ECM and serves a major roll in influencing cell behavior. Various laminins can promote stem cell differentiation, adhesion, and migration.[6-8] Additionally, these proteins appear to be crucial for cancer metastasis and viral invasion.[9] Other proteins also affect cell behavior, such as tenascins and proteoglycans.[10-17] For the ECM to dynamically remodel itself, it must first be broken down. This role is accomplished by matrix metalloproteases (MMPs). MMPs are a subclass of metazinicin proteins that are zinc dependent[18-21] actively secreted by a host of cells, including fibroblasts and chondrocytes, and involved in tissue remodeling during development, playing a large role in inflammation and other disease states.

One of the most important ECM components is fibronectin, a proteoglycan. Fibronectin exists in many different isoforms inside the body, including both an insoluble and soluble form.[22-24] The soluble form is found in blood plasma and plays a role in blood clotting and cell adhesion. The insoluble form is primarily located in the ECM and is implicated in adhesion, migration, and the maintenance of phenotype. The insoluble form is a multimer with a molecular weight (MW) ranging from 200 to 250 kDa and a carbohydrate content of ~5%. Fibronectin has ten domains that are composed of different repeating units, which are recognized by a variety of cell types and proteins. Fibronectin's capacity to bind many different cell types and up to 20 different integrins mediates its influence on a wide variety of cell types and tissues.[25] Fibronectin is especially important for vertebrate development in which it is responsible for cell adhesion, migration, differentiation, and growth.[26] Fibronectin's ability to

be remodeled, unmasking specific domains makes it a dynamic protein capable of modulating affinities and most likely, is the mechanism to modulate cell behavior.[27] The two most important cell-binding domains are the type III repeat found in the 10th domain (Arg-Gly-Asp (RGD))and the type III repeat found in the 9th domain (Phe-His-Ser-Arg-Asn (PHSRN)).[28] The 10th domain type III binds a host of integrins and mediates cell adhesion to the ECM, while the 9th domain type III repeat has been shown to act as a synergy peptide for integrin binding. For some integrins, both domains are required for cell-ECM adhesion.[29]

Cells interact with constituent proteins of the ECM predominately through a set of proteins called integrins. Integrins are heterodimeric proteins consisting of an alpha and beta chain with one single membrane span.[30,31] Twelve alpha and 24 beta chains combine to form up to 24 known integrins that are found on all cell types.[32] The majority of the proteins interact with the external environment and are found outside the cell. Inside the cell, a small tail projects into the cytoplasm, serving as an activation and attachment site for the actin cytoskeleton.[33] These attachments allow for the force to be transmitted across the plasma membrane, which is crucial for cell migration and adhesion. In addition to serving as anchor points to the ECM, integrins transmit information to the cell concerning the cell's environment, location, and adhesive state. These signals are integrated inside the cell and affect its adhesion, migration, and death.[34] Additionally, integrins can be activated internally through proteins, such as talin, into a higher affinity state.[35,36] Talin acts by binding the cytoplasmic tail of the integrin, and induces a conformational change in the extracellular head portion.[37] The conformational change raises the affinity of the integrin towards various extracellular matrix proteins. Proteins can also deactivate integrins. Typically, proteins such as Dok1 and ICAP1 competitively bind the cytoplasmic tail to displace talin, lowering the integrin affinity.[38,39] As such, these processes are called inside-out signaling, and coupled with the delivery of

information to the cell, integrins serve as conduits for information for the cell that allow it to not only sense its environment, but also respond to it.

When integrins bind their environment, a protein cascade is initiated that leads to the formation of focal adhesions.[40-45] Currently, several subsets of focal adhesions exist. Focal complexes are found at the periphery of a migrating cell.[46] Focal adhesions are larger protein complexes found at the center of cells and at the end of stress fibers in strongly adhered cells.[47] Fibrillar adhesions are a subset of elongated focal adhesions containing tenesin.[48] 3D matrix adhesions are attachments that have been described for fibroblasts adhered to various 3D substrates.[49-52] Various proteins that constitute focal adhesions have multiple interacting proteins, which allow the cell to construct various focal adhesion types. Currently, it is not known how matrix composition affects the protein make up of the focal adhesions. Two important kinases found at focal adhesions are focal adhesion kinase (FAK) and Src. Each of these proteins activates different proteins and modulates focal adhesion composition and activity. FAK can bind the integrin tail directly to proteins, such as p130CAS and paxillin.[53,54] Both of these proteins are phosphorylated upon binding, and even though FAK is an important kinase, it also serves as an important scaffold protein for focal adhesions.[55-57] In addition, FAK acts as GTPase activator.[58] Src also acts as a kinase.[59,60] It activates upon binding to FAK and can also bind the integrin cytoplasmic tail. Src is believed to help regulate focal adhesion turnover.[61] Another protein that regulates focal adhesion turnover is PTP-TEST.[62] This protein acts as a dephosphorylating agent and helps regulate focal adhesion activity.[63] Other important proteins are p130CAS and paxillin.[64] Both act as a scaffold proteins with many binding partners and partner with other proteins to help regulate focal adhesion function and behavior in the cell. One partner protein is Crk.[65] Together, these proteins regulate Ras activity and other GEFs.

Vinculin is another important protein[66] and sequesters the Arp2/3 protein to the focal adhesions to promote localized actin branching.[67]

Integrin-cell surface binding is not sufficient for integrin clustering, which leads to focal adhesion formation.[68] Instead, this process must be initiated through intracellular events. Proteins Rho and R-Ras have been shown to mediate this process and thereby, control the integrin activity.[69,70] Initially, when a focal adhesion is formed at the leading edge of cells, it is composed of mostly paxillin and al-actinin, and as the adhesion matures other proteins such as vinculin, FAK, Src, and talin bind to the site.[71,72] Next, zyxin and tensinin are recruited to act as stabilize the adhesion,[73] and finally in order for the cell to effectively migrate, focal adhesions need to be turned over. It is believed that this process is mediated by FAK, Src, and Caplain,[74-77] that help increase focal adhesion turnover rate in the cell when they are present. Another possible regulating process of integrin function is binding forces. It is believed this process is regulated through force-sensitive proteins, such as FAK, Src, and Talin.[77-79]

Rho and Rac are as the master control proteins of cell migration and adhesion. Theses proteins are GTPases that regulate the formation of stress fibers, focal adhesions, and membrane ruffling.[80,81] Rho specifically modulates contractility, stress formation fibers, and focal adhesion formation.[82,83] Their activity is regulated by Rho kinases that phosphorylate the protein. Rho upregulates MAPK kinase and myosin light chain phosphorylation to increase contractility.[84,85] Rho also downregulates cofilin, which slows actin polymerization.[86] The sum of these and other actions leads to the formation of stress fibers. Rho significantly upregulates focal adhesion formation by inducing integrin clustering in fibroblasts.[87] This effect is also observed with Rac; focal complexes of high-affinity integrin complexes are formed. However, Rac's major function is the cell is to regulate membrane protrusions and ruffling, and its mechanism of activation primarily occurs through increasing actin polymerization.[88] As such,

Rac activates PI 5-kinase, Arp 2/3 complex, and PAK,[89] all of which remove actin-capping proteins and increase actin polymerization. Since Rho and Rac are GTPases, they are controlled by both GAPs and GEFs that are specific to each protein.[90,91] These controls are governed by growth factors and other cell surface receptors.

A number of different cell surface receptor-ligand interactions have been investigated to study the dynamic processes of cell adhesion and migration. Simple methods have used ECM-derived protein fragments. These ligands are limited by the inability to control their orientation and the difficulty of either generating or synthesizing such ligands. The discovery of the minimal adhesion sequence in fibronectin, RGD, represents a more appealing alternative.[92] Peptides can easily be readily synthesized or commercially purchased without the need to modify proteins. Another peptide sequence that has been found to affect cell adhesion, PHSRN, acts as a synergy peptide with RGD to enhances cell migration rate.[93] These two sequences are located in fibronectin, and their orientation has been shown to affect cell adhesion to its surface. When introduced to various materials, these two peptide sequences have been shown to promote cell adhesion and allow for the generation of materials for biological studies.[94]

Many factors determine not only how the ECM will respond to cell adhesion, but also how the composition and orientation influence cell behavior. To isolate the myriad variables, the ECM has been simplified with a number of different model systems. Polymers are one of the most popular systems and allow for the flexibility in chemical composition, structure, and various physical properties to modulate diverse aspects of the ECM.[95] Layer-by-layer depositions have been employed to create model systems simply.[96] In general, the layers must alternate electric charge or hydrophobicity and are not as compositionally variable as polymer materials. In contrast, self-assembled monolayers are synthetically well defined, and by nature are synthetically flexible.[97] Numerous SAMs have been used, including phosphonates coupled

6

with indium tin oxide (ITO), iron oxide, and glass and siloxanes coupled with glass, ITO, and iron oxide. Perhaps the most well studied and most often used SAM systems are thiol SAMs on noble metals.[98] SAMs have been generated from silver, gold, and even nickel. However, the most common of these metals is gold.

1.3 SAM Structure and Function

SAMs of alkanethiolates on gold are the most well studied system for a number of reasons. Gold is easy to obtain in a variety of forms, including solids and colloids. Thin films can be prepared using different deposition techniques, such as physical vapor deposition, sputtering, and electrodeposition. Crystalline substrates are easily obtained with few defects other relatively large areas. Single crystals are also available for spectroscopic studies. Gold is also relatively easy to pattern. Photolithography, etching, and micromachining have been used to pattern gold substrates. Gold is also one of the most stable metals under room temperature and ambient air conditions and does not oxidize as easily as other noble metals. Thus, gold does not have to be handled under UHV conditions. Thiols bind gold strongly and do not form other side products. This high affinity allows the thiols to not only bind gold, but also to displace other material adhered to the surface. Additionally, thin gold films are commonly used in several spectroscopies such as surface plasmon resonance (SPR), reflection adsorption infrared spectroscopy (RAIRS), and elipsometry making the transition to studying SAMs with these techniques easier. Gold is inert to biological systems and does not poison cells like other metals. Additionally, SAMs composed of olgio(ethylene glycol) form resistant surfaces to non-specific protein and cell adsorption and adhesion. Other common metals used for thiol SAMs are silver and nickel; however, these metals are not as well studied and are not compatible with cell culture.

SAM Substrates can be formed from different systems. One of the most popular methods has been thin-layer deposition on flat substrates, such as glass, silicon, quartz, and mica. The gold is deposited by physical vapor deposition in two layers.[99-102] A ~10-200 nm chrome or titanium layer is first deposited on the substrate because gold does not directly adhere to many typical flat substrates. Next, a 100-1000 nm gold layer is deposited. The metal layers are polycrystalline in nature and can form grains and islands. These films have dominant <111> texture at the exposed surface.[103-106] Metal that is deposited on quartz and mica have a stronger crystal structure than glass.[107] Mica surfaces can provide grain structure of 1000 nm with flat <111> terraces. Quartz can also provide structurally uniform gold surfaces by thermal annealing. By starting with substrates of other dominant crystal structure such as <100>, substrates have been fabricated with other crystal structures.[108,109] Additionally, other deposition methods, including underpotential and electroless, have been used to create surfaces with alternate crystal structures.[110]

Many factors affect grain structure and size of the deposited surfaces. By raising the temperature from 0 °C to 400 °C, the average gold grain size can be increased from 200 to 106 nm^2.[111] Additionally, the angle of deposition and deposition rate can affect the grain size and shape of the surface; the faster the deposition, the larger the grain size.[112] To modify the grain size after deposition, thermal annealing of the substrates has been used to enhance the overall <111> structure of the surface.[113,114]

Film thickness is another important parameter in film deposition. Thin, translucent films are useful for imaging applications, which make them desirable for biological studies. However, various characteristics of these films must be controlled. For thinner (>15 nm) gold layers, the adhesion layer can migrate to the surface.[115] This process can be problematic for biological substrates. If the adhesion layer is cytotoxic nickel, tin, or chrome, then cell death

8

may be induced. Thus, titanium is typically the adhesion layer used for biological substrates for this reason. Additionally, thicker substrates are useful for spectroscopic and electrochemical applications.

Even though planar SAM systems are well studied and characterized, SAMs can be formed on other metal supports. Metal features have been machined using photolithography, molding, or photolithography.[1156,117] However, the substrates' features introduce structural defects into the metal substrate and therefore, the SAMs.[118] Perhaps the second most popular substrates after planar supports are colloid gold nanoparticles.[119,120] These nanoparticles can be synthesized easily utilizing the Brust synthesis and are spectroscopically well studied.[121] SAMs on colloid gold nanoparticles have been used for a variety of applications including hypothermal cancer treatments and MRI contrast imaging agents.[122]

Once the substrate has been fabricated, the SAM can be formed in a variety of ways. The most common method is solution deposition.[123] Gas phase adsorption is performed as well but suffers from a lack of generality and does not produce a SAM with same level of packing as solution phase adsorption. Typically, substrates are immersed in 1 mM ethanolic thiolate solutions for 12-18 h. The SAMs are formed in two mechanistic steps. The thiolate molecule adsorbs to the surface following a Langmuir isotherm. The adsorption takes place on the order of milliseconds to seconds, followed by slow reorganization of the thiolate molecules into the lowest energy configuration; this step occurs over hours. The reorganization maximizes the thiolate packing density and minimizes the SAM defects. This final structure can be affected by a number of factors, including solvent, temperature, immersion time, substrate cleanliness, and alkane chain length.

Solvent effects SAM formation; however, how it effects SAM formation is not thoroughly understood. Ethanol is the solvent of choice due to its purity, availability, and low

toxicity.[123] Generally, the choice of solvent can affect both the SAM formation rate and defect quantity vs. ethanol. Generally, more polar solvents such as water form SAMs with fewer defects than ethanol, which is most likely due to low alkanethiolate solubility.[124-126] Also, solvents like heptane and hexane have been shown to increase SAM formation rates.[127,128] Increasing the temperature from 25 °C has been shown to increase adsorption kinetics, lower the defect rate, and help remove adventitious materials that are bound to the gold substrate.[129,130] The higher temperature increases the crossing of certain activation barriers in SAM formation, which has been shown to be most relevant to the first few minutes of formation. As expected, concentration and immersion time are inversely related with lower concentrations requiring longer immersion times.[131] RAIRS studies have shown that the overall structure of SAMs does not change after 18 h.[123] However, electrochemistry and STM have shown that SAMs do show a decrease in both pinhole and alkane conformation defects over the order of 7-10 days. [132]

Thiol solutions can contain common purities that affect SAM formation. Generally, it has been found that solutions with <5% impurities can form SAMs.[133] However, if the impurities are less soluble than the alkanethiols, it can lead to physisorption of the material, which can affect SAM formation. The cleanliness of the substrate is also important. Materials that are physisorbed to the surface impede SAM adsorption and formation and can introduce defects to the SAM surface. However, due to the strength of the thiol gold bond, most of the adventitious materials can be competitively desorbed from the surface. This process slows down SAM formation and some materials cannot be removed in the 12-18 h timeframe allowed for SAM formation.[123]

Mixed SAMs have been used to install multiple functionalities on the surface. Typically mixed SAMs are formed through solution mixtures, but through SAM desorption and backfill it

can be done after SAM formation. Varying ratios of two different thiols or asymmetric disulfides in solution can be used to create SAMs with mixed functionalities. These SAMs are especially useful for biology where only a small percentage of ligand is needed on the surface for biorecognition and the rest can be another background alkanethiol. If solutions of alkanethiols are used to create these SAMs, their molar ratio reflects but does not always equal the surface ratio.[134,135] Many factors influence the overall distribution including solvent, alkanethiol structure, and adsorption time. Asymmetric disulfides have also been used with some limitations.[136] Most notably, the ratio is restricted to 1:1. However, over time the SAMs will adopt the more energetically favorable state and may deviate from the initial 1:1 ratio. Disulfides are also less soluble than their thiol counterparts and form SAMs with a greater defect rate.[137]

The gold-thiol bond has been well studied both thermodynamically and spectroscopically. To determine the gold-thiol binding energy, Dubois used temperature programming to desorb thiols from gold and determined that it occurs dissociatively in the gas phase. The barrier to recombinative dissociation is roughly 30 kcal/mol, which corresponds to theoretical calculations.[138,139] This value corresponds to a high degree of charge transfer from the thiol to the gold. Scoles and coworkers verified these numbers by using different experimental protocols.[140] For liquid phase desorption, the barrier appears to be lower. SAMs were desorbed while immersed in a solvent and it was found the barrier was approximately 20 kcal/mol.[141] By using these numbers, combined with the segmental heat of interaction, heat of dissolution, and heat immersion, the strength of the gold-thiol bond is believed to ~50 kcal/mol.[138] One ambiguity remaining in the reaction is the final form of the hydrogen after gold-thiol bond formation. In vacuum, it is believed that the hydrogen simply forms a gas, as

reductive elimination is weakly activated by gold. In solution, hydrogen could also be converted to water with gold serving as the catalyst.[142,143]

Once the gold thiol bond has formed on the surface, the SAMs can adopt many different configurations. The most accepted and common form the SAM adopts is the $\sqrt{(3 \times 3)}$R30° overlayer with the alkane chains adopting a c(4x2) superlattice.[144-148] These structures are not only driven by the gold-thiol bond formation, but van der Waals interactions between alkane chains in the overlayer. Both the nearest neighbor distances and geometric arrangement affect the structure of the alkane overlayer of SAMs.[149] The interthiol distance constrains ability of alkane chains to pack closely to maximize the van der Waals interactions. For these reasons, the alkane chains are tilted 30° to the surface normal of the substrate to maximize the van der Waals interaction between the chains. Each of the thiols is individually bonded to the gold; neighboring thiols do not interact with each other. A majority of the SAM structure studies are performed on substrates with dominant <111> structure. The few studies with substrates of different crystallographic directions have shown the effect of the underlying substrate on the final SAM structure. For <100> gold surfaces, the alkane chains adopted a c(2x2) structure as opposed to the c(4x2) structure.[150] For alkanethiolates comprising of different alkane structures such as biphenyl and terpphenyl thiols, the overall SAM structure is constrained by the steric hindrance of the chains. The steric hindrance can reduce the angle the chains take to the surface normal.[151,152] However, the underlying thiol structure appears to be unaffected. Another factor in SAM structure is the odd-even affect for straight chain alkanethiolates.[153,154] Due to constant 30° of tilt found in these SAMs, it has been observed that the even numbered alkanethiolates have a slightly lower free energy than their odd number counterparts.[155] Another factor affect SAM stability is the overall chain length, alkanes longer than n=10 have shown more long term stability than their shorter chained brethren. [156]

Several factors affect the mechanism of SAM formation. An interplay exists between the formation of the covalent gold-thiol bonds, hydrogen bonding, and the van der Waals interaction between chains. The gold surface structure dictates available reaction sites for the thiol to bind. These sites determine the structure of the thiol layer while the van der Waals and hydrogen bonding of the alkane chains add an additional 1 kcal/mol of stabilization per methylene unit.[157] For gas phase reactions, several low coverage phases proceed the fully formed SAM.[141] The alkanethiols lie flat on the gold surface and as other alkanethiols pack onto the substrates, and these alkanethiols eventually form a well packed SAM.[143] The conversion from the striped phase constitutes the slow step in SAM formation. In solution, the complexity of the environment has stymied efforts to study the mechanism of assembly.[143,158] Qualitatively, the SAM formation follows a Langmuir isotherm with fast adsorption of thiols on solution and a slow packing and order step.[143] It is believed both gas and solution phases roughly follow the same mechanism. However, this has not been demonstrated effectively.

Defects in SAMs can come from a number of sources including the surface cleanliness, impurities, and substrate preparation. However, another major source of defects are the dynamic nature of SAMs. In solutions, they are not simply the well-ordered substrates of theory. The substrate of choice, polycrystalline gold, has many defects from intergrain boundaries, faceting, and a varying density of atomic steps. These surface defects impact SAM formation and can introduce structural defects into the SAM.[140,159,160] Other types of defects are introduced during the SAM induced rearrangement of the gold surface atoms.[143,161] A clean gold surface has a higher density of reactions sites than can be filled by available thiols. As the thiols bind the gold, single atom vacancies form in the gold structure and cannot be concealed by the SAM itself. Impurities, if they have a stronger affinity for the gold surface, can impact SAM formation and structure by impeding SAMs in the blocked areas. Defects can be introduced

once the SAM is removed from its solution. By its nature, SAM formation is a thermodynamic process in equilibrium between well-formed SAM and single alkanethiolates.[162] Once the SAM is removed from solution and used for other studies, the thiols start desorbing from the surface, which can introduce defects.

Once SAMs are formed, they can be removed a using a number of different methods. First, by applying a negative potential to the surface, the SAMs can be reductively desorbed from the surface.[163,164] The thiol leaves the surface negatively charged while the metal goes from positively charged to neutral. The process is reversible. Once the potential is removed, thiolates in solution can reabsorb to the surface. Another method to remove a SAM is through a displacement exchange.[165] By removing the SAM from its original alkanethiolate solution and placing it in a new solution, the new alkanethiols will displace the original ones from the surface over time. The rate typically depends on the inter chain attraction of the new alkanethiolate vs the original one and the amount of defects found within the original SAM.[166] The defects present serve as nucleation point for new SAM formation and greatly speed exchange.[167] SAMs can also be photooxidized with UV light.[168] When exposed, the thiols are oxidized to sulfonates, which can be washed away with a polar solvent.[169]

1.4 SAMs for Biology

For biological applications, the most important alkanethiolates are terminated in olgio (ethylene glycols).[170] SAMs composed from these alkanethiolates resist non-specific adsorption and adhesion of both proteins and cells. This feature makes SAMs a unique platform for biology. Rather than studying whole proteins on ill-defined surfaces, specific ligands can be presented against an inert background.[171] SAMs of these molecules pack normally, however, the ethylene glycol chains adopt a number of different conformations that provide the resistance to protein and cell binding.[172] The helical structures on the surface yield a quasi-crystalline surface and the

amorphous phase leads to a liquid like phase on the surface. Above room temperature, other phases such as an all trans conformer are visible with NEFAXS. It is believed these structures resist proteins and cell adsorption for two reasons. These structures adsorb a significant amount of water on the surface, which in turn must be removed before a protein can adsorb to the surface. The water removal generates an enthalpic penalty for binding on the surface. Second, protein bind restricts the possible conformers available to the ethylene glycol chains and providing an entropic penalty to protein and cell binding. The combination of these two penalties provides an energy barrier to protein binding that allows these SAMs to resist protein binding for a finite time (~1-2 weeks).[173,174]

Several factors influence the ability of the SAMs resistance to non-specific binding of cells and proteins. The substrate cleanliness and age have a strong effect. The substrate must be clean and as free from defects as possible. The defects introduced from a poorly prepared or poorly cleaned SAM generate binding sites for protein adsorption to the surface. If the substrate is not freshly prepared, the adventitious materials and oxidation that take place on the gold surface can introduce defects as well. Additionally, the ethylene glycol purity is of utmost importance. For the SAM to resist protein and cell binding the most strongly, the thiol must be >99% pure. If not, the impurities can introduce surface defect sites. In the same vein, the solution must be freshly prepared, so no disulfides or other impurities are present in the solution. The ethylene glycol chain length is important as well. For the SAMs to resist protein and cell binding, the chain length has to exceed 3 units.[175]Another factor is formation time. The SAMs must be allowed to form properly over an 18h time to minimize defects.[176] For mixed SAMs, ethylene glycol portion must exceed 95% of the surface density. Below this number, proteins and cells adhere to the other thiols on surface. [172]

Studies of SAMs under physiological conditions have been sparse and are not as thorough as solution and gas phase studies. Grunze and co-workers studied PEG SAMs exposed to water.[177] They found that the chains adopted an amorphous conformation that mirrored solvated PEG chains in solution. For shorter PEG chains (3-6 units), studies have shown they adopt a similar state in water. [178] Another important but poorly understood area is the long-term effect of water immersion of SAMs on their stability. SAMs terminated with EG form significant defects after 4-5 weeks in water containing calf bovine serum.[179] Typically, SAMs of EG can resist non-specific protein adsorption and adhesion for only 1-2 weeks as a consequence of this. It is believed the cells and proteins can oxidize the thiolates and introduce defects into the SAM to generate binding sites.

1.5 Covalent and Non-Covalent SAM Modification

SAMs are modified after formation to enhance their usefulness. Simple surface functional groups are useful for wettability studies and fundamental structure studies but are limited in biological and other applications.[180-183] Biochemical applications demand surfaces that present complex ligands such as peptides, carbohydrates, and signaling molecules. Directly synthesizing thiol forms of these molecules can often be laborious even for simple biomolecules. By providing a reactive functional group on the SAM surface, these syntheses can effectively split in 2. Instead of synthesizing the biomolecule of interest with a complex thiol, all that is required is to attach the surface group's reactive pair. Additionally, ligands can be synthesized that are not compatible with thiol chemistry and the underlying SAM structure is not disrupted by the larger peptides and other ligands attached to the surface. Another important advantage, only a small amount is ligand is needed for surface immobilization, which allows for the reduced use of difficult to synthesize ligands.

For a reaction to be successfully adapted to a surface, it must have a number of characteristics. It must take place with high yield. Low yielding reactions defeat the purpose of immobilizing ligands to the surface. Ideally, the reaction should be quantitative so that the amount of ligand on the surface can easily be estimated from the surface density of the reactive thiol. Additionally, the reaction conditions must be mild enough to not damage or remove the underlying SAM structure. For biological surface reactions, additional constraints are imposed. The reaction needs to be bio-orthogonal, which entails the reactive pair being absent from biology. Also, the reaction needs to take place under physiological conditions so the reaction does not stress or cause harm to cells. These two constraints severely limit the number of possible reactions.

Many different organic reactions have been adapted to the surface and fall into two broad groups. In the first, the reaction groups are present and reactive on the surface without further modification. Many examples are present in the literature. Mrksich and co-workers have pioneered the use of SAMs terminated with malemide groups to react with thiols in solution by Michael addition.[184] Disulfides have been used as well to exchange various thiolated ligands on the surface.[185] Choi et al have demonstrated olefin metasis on the surface catalyzed by palladium. However, the reaction is limited by the 50 ° C temperature required for reaction.[186] Perhaps the most popular has been the copper catalyzed triazole formation.[187] The reaction is fast, nearly quantitative, and takes place at room temperature. Both the alkyne and azide can easily be incorporated into a number of different ligands and thiols, which allows for great synthetic flexibility. Staudinger ligation is reaction suitable for biological applications.[188] The reaction of substituted phosphanes and azides can take place at physiological conditions without the need of the catalyst and is chemoselective. The reaction has been used to modify the surfaces of cells and glass slides.

In the other group of surface reactions, the surface must be activated for the reaction to proceed. The activation allows for the creation of 'smart' surfaces. These surfaces can be patterned by controlling the unmasking of the reactive group, followed by a subsequent reaction to spatially control the reaction. Additionally, it is possible to temporally control the reaction to create a dynamic surface for cell studies. The most basic masking reaction is amide formation through a NHS ester or anhydride intermediate.[189,190] Carboxylate terminated SAMs are activated with either trifluoroacetic acid anhydride or a mixture of NHS/DCC. Subsequent reaction with an amine containing ligand generates amide linkages on the surface. Reaction yields for the anhydride reaction is limited to 50% and for the activated ester intermediate, falls somewhere between 80-100%. Other reactions take advantage of external stimuli to convert the surface groups for reaction such as electrochemical, photoradiation, or chemical oxidation.

Mrksich and co-workers pioneered the use of the hydroquinone-terminated SAMs on the surface.[191] When oxidized on the surface, the hydroquinone transforms to quinone form and becomes suitable for a diels-alder reaction with cyclopentadiene-terminated ligands. This work was extended by Muhammad and co-workers. The hydroquinone was oxidized as before, but oxyamine-terminated ligands were used instead of cyclopentadiene; for this reaction, the transformed quinone form served as a ketone leading to formation of an oxime on the surface.[192]

This reaction afforded many advantages over the diels alder reaction. The oxyamine-ketone is orthogonal to biology and can take place in the presence of cells. The oxyamine-terminated ligands are more stable than their cyclopentdiene counterparts, which have a tendency to dimerize in solution over time. Also, both oxime and hydroquinone are electroactive with characteristic peaks. These peaks allow both the oxime and unreacted product to be distinguished and quantified on the surface. Also, the reaction between the

hydroquine and oxyamine is reversible.[193] Once the oxime product is formed on the surface, it is stable at low pHs when cycled between the oxidized and reduced forms. However, when the oxime is cycled at pH 7, the oxime product is cleaved on the surface and leaves as an alcohol. The reversibility allows for multiple rounds of reactions to take place on the same surface.

The structure of SAMs affects reactions that take place on the surface. The surface reaction kinetics and mechanisms can be dramatically different than solution phase ones due to the geometric constraints and environmental variations on the surface. Additionally, the solution composition has been shown to be dramatically different at the SAM interface vs. the bulk solution.[194,195] Other factors such as chain organization, surface functional group density and orientation, lateral steric effects, and the portioning of the reactants at the interface also affect surface reactions. Using RAIRS, the conversion of a carboxylic acid to the NHS ester was studied with respect to the chain organization.[196] It was found that the surface reactions proceeded as much as 2 orders of magnitude slower than their solution counterparts. Vaidya et al. studied hydrolysis rates of ester on SAMs and found the ester hydrolyzed more slowly on the SAM surface compared to the solution.[197] These two results demonstrate the effect geometric and steric constraints on surface reactions.

When reactive surface groups become crowded, lateral steric effects can negatively or positively impact surface reaction rates. For enzymatic catalysis on the surface, reaction rates were linear until roughly 70% surface density of reactive surface group. For densities greater than 70%, the reaction rates decreased rapidly.[198] Counter to these results, one group observed an increase in reaction rates with increasing surface density for a polymerization reaction.[199] The lateral steric effects appear to be very reaction dependent. Another factor affecting surface reactions are the position of reactive sites on the surface. If the reactive sites are not presented on the surface and are buried within the SAM, the reaction rates suffer.[200] Additionally, making

the thiol containing the reactive group longer than the background thiols can reduce steric effects. The longer thiol will extend away from the bulk SAM reducing the surface steric effects.[201] For example, tethering a reactive site to a dodecane thiol positions the reactive site away from a background of decane thiol. Also, reactant partitioning affects the surface reaction rates. Studies have suggested if the reactant concentration is higher at the interface vs. the bulk solution, the apparent reaction rate increased.[202] However, significant work in this field has not been performed to establish definitive structure-activity relationships at the solution-SAM interface, and many questions still remain.

In addition to covalent modification, SAMs can be modified non-covalently as well using either electrostatic or hydrophobic interactions. Using SAMs composed of hydrophobic molecules, many different molecules have been adsorbed to the surface from solution including proteins, polymers, and organic dyes.[203] Using this method has its limitations, the thickness of the adsorbed layer cannot be easily controlled on the surface and the orientations of molecules cannot easily be controlled. Orientation control is especially important for proteins involved in certain surface assays. Lipid vesicles can also be fused to both hydrophilic and hydrophobic SAMs.[204] If the SAM is hydrophilic, the polar head group will associate with the SAM and generate bilayers on the surface. If the SAM is hydrophobic the tails will associate with the surface and form a monolayer. The bilayer formation provides an excellent platform for cell membrane studies. They can incorporate many proteins found on the cell surface and are amenable to a number surface spectroscopies.[205] To gain the most specificity and control over non-covalent interaction on the SAM surface, supramolecular chemistry has been used to modify SAMs.[206,207] These interactions rely on different host-guest interaction on the surface such as metal-ligand, hydrogen bond networks, or electrostatic interactions.

1.6 Patterning Planar SAMs

Patterning SAMs has been performed using many different lithography techniques and can also occur destructively. Many methodologies have been developed to pattern the surface ranging from 1 cm to 100 nm in size. Both non-destructive and destructive methods have been used on the surface. Destructive patterning methods rely on removing a portion of the SAM using photons, electrons, or atoms and replacing the damaged portions with SAMs of their own to generate the pattern on the surface.

The most popular method to pattern SAMs to date has been microcontact printing. (μCP) It was developed by Whitesides and co-workers and has become nearly ubiquitous due its ease and versatility.[208] The stamps used to generate the patterns can be fabricated from commercially available materials using a process called soft lithography. Soft lithography is a microfabrication technique that does not relies on the need for materials such as glass and silicon. Instead, polymers like polydimethyl siloxane (PDMS) are used to generate the microstructures. PDMS is a commercially available elastomer that can generate structures down to 100 nm.[209,210] The polymers' flexibility and low surface energy allow for a large range of pattern sizes to be generated on the surface. The low surface energy makes it easy to contact then remove the stamp from various surfaces and its flexibility allows for excellent contact between the substrate and stamp. The stamps are fabricated such that the desired features stand in relief from the stamp surface.[211] To carry out μCP, a PDMS stamp is fabricated and then inked with alkanethiol by immersing it in an alkanethiolate solution. The solvent is dried and stamp is pressed on the surface. Where the PDMS contacts the gold surface, a partial SAM is formed. The stamp is lifted and the surface is backfilled with another alkanethiolate by immersing in a solution.

Alkanethiols are transferred to the surface through a number of different mechanisms. The most direct is diffusion from the stamp onto the substrate. Next, the ink can diffuse away

from the features contacting the surface over time.[212] Finally, the alkanethiol in the stamp can enter the gas phase and diffuse to the surface from the stamp.[213] The last two methods of ink transfer are not generally desirable and are controlled by limiting the stamp's contact time with the surface.[214]

SAMs formed by μCP have considerable defects when initially formed and have been studied with a variety a spectroscopic methods.[215-217] Many different crystal structures are formed on the surface after inking with alkanethiols at 1-10 mM including striped phases as well as denser regions of SAMs packed similarly to solution formed ones.[218] For stamps inked with 100 mM alkanethiols, the SAM structures were more ordered and could not be distinguished from SAMs formed in solution. Most defects were only eliminated with longer stamp contact times of 1 min to 1h, which is less time than solution formation.

Though useful, several limitations constrain μCP. The inks must be hydrophobic in order to diffuse into the PDMS stamp. Hydrophilic molecules cannot impregnate the stamp so they do not transfer into the PDMS. Some work has been done with alternate polymers and oxidized PDMS for hydrophilic μCP.[219] However, most these methods lack the simplicity of regular μCP. Additionally, The PDMS cannot support small structure spaced at large intervals, because the stamp cannot support the regions between features.[220] The stamp will collapse between the features and contact the surface leading to pattern distortion. Also, the stamp can be distorted non-uniformly during application of the stamp. Too much force can lead to the collapse of the stamp as well as distortion of the stamp features. [221]

Photolithography or beam lithography is another popular method used to pattern SAMs. These methods can generate patterns on the order of 10 nm and are much more reproducible than μCP. The most simple of these methodologies involves simply desorbing the SAM using photooxidation.[222] By exposing through a photomask, the reaction can be spatially

controlled with resolution down to 300 nm. For complete desorption, ~20 min exposure times are required with lamps, but with a laser, exposure can be reduce to 1 min.[223] Alternatively to photooxidiation, the SAM can be desorbed thermally by local heating with a laser.[224] In addition to destructive photo patterning methods, SAMs have been made with photosensitive molecules. Upon exposure, a hidden molecule is revealed and the surface is available for further reaction. Mrksich and co-workers used this method to photoprotect hydroquinone alkanethiols.[225] After photodeprotection, the hydroquinones were activated and then reacted with cyclopentadiene ligands. We have extended this work using photoprotected hydroquinone and oxyamine terminated alkanethiols followed by subsequent surface activation and functionalization to study cell polarity and adhesion. [226]

As an alternative to photons, electrons, x-rays, and atomic beams can be used to pattern SAMs. [227] When the SAMs are irradiated with these beams, they undergo several chemical reactions. Bonds are broken and formed leading to SAM that is easily desorbed after treatment. Once treated with certain etchants, the SAMs act as a negative resist. SAMs containing biphenyl rings instead of alkane chains serve as positive photoresists instead.[228] Upon irradiation, the biphenyls crosslink into one another and are difficult to desorb from the surface. For atomic beam lithography, SAMs are damage by a beam of rare excited rare gases.[229] Diffraction effects do not limit the atomic beams, which allow for a higher degree of precision. The SAMs can either be destroyed if the exposure time long enough or merely desorbed to make them more susceptible to exchange after exposure. These methodologies allow for formation of patterns down to the 10 nm region.

One of the most powerful patterning methodologies is scanning probe lithography. Scanning probes such as AFM have been used to not only characterize SAMs, but either remove them mechanically or create new SAM patterns.[230] Dip pen nanolithography, pioneered by

Mirkin and co-workers, has been the most popular of these methods to date.[231] The method creates SAMs on the order of 50 nm reliably over larger areas of substrate. To perform DPN, an AFM tip is inked with alkanethiol and then spotted on the surface. By controlling the tip contact time, various spot diameters on the surface can be generated. If the tip is dragged, lines can be formed and if larger patterns are desired, arrays of spots can be used. Once the pattern has been formed on the surface, the remaining area can be backfilled with a different alkanethiol. DPN has proven used for cell biology studies, and has been used to study cell polarity can cell adhesion on the nanoscale.[232] However, DPN is limited by its serial nature. Spots must be generated individually, which limits pattern throughput. This drawback has been overcome with the advent of parallel DPN; multiple tips contact the surface at once and generate multiple patterns.[233] In contrast to DPN, SAMs can be removed from the surface. The removal can be accomplished through local electrochemical desorption, mechanical scratching, or directed photooxidation.[234] These methods are destructive and can permanently damage the substrate beneath leading to problems with subsequent SAM formation.

One of most important pattern goals for biology is generating gradients. They are important for studies of chemotaxsis, cell adhesion, cell migration, and tissue formation.[235] Gradients have been generated a number of different ways. A gold substrate has been dipped in one alkanethiol followed by immersion in a second thiol. The first thiol forms an incomplete SAM based on the immersion time followed by the backfill of the second thiol. Thiol diffusion can also be used.[237] Thiols diffusing through a polysaccharide matrix have been used, as well as diffusion gradients through PDMS induced by organic solvents. By establishing a potential gradient on the surface, SAMs can be desorbed in a gradient, and then followed by a backfill with a second thiol.[238] Finally by coupling photosensitive surface group with grayscale

photolithography, this methodology has been used to generate surfaces for studies of cell polarity, adhesion, and division. [239]

1.7 Non-biological Applications of SAMs

SAMs are enormously useful in biology, but have found myriad uses outside its scope. They are particularly useful as etch resists. Since SAMs are composed of molecules ~2 nm in width their theoretical spatial resolution is higher than for typical photoresists.[240] They have used as resists with Au, Ag, Cu, Pd, and many others. Additionally, SAMs have been used barriers to electron transport.[241] The alkane chain component serves as effective insulator given the chain length is long enough. Additionally, biphenyl SAMs have been used as molecular wires.[242] These nanometer wires have been used as rectifiers, conductors, and even transistors. SAMs have also served as crystallization substrates.[243] Many SAM parameters can be tuned such as surface composition, orientation, substrate roughness, and the functional surface group.[244] These parameters can be tuned to effect the crystal size and orientation during nucleation.

SAMs have found significant use as platform for electrochemical studies both theoretical and applied. Two types of experiments are usually undertaken. One strategy seeks to completely block access to the metal through the formation of long chain alkanes based SAMs.[245] In the second approach, SAMs are fabricated from alkanethiols containing an electroactive group.[246] These studies are used to look at electron transfer kinetics without diffusion effects. Many different electron phenomena have been studied with these electrochemical setups. Electron transfer was studied through straight chain alkanes under the following parameters: distance from the surface, electrolyte, temperature, and metal. Unsaturated chains were studied as well under these parameters.[247] Additionally, coupled proton-electron transfer reactions like the reduction and oxidation of hydroquinone were

studied.[248] Solvation effects on electron transfer were studied at the solvent hydrophobic SAM interface.[249] Additional studies include the effect of counterion movement on electron transfer kinetics, dynamic molecules in lipid bilayers, and the effect of orientation and conformation on protein electron transfer rates.[250] Gold is the primary choice for its ease of use, but mercury is used as well due to its lack of defects and ability to create a clean surface by simply extruding a drop from a needle.

1.8 Biological Applications of SAMs

SAMs are able substrates for biological studies for a number of reasons. SAMs are spectroscopically well defined. As noted above, many different spectroscopic methods have been used to characterize the structure and function of SAMs. This knowledge makes predicting and understanding ligand presentation on the surface relatively easy to understand. SAMs are compatible a number of surface spectroscopies such as SPR, RAIRS, and electrochemistry. These techniques allow surface interactions to be characterized, which can be useful for binding assays. The thiols are synthetically flexible allowing for the synthesis of broad spectrum of tail groups. This feature makes the SAMs flexible in their application and composition. Gold is an easy metal to work with because it does not oxidize in air and can easily be coated on glass in thin films. Similarly, gold is not cytotoxic making the metal compatible with cell culture. Thin gold surfaces are translucent, so the substrates are compatible with high-resolution microscopy. Perhaps most importantly, SAMs of alkanethiols terminated with olgio EG are resistant to non-specific adsorption and adhesion of cells. These SAMs create masked regions to cells, and by creating cell adhesive patches on the surface, cells can be patterned.

Many cell adhesion studies have been undertaken with SAMs as the platform. For cell adhesion studies, patterned SAM surfaces present the tripeptide, RGD, or fibronectin immobilized to hydrophobic patches to allow cells to adhere to the surface under spatial control.

Whitesides and co-workers studied geometric effects on cell viability μCP.[251] They found that the shape greatly affect cell survival rates on the surface. Additionally, we have looked at ligand effects on the surface. DPN was used to generate nanopeptide arrays on the surface and both cyclic and linear RGD was immobilized to the surface.[233] It was found both the ligand density and strength affect the distribution of focal adhesions, and overall cell polarity on these substrates. Cells were also patterned by electrochemical desorption. Using microfluidic cassettes to control electrolyte flow, local electrochemical desorption of SAMs was performed.[252] Cells were seeded to the desorbed regions to generate cell adhesive patterns on the surface. Other groups have looked at lamellipodal distribution on μCP patterns.[253] Protein arrarys were created using μCP to study density effect on Ras activation and focal adhesion distribution. Various proteins were adsorbed on the μCP printed surfaces and the cellular responses were studied.[254] Using a FRET biosensor, RhoA activation was studied on patterned SAM surfaces.[255] It was found that RhoA activity was significantly at the cell periphery than its interior.

SAMs also have been used as substrates in other cell behavior studies. Stem cell differentiation of meschemyl stem cells into adipocytes was undertaken by μCP.[256] Geometric and size effects were studied by μCP printed patterns of fibronectin. Additionally cell polarity was looked at by a photodeprotection/electrochemical activation scheme.[226] It was found that cell-cell contact overrode surface cues and force the cells to polarize away from one another. Additionally, microfluidic lithography has been used to generate surface gradients and in combination with μCP cells were patterned on the surface at a certain starting point and given an option to move up or down the gradient.[257] Cells migrated up the gradient. Many additional studies have been performed using SAMs demonstrating both its flexibility and usefulness for biological applications.[98]

1.9 Dissertation Goals and Organization

My overall research goal for this dissertation is to design simple research tools based on SAMs for cell studies. I hope to create tools that need a minimum of organic synthesis and rigorous microfabrication in order to broaden their appeal without sacrificing flexibility or usefulness. I have pursued these goals with the use of microfluidic controlled surface chemistry using a power supply in chapter 2. I then generated SAM patterns by microfluidic controlled gold etching in chapter 3. In chapter 4, a method was developed to pattern SAMs with the synthesis of a precursor thiol for both gold and ITO SAMs. This method was extended to serve as platform for protein affinity studies in chapter 5. In chapter 6, the DPN studies initated by previously in our lab were extended with parallel DPN. In chapter 7, cells were patterned in 3 dimensions using a chemically flexible hydrogel. Finally, the dissertation summary and conclusion is in chapter 8.

1.10 References

1. Myllyharju, J; Kivirikko, K.I. *Ann. Med.* **2001**, *33*, 7.

2. Hulmes, D.J. *Essays Biochem.* **1992**, *27*, 49.

3. Kadler, K.E.; Holmes, D.F.; Trotter, J.A.; Chapman, J.A.; *Biochem. J.* **1996**, *316*, 1.

4. Ottani, V.; Raspanti, M. Ruggeri A. *Micron.* **2001**, *32*, 251.

5. Hulmes, D.J. *J. Struct. Biol.* **2002**, *137*, 2.

6. Aumailley, M; Smyth, N. *J. Anat.* **1998**, *193*, 1.

7. Colognato, H.; Yurchenco, P.D. *Dev. Dyn.* **2000**, *218*, 213.

8. Miner J.H.; Patton, B.L.; Lentz, S.I, *et al. J Cell Biol.* **1997**, *137*, 685.

9. Patarroyo, M.; Tryggvason, K.; Virtanen, I. *Semin. Cancer. Biol.* **2002**, *12*, 197.

10. Bourdon, M.A.; Wikstrand, C.J.; Furthmayr, H.; Matthews, T.J.; Bigner, D.D. *Cancer Res.* **1983**, *43*, 2796.

11. Jones, F.S.; Jones P.L. *Dev. Dyn.* **2000**, *218*, 235.

12. Iozzo, R.V. *Annu Rev. Biochem.* **1998**, *67*, 609.

13. Lander, A.D.; Selleck, S.B. *J. Cell Biol.* **2000**, *148*, 227.

14. Sugahara, K.; Kitagawa, H. *Curr. Opin. Struct. Biol.* **2000**, *10*, 518.

15. Yamaguchi, Y. *CMLS Cell Mol. Life Sci.* **2000**, *57*, 276.

16. Kresse, H.; Schonherr, E. *J. Cell Physiol.* **2001**, *189*, 266.

17. Tumova, S.; Woods, A.; Couchman, J.R. *Int. J. Biochem. Cell Biol.* **2000**, *32*, 269.

18. Nagase, H.; Woesner, J.F. *J. Biol. Chem.* **1999**, *274*, 21491.

19. McCawley, L.J.; Matrisian, L.M. *Curr. Opin. Cell Biol.* **2001**, *13*, 534.

20. Egeblad, M; Werb, Z. *Nature Rev.* **2002**, *2*, 161.

21. Sternlicht, M.D.; Werb, Z. *Annu. Rev. Cell Dev. Biol.* **2001**, *17*, 463.

22. George, E.L.; Rayburn H.; Hynes, R. *J. Cell Biochem.* **1993**, *111, 4353*.

23. Pankov, R.; Yamada, K.M. *J. Cell Sci.* **2002**, *115*, 3861.

24. Vogel, V. *Annu. Rev. Biophys. Biomol. Struct.* **2006**, *35*, 459.

25. Krammer, A.; Craig, D.; Thomas, W.E.; Schulten, K.; Vogel, V. *Matrix Biol.* **2002**, *21*, 139.

26. Danen, E.H.J.; Aota, S.I.; Vankraats, A.A.; Yamada, K.M.; Ruiter, D.J.; Vanmuijen, G.N.P. *J. Biol. Chem.* **1995**, *270*, 21612.

27. Baron, M.; Main, A.L.; Driscoll, P.C.; Mardon, H.J.; Boyd, J.; Campbell, I.D. *Biochemistry* **1992**, *31*, 2068.

28. Altroff, H.; Schlinkert, R.; van der Walle, C. F.; Bernini, A.; Campbell, I. D.; Werner, J. M.; Mardon, H. J. *J. Biol. Chem.* **2004**, *279*, 55995.

29. Ochsenhirt, S. E.; Kokkoli, E.; McCarthy, J. B.; Tirrell, M. *Biomaterials* **2006**, *27*, 3863.

30. Humphries, J. D.; Byron, A.; Humphries, M. J. *J. Cell Sci.* **2006**, *119*, 3901.

31. Hynes, R. O. *Cell* **2002**, *110*, 673.

32. Calderwood, D. A.; Shattil, S. J.; Ginsberg, M. H. *J. Biol. Chem.* **2000**, *275*, 22607.

33. Calderwood, D. A. *J. Cell Sci.* **2004**, *117*, 657.

34. Zaidel-Bar, R.; Itzkovitz, S.; Ma'ayan, A.; Iyengar, R.; Geiger, B. *Nat. Cell Biol.* **2007**, *9*, 858.

35. Ginsberg, M. H.; Partridge, A.; Shattil, S. J. *Nat. Cell. Biol.* **2005**, *17*, 509.

36. Tadokoro, S.; Shattil, S. J.; Eto, K.; Tai, V.; Liddington, R. C.; de Pereda, J. M.; Ginsberg, M.H.; Calderwood, D. A. *Science* **2003**, *302*, 103.

37. Petrich, B.G.; Fogelstrand, P.; Partridge, A.W.; Yousefi, N.; Ablooglu, A. J.; Shattil, S.J.; Ginsberg, M.H. *J. Clin. Invest.* **2007**, *117*, 2250.

38. Kiema, T.; Lad, Y.; Jiang, P.; Oxley, C.; Baldassarre, M.; Wegener, K. L.; Campbell, I.D.; Ylanne, J.; Calderwood, D.A. *Mol. Cell* **2006**, *21*, 337.

39. Calderwood, D.A.; Fujioka, Y.; de Pereda, J.M.; Garcia-Alvarez, B.; Nakamoto, T.; Margolis, B.; McGlade, C.J.; Liddington, R.C. Ginsberg, M.H. *Proc. Natl. Acad. Sci. U.S.A.* **2003**, *100*, 2272.

40. Geiger, B.; Bershadsky, A.; Pankov R.; Yamada, K.M. *Nat. Rev., Mol. Cell. Biol.* **2001**, *2*, 793.

41. Cukierman, E.; Pankov R.; Yamada, K.M. *Curr. Opin. Cell Biol.* **2002**, *14*, 633.

42. Geiger, B.; Bershadsky, A. *Cell* **2002**, *110*, 139.

43. Wehrle-Haller, B.; Imhof, B. *Trends Cell Biol.* **2002**, *12*, 382.

44. DeMali, K.A.; Wennerberg, K.; Burridge, K. *Curr. Opin. Cell Biol.* **2003**, *15*, 572.

45. Yamada, K.M.; Pankov, R.; Cukierman, E. *Braz. J. Med. Biol. Res.* **2003**, *36*, 959.

46. Zamir, E.; Geiger, B. *Cell. Sci.* **2001**, *114*, 3583.

47. Pankov, R.; Cukierman, E.; Katz, B.Z.; Matsumoto, K.; Lin, D.C.; Lin, S.; Hahn, C.; Yamada, K.M. *J. Cell Biol.* **2000**, *148*, 1075.

48. Cukierman, E.; Pankov, R.; Stevens, D.R.; Yamada, K.M. *Science* **2001**, *294*, 1708.

49. Tamariz, E.; Grinnell, F. *Mol. Biol. Cell* **2002**, *13*, pp. 3915.

50. Wozniak, M.A.; Desai, R.; Solski, P.A.; Der, C.J.; Keely, P.J. *J. Cell Biol.* **2003**,*163*, 583.

51. Wang, Y.; Wang, Y.; Wang, C.; Sung, J.; Chiu, W.; Lin, S.; Chang, Y.; Tang, M. *J. Biol. Chem.* **2003**, *278*,21886.

52. Schaller, M.D.; Borgman, C.A.; Cobb, B.S.; Vines, R.R. *Proc. Natl. Acad. Sci. U.S.A.* **1992**, *89, 5192.

53. Hildebrand, J.D.; Schaller, M.D.; Parsons, J.T. *J. Cell Biol.* **1993**, *123*, 993.

54. Polte, T.R.; Hanks, S.K. p130Cas. *Proc. Natl. Acad. Sci. U.S.A.* **1995**, *92*, 10678.

55. Harte, M.T.; Hildebrand, J.D.; Burnham, M.R.; Bouton, A.H.; and Parsons, J.T. *J. Biol. Chem.* **1996**, *271,* 13649.

56. Schaller, M.D.; Hildebrand, J.D.; Parsons, J.T. *Mol. Biol. Cell* **1999**, *10*, 3489.

57. Zhai, J.; Lin, H.; Nie, Z.; Wu, J.; Canete-Soler, R. *J. Biol. Chem.* **2003**, *278*, 24865.

58. Hanks, S.K.; Polte, T.R. *BioEssays* **1997**, *19*, 137.

59. Frame, M.C.; Fincham, V.J.; Carragher N.O.; Wyke, J.A. *Nat. Rev., Mol. Cell. Biol.* **2002**, *3*, 233.

60. Burnham, M.R.; Bruce-Staskal, P.J.; Harte, M.T.; Weidow, C.L.; Ma, A.; Weed, S.A.; Bouton, A.H. *Mol. Cell. Biol.* **2000**, *20, 5865.

61. Angers-Loustau, A.; Cote, J.F.; Tremblay, M.L. *Biochem. Cell. Biol.-Biochimie & Biologie Cellulaire* **1999**, *77,* 493.

62. Angers-Loustau, A.; Cote, J.F.; Charest, A.; Dowbenko, D.; Spencer, S.; Lasky, L.A.; Tremblay, M.L. *J. Cell Biol.* **1999**, *144*, 1019.

63. Mayer, B.J.; Hanafusa, H. *J. Virol.* **1990**, *64*, 3581.

64. Uemura, N.; Griffin, J.D. *J. Biol. Chem.* **1999**, *274*, 37525.

65. Klemke, R.L.; Leng, J.; Molander, R.; Brooks, P.C.; Vuori, K.; Cheresh, D.A. *J. Cell Biol.* **1998**, *140*, 961.

66. DeMali, K.A.; Barlow, C.A.; Burridge, K. *J. Cell Biol.* **2002,** *159*, 881.

67. Svitkina, T.M.; Borisy, G.G. *J. Cell Biol.* **1999**, *145*, 1009.

68. Berrier, A.L.; Mastrangelo, A.M.; Downward, J.; Ginsberg, M.; LaFlamme, S.E. *J. Cell Biol.* **2000**, *151*, 1549.

69. Kwong, L.; Wozniak, M.; Collins, A.; Wilson, S.; Keely, P. **2003**, *23*, 933.

70. Furuhjelm, J.; Peranen, J. *J. Cell. Sci.* **2003**, *116*, 3729.

71. Laukaitis, C.M.; Webb, D.J.; Donais, K.; Horwitz, A.F. *J. Cell Biol.* **2001**, *153*, 1427.

72. Edlund, M.; Lotano, M.A.; Otey, C.A. *Cell Motil. Cytoskelet.* **2001**, *48*, 190.

73. Zaidel-Bar, R.; Ballestrem, C.; Kam, Z.; Geiger, B. *J. Cell. Sci.* **2003**, *116*, 4605.

74. Parsons, J.T.; Parsons, S.J. *Curr. Opin. Cell Biol.* **1997**, *9*, 187.

75. Huttenlocher, A.; Palecek, S.P.; Lu, Q.; Zhang, W.; Mellgren, R.L.; Lauffenburger, D.A.; Ginsberg, M.H.; Horwitz, A.F. *J. Biol. Chem.* **1997**, *272*, 32719.

76. Bhatt, A.; Kaverina, I.; Otey, C.; Huttenlocher, A. *J. Cell. Sci.* **2002**, *115*, 3415.

77. Dourdin, N.; Bhatt, A.K.; Dutt, P.; Greer, P.A.; Arthur, J.S.C.; Elce, J.S.; Huttenlocher, A. *J. Biol. Chem.* **2001**, *276*, 48382.

78. Felsenfeld, D.P.; Schwartzberg, P.L.; Venegas, A.; Tse, R.; Sheetz, M.P. *Nat. Cell Biol.* **1999**, *1*, 200.

79. Grinnell, F.; Ho, C.H.; Tamariz, E.; Lee, D.J.; Skuta, G. *Mol. Biol. Cell* **2003,** *14*, 384.

80. Ridley, A.J.; Hall, A. *Cell* **1992**, *70*, 389.

81. Ridley, A.J.; Paterson, H.F.; Johnston, C.L.; Diekmann, D.; Hall, A. *Cell* **1992**, *70*, 401.

82. Etienne-Manneville, S.; Hall, A. *Nature* **2002**, *420*, 629.

83. Chrzanowska-Wodnicka, M.; Burridge, K., *J. Cell Biol.* **1996**, *133*, 1403.

84. Kimura, K.; Ito, M.; Amano, M.; Chihara, K.; Fukata, Y.; Nakafuku, M.; Mamamori, B.; Feng, J.H.; Nakano, T.; Okawa, K. *et al. Science* **1996**, *273*, 245.

85. Maekawa, M.; Ishizaki, T.; Boku, S.; Watanabe, N.; Fujita, A.; Iwamatsu, A.; Obinata, T.; Ohashi, K.; Mizuno, K.; Narumiya, S. *Science* **1999**, *285*, 895.

86. Chrzanowska-Wodnicka, M.; and Burridge, K. *J. Cell Biol.* **1996,** *133*, 1403.

87. Tolias, K.F.; Cantley, L.C.; Carpenter, C.L. *J. Biol. Chem.* **1995**, *270*, 17656.

88. Miki, H.; Suetsugu, S.; Takenawa, T. *EMBO J.* **1998**, *17*, 6932.

89. Machesky, L.M.; Insall, R.H. *Curr. Biol.* **1998**, *8*, 1347.

90. Zheng, Y.; Bagrodia, S.; Cerione, R.A. *J. Biol. Chem.* **1994**, *269*, 18727.

91. Kozma, R.; Ahmed, S.; Best, A.; Lim, L. *Mol. Cell. Biol.* **1995**, *15*, 1942.

92. Danilov, Y.; Juliano, R. *Exp. Cell Res.* **1989**, *182*, 186.

93. Ochsenhirt, S. E.; Kokkoli, E.; McCarthy, J. B.; Tirrell, M. *Biomaterials* **2006**, *27*, 3863.

94. Feng, Y.; Mrksich, M. *Biochemistry (N. Y.)* **2004**, *43*, 15811.

95. Cheung, H.; Lau, K.; Lu, T.; Hui, D. *Composites Part B: Engineering* **2007**, *38*, 291.

96. Tang, Z.; Wang, Y.; Podsiadlo, P.; Kotov, N. *Adv Mater.* **2006**, *18*, 3203.

97. Ulman, *Chem. Rev.* **1996**, *96*, 1533.

98. Love, J. C.; Estroff, L. A.; Kriebel, J. K.; Nuzzo, R. G.; Whitesides, G. M. *Chem. Rev.* **2005**, *105*, 1103.

99. Baudrand, D. *Plat. Surf. Finish.* **2000**, *87*, 42.

100. Hou, Z.; Abbott, N. L.; Stroeve, P. *Langmuir* **1998**, *14*, 3287.

101. Dubois, L. H.; Nuzzo, R. G. *Annu. Rev. Phys. Chem.* **1992**, *43*, 437.

102. Laibinis, P. E.; Whitesides, G. M.; Allara, D. L.; Tao, Y. T.; Parikh, A. N.; Nuzzo, R. G. *J. Am. Chem. Soc.* **1991**, *113*, 7152.

103. Love, J. C.; Wolfe, D. B.; Haasch, R.; Chabinyc, M. L.; Paul, K. E.; Whitesides, G. M.; Nuzzo, R. G. *J. Am. Chem. Soc.* **2003**, *125*, 2597.

104. Dubois, L. H.; Zegarski, B. R.; Nuzzo, R. G. *J. Chem. Phys.* **1993**, *98*, 678.

105. Schweizer, M.; Hagenstrom, H.; Kolb, D. M. *Surf. Sci.* **2001**, *490*, L627.

106. Herrero, E.; Buller, L. J.; Abruna, H. D. *Chem. Rev.* **2001**, *101*, 1897.

107. Semaltianos, N. G.; Wilson, E. G. *Thin Solid Films* **2000**, *366*, 111.

108. Skaife, J. J.; Brake, J. M.; Abbott, N. L. *Langmuir* **2001**, *17*, 5448.

109. Wanunu, M.; Vaskevich, A.; Rubinstein, I. *J. Am. Chem. Soc.* **2004**, *126*, 5569.

110. Twardowski, M.; Nuzzo, R. G. *Langmuir* **2002**, *18*, 5529.

111. Semaltianos, N. G.; Wilson, E. G. *Thin Solid Films* **2000**, *366*, 111.

112. Skaife, J. J.; Brake, J. M.; Abbott, N. L. *Langmuir* **2001**, *17*, 5448.

113. Wanunu, M.; Vaskevich, A.; Rubinstein, I. *J. Am. Chem. Soc.* **2004**, *126*, 5569.

114. Twardowski, M.; Nuzzo, R. G. *Langmuir* **2002**, *18*, 5529.

115. Hampy, R. E.; Yost, F. G.; Ganyard, F. P. *J. Vac. Sci. Technol.* **1979**, *16*, 25.

116. Yang, H.; Love, J. C.; Arias, F.; Whitesides, G. M. *Chem. Mater.* **2002**, *14*, 1385.

117. Black, A. J.; Paul, K. E.; Aizenberg, J.; Whitesides, G. M. *J. Am. Chem. Soc.* **1999**, *121*, 8356.

118. Aizenberg, J.; Black, A. J.; Whitesides, G. M. *Nature (London)* **1998**, *394*, 868.

119. Jana, N. R.; Gearheart, L.; Murphy, C. J. *Langmuir* **2001**, *17*, 6782.

120. Henglein, A.; Giersig, M. *J. Phys. Chem. B* **1999**, *103*, 9533.

121. Strong, L.; Whitesides, G. M. *Langmuir* **1988**, *4*, 546.

122. Daniel, M.; Astruc, D. *Chem. Rev.* **2004**, *104*, 293-346.

123. Bain, C. D.; Troughton, E. B.; Tao, Y. T.; Evall, J.; Whitesides, G. M.; Nuzzo, R. G. *J. Am. Chem. Soc.* **1989**, *111*, 321.

124. Yamada, R.; Sakai, H.; Uosaki, K. *Chem. Lett.* **1999**, 667.

125. Schneider, T. W.; Buttry, D. A. *J. Am. Chem. Soc.* **1993**, *115*, 12391.

126. Ishida, T.; Mizutani, W.; Azehara, H.; Sato, F.; Choi, N.; Akiba, U.; Fujihira, M.; Tokumoto, H. *Langmuir* **2001**, *17*, 7459.

127. Peterlinz, K. A.; Georgiadis, R. *Langmuir* **1996**, *12*, 4731.

128. Dannenberger, O.; Wolff, J. J.; Buck, M. *Langmuir* **1998**, *14*, 4679.

129. Kawasaki, M.; Sato, T.; Tanaka, T.; Takao, K. *Langmuir* **2000**, *16*, 1719.

130. Yamada, R.; Wano, H.; Uosaki, K. *Langmuir* **2000**, *16*, 5523.

131. Bensebaa, F.; Voicu, R.; Huron, L.; Ellis, T. H.; Kruus, E. *Langmuir* **1997**, *13*, 5335.

132. Chidsey, C. E. D. *Science* **1991**, *251*, 919.

133. Love, J. C.; Wolfe, D. B.; Haasch, R.; Chabinyc, M. L.; Paul, K. E.; Whitesides, G. M.; Nuzzo, R. G. *J. Am. Chem. Soc.* **2003**, *125*, 2597.

134. Bain, C. D.; Whitesides, G. M. *J. Am. Chem. Soc.* **1988**, *110*, 6560.

135. Laibinis, P. E.; Fox, M. A.; Folkers, J. P.; Whitesides, G. M. *Langmuir* **1991**, *7*, 3167.

136. Heister, K.; Allara, D. L.; Bahnck, K.; Frey, S.; Zharnikov, M.; Grunze, M. *Langmuir* **1999**, *15*, 5440.

Azehara, H.; Yoshimoto, S.; Hokari, H.; Akiba, U.; Taniguchi, I.; Fujihira, M. *J. Electroanal. Chem.* **1999**, *473*, 68.

137. Porter, M. D.; Bright, T. B.; Allara, D. L.; Chidsey, C. E. D. *J. Am. Chem. Soc.* **1987**, *109*, 3559.

138. Nuzzo, R. G.; Zegarski, B. R.; Dubois, L. H. *J. Am. Chem. Soc.* **1987**, *109*, 733.

139. Fischer, D.; Curioni, A.; Andreoni, W. *Langmuir* **2003**, *19*, 3567.

140. Lavrich, D. J.; Wetterer, S. M.; Bernasek, S. L.; Scoles, G. *J. Phys. Chem. B* **1998**, *102*, 3456.

141. Schlenoff, J. B.; Li, M.; Ly, H. *J. Am. Chem. Soc.* **1995**, *117*, 12528.

142. Kluth, G. J.; Carraro, C.; Maboudian, R. *Phys. Rev. B: Condens. Matter* **1999**, *59*, R10449.

143. Trevor, J. L.; Lykke, K. R.; Pellin, M. J.; Hanley, L. *Langmuir* **1998**, *14*, 1664.

144. Dubois, L. H.; Zegarski, B. R.; Nuzzo, R. G. *J. Chem. Phys.* **1993**, *98*, 678.

145. Schreiber, F. *Prog. Surf. Sci.* **2000**, *65*, 151.

146. Poirier, G. E. *Chem. Rev.* **1997**, *97*, 1117.

147. Poirier, G. E. *Langmuir* **1997**, *13*, 2019.

148. Camillone, N., III; Chidsey, C. E. D.; Liu, G. Y.; Scoles, G. *J. Chem. Phys.* **1993**, *98*, 3503.

149. Fischer, D.; Curioni, A.; Andreoni, W. *Langmuir* **2003**, *19*, 3567.

150. Andreoni, W.; Curioni, A.; Gronbeck, H. *Int. J. Quantum Chem.* **2000**, *80*, 598.

151. Zharnikov, M.; Grunze, M. *J. Phys.: Condens. Matter* **2001**, *13*, 11333.

152. Frey, S.; Stadler, V.; Heister, K.; Eck, W.; Zharnikov, M.; Grunze, M.; Zeysing, B.; Terfort, A. *Langmuir* **2001**, *17*, 2408.

153. Geyer, W.; Stadler, V.; Eck, W.; Zharnikov, M.; Golzhauser, A.; Grunze, M. *Appl. Phys. Lett.* **1999**, *75*, 2401.

154. Fuxen, C.; Azzam, W.; Arnold, R.; Witte, G.; Terfort, A.; Woell, C. *Langmuir* **2001**, *17*, 3689.

155. Stapleton, J. J.; Harder, P.; Daniel, T. A.; Reinard, M. D.; Yao, Y.; Price, D. W.; Tour, J. M.; Allara, D. L. *Langmuir* **2003**, *19*, 8245.

156. Park, B.; Chandross, M.; Stevens, M. J.; Grest, G. S. *Langmuir* **2003**, *19*, 9239.

157. Dubois, L. H.; Nuzzo, R. G. *Annu. Rev. Phys. Chem.* **1992**, *43*, 437.

158. Chen, S. H.; Frank, C. W. *ACS Symp. Ser.* **1990**, *447*, 160.

159. Sun, L.; Crooks, R. M. *Langmuir* **1993**, *9*, 1951

160. O'Dwyer, C.; Gay, G.; de Lesegno, B. V.; Weiner, J. *Langmuir* **2004**, *20*, 8172.

161. Yang, G.; Liu, G.-Y. *J. Phys. Chem. B* **2003**, *107*, 8746.

162. Rai, B.; Sathish, P.; Malhotra, C. P.; Pradip; Ayappa, K. G. *Langmuir* **2004**, *20*, 3138.

163. Shepherd, J. L.; Kell, A.; Chung, E.; Sinclar, C. W.; Workentin, M. S.; Bizzotto, D. *J. Am. Chem. Soc.* **2004**, *126*, 8329.

164. Quinn, B. M.; Kontturi, K. *J. Am. Chem. Soc.* **2004**, *126*, 7168.

165. Collard, D. M.; Fox, M. A. *Langmuir* **1991**, *7*, 1192.

166. Yang, G.; Amro, N. A.; Starkewolfe, Z. B.; Liu, G.-y. *Langmuir* **2004**, *20*, 3995.

167. Chidsey, C. E. D.; Bertozzi, C. R.; Putvinski, T. M.; Mujsce, A. M. *J. Am. Chem. Soc.* **1990**, *112*, 4301.

168. Huang, J.; Hemminger, J. C. *J. Am. Chem. Soc.* **1993**, *115*, 3342.

169. Zhang, Y.; Terrill, R. H.; Bohn, P. W. *Chem. Mater.* **1999**, *11*, 2191.

170. Prime, K. L.; Whitesides, G. M. *Science* **1991**, *252*, 1164.

171. Martins, M. C. L.; Ratner, B. D.; Barbosa, M. A. *J. Biomed. Mater. Res. A* **2003**, *67A*, 158.

172. Zwahlen, M.; Herrwerth, S.; Eck, W.; Grunze, M.; Haehner, G. *Langmuir* **2003**, *19*, 9305.

173. Kreuzer, H. J.; Wang, R. L. C.; Grunze, M. *J. Am. Chem. Soc.* **2003**, *125*, 8384.

174. Kim, H. I.; Kushmerick, J. G.; Houston, J. E.; Bunker, B. C. *Langmuir* **2003**, *19*, 9271.

175. Jiang, X.; Bruzewicz, D. A.; Thant, M. M.; Whitesides, G. M. *Anal. Chem.* **2004**, *76*, 6116.

176. Ostuni, E.; Chapman, R. G.; Holmlin, R. E.; Takayama, S.; Whitesides, G. M. *Langmuir* **2001**, *17*, 5605.

177. Fick, J.; Steitz, R.; Leiner, V.; Tokumitsu, S.; Himmelhaus, M.; Grunze, M. *Langmuir* **2004**, *20*, 3848

178. Vanderah, D. J.; Arsenault, J.; La, H.; Gates, R. S.; Silin, V.; Meuse, C. W.; Valincius, G. *Langmuir* **2003**, *19*, 3752.

179. Engelkes, V. B.; Beebe, J. M.; Frisbie, C. D. *J. Am. Chem. Soc.* **2004**, *126*, 14287.

180. Colorado, R., Jr.; Lee, T. R. *Langmuir* **2003**, *19*, 3288. Pemberton, J. E. *Langmuir* **2003**, *19*, 6422.

181. Leggett, G. J. *Anal. Chim. Acta* **2003**, *479*, 17.

182. Houston, J. E.; Kim, H. I. *Acc. Chem. Res.* **2002**, *35*, 547.

183. Jennings, G. K.; Yong, T.-H.; Munro, J. C.; Laibinis, P. E. *J. Am. Chem. Soc.* **2003**, *125*, 2950.

184. Houseman, B. T.; Gawalt, E. S.; Mrksich, M. *Langmuir* **2003**, *19*, 1522.

185. Smith, E. A.; Wanat, M. J.; Cheng, Y.; Barreira, S. V. P.; Frutos, A. G.; Corn, R. M. *Langmuir* **2001**, *17*, 2502.

186. Lee, J. K.; Lee, K.-B.; Kim, D. J.; Choi, I. S. *Langmuir* **2003**, *19*, 8141.

187. Kolb, H. C.; Finn, M. G.; Sharpless, K. B. *Angew. Chem., Int. Ed. Engl.* **2001**, *40*, 2004.

188. Saxon, E.; Bertozzi, C. R. *Annu. Rev. Cell Dev. Biol.* **2001**, *17*, 1.

189. Yan, L.; Marzolin, C.; Terfort, A.; Whitesides, G. M. *Langmuir* **1997**, *13*, 6704.

190. Lahiri, J.; Isaacs, L.; Tien, J.; Whitesides, G. M. *Anal. Chem.* **1999**, *71*, 777.

191. Yousaf, M. N.; Mrksich, M. *J. Am. Chem. Soc.* **1999**, *121*, 4286.

192. Chan, E. W. L.; Yousaf, M. N. *J. Am. Chem. Soc.* **2006**, *128*, 15542.

193. Chan, E. W. L.; Yousaf, M. N. *ChemPhysChem* **2008**, *3*, 746.

194. Creager, S. E.; Clarke, J. *Langmuir* **1994**, *10*, 3675.

195. Schwendel, D.; Hayashi, T.; Dahint, R.; Pertsin, A.; Grunze, M.; Steitz, R.; Schreiber, F. *Langmuir* **2003**, *19*, 2284

196. Schoenherr, H.; Feng, C.; Shovsky, A. *Langmuir* **2003**, *19*, 10843

197. Vaidya, B.; Chen, J.; Porter, M. D.; Angelici, R. J. *Langmuir* **2001**, *17*, 6569.

198. Houseman, B. T.; Mrksich, M. *Angew. Chem., Int. Ed. Engl.* **1999**, *38*, 782.

199. Jones, D. M.; Brown, A. A.; Huck, W. T. S. *Langmuir* **2002**, *18*, 1265.

200. Kwon, Y.; Mrksich, M. *J. Am. Chem. Soc.* **2002**, *124*, 806.

201. Lahiri, J.; Isaacs, L.; Tien, J.; Whitesides, G. M. *Anal. Chem.* **1999**, *71*, 777.

202. Chechik, V.; Stirling, C. J. M. *Langmuir* **1998**, *14*, 99.

203. Ko, B. S.; Babcock, B.; Jennings, G. K.; Tilden, S. G.; Peterson, R. R.; Cliffel, D.; Greenbaum, E. *Langmuir* **2004**, *20*, 4033

204. Creager, S. E.; Rowe, G. K. *Langmuir* **1993**, *9*, 2330.

205. Jenkins, A. T. A.; Bushby, R. J.; Evans, S. D.; Knoll, W.; Offenhaeusser, A.; Ogier, S. D. *Langmuir* **2002**, *18*, 3176.

206. Twardowski, M.; Nuzzo, R. G. *Langmuir* **2003**, *19*, 9781.

207. Jeoung, E.; Carroll, J. B.; Rotello, V. M. *Chem. Commun.* **2002**, 1510.

208. Xia, Y.; Whitesides, G. M. *Angew. Chem., Int. Ed. Engl.* **1998**, *37*, 550.

209. Choi, K. M.; Rogers, J. A. *J. Am. Chem. Soc.* **2003**, *125*, 4060.

210. Clarson, S. J.; Semlyen, J. A. *Siloxane polymers*; Prentice Hall: Englewood Cliffs, NJ, 1993.

211. Gates, B. D.; Xu, Q.; Love, J. C.; Wolfe, D. B.; Whitesides, G. M. *Annu. Rev. Mater. Res.* **2004**.

212. Guo, Q.; Teng, X.; Yang, H. *Nano Lett.* **2004**, *4*, 1657.

213. Trimbach, D.; Feldman, K.; Spencer, N. D.; Broer, D. J.; Bastiaansen, C. W. M. *Langmuir* **2003**, *19*, 10957.

214. Delamarche, E.; Schmid, H.; Bietsch, A.; Larsen, N. B.; Rothuizen, H.; Michel, B.; Biebuyck, H. *J. Phys. Chem. B* **1998**, *102*, 3324.

215. Bohm, I.; Lampert, A.; Buck, M.; Eisert, F.; Grunze, M. *Appl. Surf. Sci.* **1999**, *141*, 237.

216. Losic, D.; Shapter, J. G.; Gooding, J. J. *Electrochem. Commun.* **2001**, *3*, 722.

217. Trimbach, D.; Feldman, K.; Spencer, N. D.; Broer, D. J.; Bastiaansen, C. W. M. *Langmuir* **2003**, *19*, 10957.

218. Larsen, N. B.; Biebuyck, H.; Delamarche, E.; Michel, B. *J. Am. Chem. Soc.* **1997**, *119*, 3017.

219. Donzel, C.; Geissler, M.; Bernard, A.; Wolf, H.; Michel, B.; Hilborn, J.; Delamarche, E. *Adv Mater* **2001**, *13*, 1164.

220. Michel, B.; Bernard, A.; Bietsch, A.; Delamarche, E.; Geissler, M.; Juncker, D.; Kind, H.; Renault, J. P.; Rothuizen, H.; Schmid, H.; Schmidt-Winkel, P.; Stutz, R.; Wolf, H. *IBM J. Res. Dev.* **2001**, *45*, 697

221. Love, J. C.; Wolfe, D. B.; Chabinyc, M. L.; Paul, K. E.; Whitesides, G. M. *J. Am. Chem. Soc.* **2002**, *124*, 1576.

222. Dammel, R. R.; Houlihan, F. M.; Sakamuri, R.; Rentkiewicz, D.; Romano, A. *Polym. Mater. Sci. Eng.* **2004**, *90*, 283

223. Friebel, S.; Aizenberg, J.; Abad, S.; Wiltzius, P. *Appl. Phys. Lett.* **2000**, *77*, 2406.

224. Shadnam, M. R.; Kirkwood, S. E.; Fedosejevs, R.; Amirfazli, A. *Langmuir* **2004**, *20*, 2667.

225. Dilmore, W.; Yousaf, M.N.; Mrksich, M. *Langmuir* **2004**, *20*, 7223-7231

226. Chan, E. W. L.; Yousaf, M. N. *Molecular BioSystems* **2008**, *4*, 746.

227. Golzhauser, A.; Geyer, W.; Stadler, V.; Eck, W.; Grunze, M.; Edinger, K.; Weimann, T.; Hinze, P. *J. Vac. Sci. Technol., B* **2000**, *18*, 3414.

228. Kaltenpoth, G.; Volkel, B.; Nottbohm, C. T.; Golzhauser, A.; Buck, M. *J. Vac. Sci. Technol., B* **2002**, *20*, 2734.

229. Johnson, K. S.; Thywissen, J. H.; Dekker, N. H.; Berggren, K. K.; Chu, A. P.; Younkin, R.; Prentiss, M. *Science* **1998**, *280*, 1583.

230. Salaita, K.; Wang, Y.; Mirkin, C. A. *Nat Nano* **2007**, *2*, 145-155.

231. Piner, R. D.; Zhu, J.; Xu, F.; Hong, S.; Mirkin, C. A. *Science* **1999**, *283*, 661-663.

232. Salaita, K.; Wang, Y.; Fragala, J.; Vega, R. A.; Liu, C.; Mirkin, C. A. *Ange. Chem. Internat'l Ed.* **2006**, *45*, 7220.

233. Hoover, D. K.; Lee, E.; Chan, E. W. L.; Yousaf, M. N. *ChemBioChem* **2007**, *8*, 1920.

234. Huo, F.; Zheng, G.; Liao, X.; Giam, L. R.; Chai, J.; Chen, X.; Shim, W.; Mirkin, C. A. *Nat Nano* **2010**, *8*, 1322.

235. Chaudhury, M. K.; Whitesides, G. M. *Science (Washington, D.C.)* **1992**, *256*, 1539.

236. Morgenthaler, S.; Lee, S.; Zuercher, S.; Spencer, N. D. *Langmuir* **2003**, *19*, 10459.

237. Liedberg, B.; Wirde, M.; Tao, Y.-T.; Tengvall, P.; Gelius, U. *Langmuir* **1997**, *13*, 5329.

238. Wang, Q.; Bohn, P. W. *J. Phys. Chem. B* **2003**, *107*, 12578.

239. Geissler, M.; Schmid, H.; Bietsch, A.; Michel, B.; Delamarche, E. *Langmuir* **2002**, *18*, 2374

240. Bard, A. J.; Abruna, H. D.; Chidsey, C. E.; Faulkner, L. R.; Feldberg, S. W.; Itaya, K.; Majda, M.; Melroy, O.; Murray, R. W.; et al. *J. Phys. Chem.* **1993**, *97*, 7147.

241. Chidsey, C. E. D. *Science* **1991**, *251*, 919.

242. Chidsey, C. E. D.; Bertozzi, C. R.; Putvinski, T. M.; Mujsce, A. M. *J. Am. Chem. Soc.* **1990**, *112*, 4301.

243. Weiner, S.; Addadi, L. *J. Mater. Chem.* **1997**, *7*, 689.

244. Aizenberg, J.; Black, A. J.; Whitesides, G. M. *J. Am. Chem. Soc.* **1999**, *121*, 4500.

245. Chidsey, C. E. D.; Murray, R. W. *Science* **1986**, *231*, 25.

246. Finklea, H. O. *Electroanal. Chem.* **1996**, *19*, 109.

247. Smalley, J. F.; Feldberg, S. W.; Chidsey, C. E. D.; Linford, M. R.; Newton, M. D.; Liu, Y.-P. *J. Phys.*

Chem. **1995**, *99*, 13141

248. Haddox, R. M.; Finklea, H. O. *J. Phys. Chem. B* **2004**, *108*, 1694.

249. Cannes, C.; Kanoufi, F.; Bard, A. J. *Langmuir* **2002**, *18*, 8134.

250. Sumner, J. J.; Creager, S. E. *J. Phys. Chem. B* **2001**, *105*, 8739.

251. Chen, C. S.; Mrksich, M.; Huang, S.; Whitesides, G. M.; Ingber, D. E. *Science* **1997**, 276, 1425.

252. Li, Y.; Yuan, B.; Ji, H.; Han, D.; Chen, S.; Tian, F.; Jiang, X. *Angew. Chem. Int. Ed.* **2007**, 46, 1094.

253. James, J.; Goluch, E.D.; Hu, H.; Liu, C. M. Mrksich, *Cell. Motil. Cyctoskeleton* **2008**, *65*, 841.

254. Xia, N.; Thodeti, C.; Hunt, T.; Xu, Q.; Ho, M.; Whitesides, G.M. *FASEB J.* **2008**, *22*, 1649.

255. Hodgson, L.; Chan, E.W.L.; Hahn, K.; Yousaf, M.N. *J. Am. Chem. Soc.* **2007**, *129*, 9264.

256. Luo, W.; Jones, S.; Yousaf, M.N. *Langmuir* **2008**, *24*, 12129.

257. Lamb, B.M.; Westcott, N.P.; Yousaf, M.N. *ChemBioChem* **2008**, *9*, 2628.

Chapter II: Electrochemical Pattering of SAMs with Microfluidics
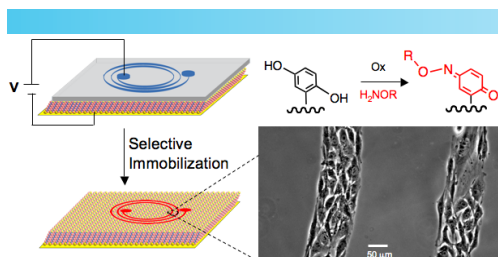
2.1 Introduction

The ability to position biological molecules on a variety of materials with spatial control has revolutionized a range of biotechnologies and has proved important for investigating fundamental studies of cell adhesion, migration and growth.[1-2] Several methods and strategies have been used to deliver or pattern molecules to the surfaces of materials including microcontact printing[3], microfluidics[4-6], photoactivation[7] and several scanning probe microscopies[8-10] for a variety of applications. For more demanding cell biological studies the most important factor is to position ligands onto an otherwise inert surface where the only net contact between material and cell is a ligand-receptor biospecific interaction. Due to the stringent requirements for generating relevant data for biological based materials tailored with ligands there have been very few convergent patterning methods, and most require specialized instrumentation[11,12] and/or multi-step synthesis[13] to produce the immobilization/capture molecules that are not accessible to the general research community.

One of the most promising strategies to pattern biomolecules on a surface is the combination of microfluidics to position molecules via flow with complementary surface chemistry to immobilize soluble molecules. This strategy has been used to pattern proteins[14] and ligands[15]

on surfaces, and in combination with electrochemistry to selectively desorb self-assembled monolayers (SAMs) of tetra (ethylene glycol) alkane thiols to pattern proteins and subsequently adhere cells.[16] This latter strategy is able to pattern cells and co-cultures, but is severely limited in its potential applications because there is no molecular level control of ligand immobilization. These methodologies would have much broader utility if they possessed the features of a general chemoselective coupling strategy to immobilize a variety of ligands with precise spatial and temporal control and an independent, real-time quantitative read-out to determine the ligand density on a molecularly well defined surface.

Herein, we show a straightforward and flexible synergistic approach that combines microfluidics, electrochemistry and a general immobilization strategy to selectively activate regions of a substrate for precise immobilization of ligands and cells in patterns for a variety of cell based assays, cell migration and cell adhesion studies. We have previously developed a general immobilization strategy and shown that hydroquinone alkanethiol SAMs can be reversibly oxidized to the quinone form, which can then chemoselectively react with soluble oxyamine tethered ligands for surface immobilization.[14] Cyclic voltammetry can be used to activate the surface, quantitatively characterize it, and distinguish the un-reactive hydroquinone-quinone redox pair and the immobilized conjugate oxime because of the distinct diagnostic peaks of each redox couple.

2.2 Experimental Section

2.2.1 Synthesis of Alkanethiols. The undecane thiols terminated with hydroquinone, tetra(ethylene glycol), and hydroquinone tera(ethylene glycol) were synthesized as reported previously.[14,15]

2.2.2 Solid Phase Peptide Synthesis and Synthesis of Rhodamine Oxime. Peptide synthesis and Rhodamine oxime was sysnthesized as previously reported. [14]

2.2.3 Microfabrication. The microchips were fabricated using soft lithography.[16] Patterns were achieved using masks drawn in Adobe Illustrator CS2 and photoplotted by the International Photoplot Store onto mylar sheets. SU-8 50 (Microchem) was patterned using the manufacturer's directions to obtain 100 μm channel depth using these masks. Slygard 184(Dow Corning) was cast onto the mold in a 1:10 curing agent:elastomer w/w. The prepolymer was degassed for 15 minutes and then poured over the mold. The prepolymer was cured for 1 hr at 75 °C. The PDMS was removed from the master and access holes were punched into the PDMS to allow fluid flow.

2.2.4 Preperation of Monolayers. Gold substrates were prepared by electron beam deposition of titanium (6 nm) and gold (24 nm) on 24 mm x 100 mm glass microscope slides. The slides were cut into 1 x 2 cm pieces and washed with absolute ethanol. The slides were then immersed in an ethanolic solution containing the proper ration of alkane thiols for 12 hr. The solutions were 1:1 tetra(ethylene glycol): hydroquinone undecanethiol for the electrochemical characterization of the surfaces studies, and 1:1 tetra(ethylene glycol): hydroquinone tetra(ethylene glycol) undecanethiol for the fluorescence data., and 99:1 tetra(ethylene glycol): hydroquinone tetra(ethylene glycol) undecanethiol for the peptide immobilization and cell adhesion patterning studies. After the slides were removed from solution, they were rinsed with ethanol and dried before use. All slides were used within a week of fabrication to minimize oxidation of the surface.

2.2.5 Electrochemistry. All electrochemical measurements were made using the Bioanalytical Systems Epsilon potentiostat. An Ag/AgCl electrode served as the reference, the gold monolayer acted as the working electrode, and a Pt wire served as the counter electrode. The

electrolyte was 1 M HClO$_4$ and the scan rate was 100 mV/s. All measurements were made in a standard electrochemical cell.

2.2.6 Selective Ligand Immobilization. A PDMS microchip was cleaned with ethanol and dried. It was then sealed reversibly to a SAM containing a mixture of hydroquinone and ethylene glycol alkanethiol. Perchloric acid at 1M was driven by vacuum into the channels. The gold was grounded to a Mastech HY1803D power supply and the electrolyte was brought to 800 mV for 8s to oxidize the surface where the electrolyte solution came into contact with the gold. The microchip was then removed from the surface and the SAM surface and microchip were cleaned with ethanol and dried. A solution of the desired oxyamine was added to the entire SAM surface to selectively immobilize the ligand to the activated regions.

2.2.7 Microscopy of Surface Immobilized Rhodamine and Cells. Scotch tape (3M) was adhered to the monolayer. The resulting substrate was then cured at 85 °C for 20 min. The tape was peeled from the substrate, resulting in transfer of the monolayer from the gold substrate to the tape and visualized. Fluorescent and brightfield microscopy was performed using a Nikon TE2000E inverted microscope. Image acquisition and processing was done using Metamorph software.

2.2.8 Cell Culture. Swiss Albino 3T3 fibroblasts (ATCC) were cultured in Dulbecco's Modified Eagle Medium (Gibco) containing 10% calf bovine serum and 1% penicillin/streptomycin. Cells were removed with a solution of 0.05% trypsin in 0.53 mM EDTA and re-suspended in serum-free medium (100,000 cells/mL). The cells were seeded to surfaces for 2 h. After 2 h, the serum containing media was added for cell growth.

2.3 Results and Discussion

2.3.1 For the electrochemical surface characterization and cell biological studies we generated mixed SAMs surfaces of hydroquinone and tetra(ethylene glycol) undecane thiol.

The hydroquinone is the chemoselective electroactive component and the ethylene glycol groups are to resist non-specific protein adsorption[9], a critical requirement for ligand mediated cell behavior studies. In order to immobilize ligands in patterns, we used a combination of microfluidics and electrochemistry to selectively electro-activate regions of the surface (Figure 1). A microchip fabricated from PDMS using soft lithography was reversibly sealed to the SAM by application of mild force. A solution of 1 M perchloric acid was flowed into the channels with a vacuum and served as the electrolyte solution for selective oxidation of the hydroquinone groups to quinone groups. The conducting gold SAM surface was grounded to a power supply (Mastech HY1803D) and the electrolyte solution was brought to 800 mV for 8s via an applied potential to oxidize the hydroquinone to quinone within the microfluidic channels. This strategy only activates the region of the surface (hydroquinone to quinone) that has access to electrolyte solution controlled by the microfabricated microfluidic channels. These activated areas can be subsequently reacted with oxyamine-tethered groups to generate specific ligand immobilization patterns. Unlike other strategies that require ligand immobilization to be flowed through the microchannels, once the surface is activated an oxyamine ligand can be added to the entire surface, but only reacts where channels had allowed solution to flow. Therefore, the first ligand immobilization pattern on the surface is directed by the channel design on the microchip. A second and subsequent ligand immobilizations can be performed by selectively activating other regions of the surface via additional microfluidic patterning activation or by activating the entire non-immobilized surface for further ligand patterning. Through the straightforward use of electrochemistry, soft lithography, and the quinone electroactive SAM system, multiple different ligand mediated patterns can be generated for a variety of biological assays and studies.
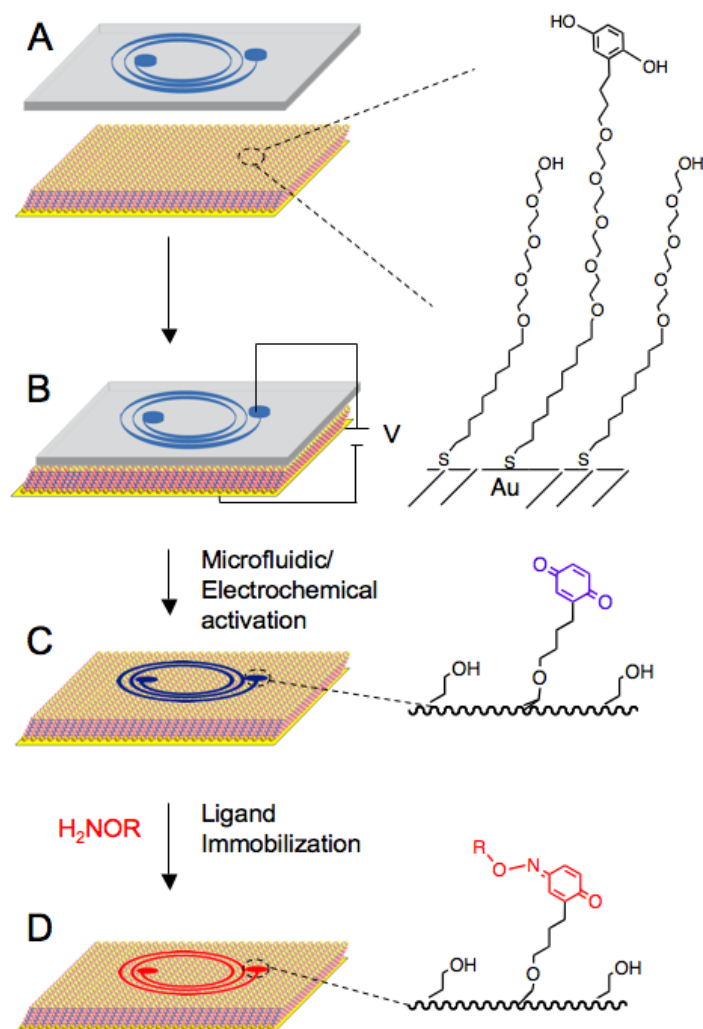
Figure 2.1. Synergistic strategy to selectively activate a SAM surface using microfluidic networks and electrochemistry. A) First, a PDMS microchip is reversibly sealed to a mixed hydroquinone and ethylene(glycol) terminated alkanethiol SAM surface. B) Electrolyte solution is flowed into the channels and 800 mV is applied to oxidize the hydroquinone to the reactive quinone. C) The surface is selectively activated only on regions where electrolyte contacts the surface. D) After removal of the microfluidic cassette, an oxyamine terminated ligand is added to the entire surface and only reacts chemoselectively to the surface where hydroquinone has been oxidized to quinone resulting in patterned and immobilized ligands, which have the same features as the microfluidic network that controlled the regions of activation.

2.3.2 Electrochemical Characterization A major advantage of an electroactive system is its ability to be reversibly activated/deactivated and to be characterized quantitatively by electrochemistry. The hydroquinone-quinone is redox active and after oxyamine-ligand conjugation to the quinone form the corresponding oxime product has a distinct diagnostic redox couple that can be monitored to determine the yield and density of ligands immobilized

to the surface. The surfaces used for the electrochemical studies to demonstrate selective activation via microchannels were 1:1 hydroquinone: tetra (ethylene glycol) undecane thiol. Figure 2 shows the surface undergoing a series of activations via microfluidic and electrochemical application and characterized by cyclic voltammetry (CV) of the entire SAM surface. The initial CV was taken of the entire SAM surface before any activation and shows the only redox couple present on the surface is the hydroquinone to quinone interconversion at 660 mV and -25 mV (Figure 2A). When the microfluidic stamp was applied to the hydroquinone surface, with the addition of 1M perchloric acid through the channels and electrochemical activation, the surface was partially activated. Only the microchannel areas were converted to quinone, which were reacted with a soluble oxyamine-acetic acid. After removal of the PDMS stamp, cyclic voltammetry of the entire surface (Figure 2B) shows partial conversion of the hydroquinone surface. In the unactivated regions of the surface, the hydroquinone/quinone redox couple was present. In the activated regions, the redox active oxime conjugate was present. This resulted in 3 distinct peaks in the cyclic voltammogram of the surface. The single broad oxidation peak (650 mV) is composed of both the oxime product and the hydroquinone species. The two peaks are fairly close in peak potential, and therefore difficult to resolve the individual oxidation peaks. However, for the reduction wave, two peaks were clearly observed. The peak at 210 mV was for the oxime reduction and the peak at -20 mV was for the quinone reduction. Our microfluidic channel pattern had an area of 0.5 cm^2 to oxidize (activate) half of a 1 cm^2 SAM surface and the ratio of the integrated two reduction peaks is consistent with the surface coverage. The two peaks have approximately equal peak heights (peak current for reduction of quinone was -6.95 µA and the peak current for the oxime was -6.57 µA) and integrated areas (peak area for the reduction of quinone was 14.21 µC and the peak area for the oxime was 13.41 µC). From the peak area data, our 1 cm^2 surfaces have 5 x 10^{13} electroactive

molecules, the unreacted portion consists of 2.57 x 10^{13} molecules and the oxime has 2.43 x 10^{13} molecules demonstrating the precise density of electroactive molecules on the surface can be determined. To show the surface is dynamic and capable of multiple ligand immobilization and therefore multiple patterns, the surfaces in Figure 2B were oxidized and the remaining quinone on the surface (outside the microchannel regions) were reacted with rhodamine-oxyamine to convert the entire surface to the oxime conjugate as shown by cyclic voltammetry (Figure 2C). The oxidation peak shifted to 600 mV and the reduction peak shifted to 250 mV to reflect complete conversion to the electroactive oxime conjugate surface. It should be noted that this surface has two different ligands (rhodamine-oxyamine and oxyamine acetic acid) immobilized in distinct patterns with quantitative precision characterized by electrochemistry that is independent of the identity of the ligand. This allows for the straightforward immobilization and characterization of a wide variety of ligands with spatial control on a surface.

2.3.3 Ligand Pattern Generation In order to demonstrate the fidelity of the microfluidic/electrochemical strategy we further characterized the surface by visualizing the patterns generated in Figure 2B since one of the two ligands (rhodamine oxyamine) used is a fluorescent ligand (30 mM added and allowed to react with the selectively activated surface for 1 h). In addition to the electrochemical characterization of the surface a fluorescence image shows rhodamine-oxyamine only bound to the activated microchannel regions (Figure 3). The mask consisted of a spiral pattern with channels of 110 µm in width. The observed fluorescent micrographs were also measured to be 110 µm in the pattern created by the rhodamine oxyamine as measured by image processing software. This shows the surface was electro-activated and patterned by the electrolyte containing microchannels with no appreciable broadening of the features. This result also demonstrates that the fidelity of the soft

lithography generated patterns to the final surface immobilized ligand patterns is easily controlled and implemented for a variety of surface applications.
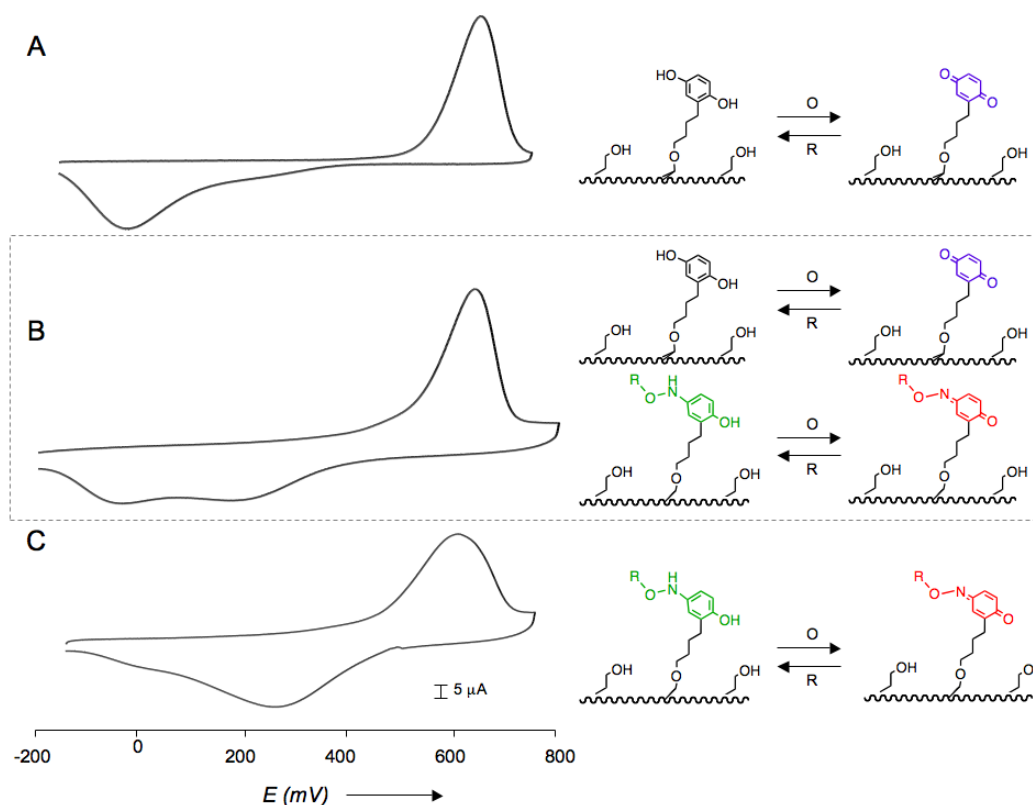
Figure 2.2. Electrochemical characterization of a 1:1 tetra(ethylene glycol):hydroquinone undecane thiol SAM surface undergoing microfluidic and electrochemical activation. The 3 cyclic voltamagrams were taken at different stages of the microfluidic activation. A) The entire SAM surface before activation. The hydroquinone on the surface undergoes a reversible redox couple at 660 mV and -25 mV. B) Selective microfluidic/electrochemical activation and subsequent oxyamine coupling to the surface. The voltammogram shows three peaks. The oxidation peak consists of both the hydroquinone and oxime peaks. It is broad and shifted slightly to 650 mV due to both species. There are two reduction peaks, one for the hydroquinone redox couple at -20 mV and other for the oxime hydroquinone couple at 210 mV. C) The remaining surface was then oxidized and rhodamine oxyamine was immobilized. The redox couple consists of only two peaks and has shifted completely from the starting surface to 600 mV and 250 mV indicating only the product oxime conjugate remains on the surface.
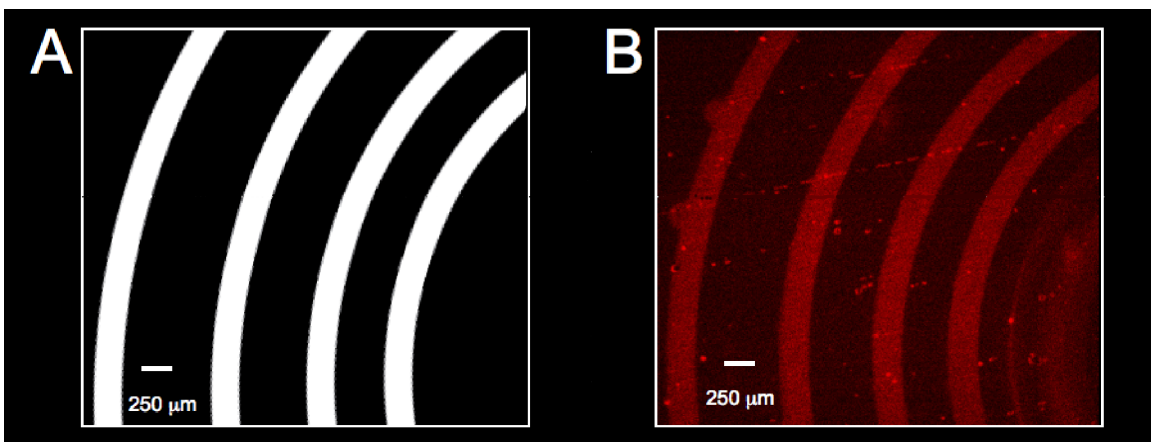
Figure 2.3. A comparison of the original mask design for the microfluidic channel and the final ligand immobilization surface pattern to demonstrate mask fidelity. A) A section of the mask design used to create the PDMS microfluidic channel. B) A fluorescent image of the surface after microfluidic/electrochemical activation and subsequent rhodamine immobilizaiton. The resolution of the fluorescent pattern is approximately the same as the microfluidic channel demonstrating no broadening of the pattern due to electrolyte leakage from the microchannel.

2.3.4 Cell Pattern Generation To extend this strategy to the level of biospecific patterning of cells, we generated surface patterns via the microfluidic/electrochemical strategy and immobilized adhesive peptide ligands to select regions. Cell surface integrin receptors are well known to bind specifically to RGD containing peptides for biospecific ligand mediated cell adhesion.[17] We used a 1:99 ratio of hydroquinone: tetra (ethylene glycol) alkanethiols in order to generate inert surfaces and activated select regions using the electrochemical and microfluidic system described. The low oxidative potential does not damage the inert properties of the surface and only oxidizes the hydroquinone to the reactive quinone within the channels for subsequent rapid RGD-oxyamine (10 mM, 2 hr to the entire surface) immobilization in patterns. In order to visualize specific cell adhesion, cells (Swiss 3T3 fibroblasts) in serum-free media at 100,000 cells/mL were added to the RGD patterned substrate. Figure 4 shows a typical cell pattern generated by the electrochemical/microfluidic immobilization strategy. As a control to show the biospecific nature of the cell adhesion, when a scrambled RDG oxyamine peptide was immobilized no cells attached to the surface. These cell adhesion studies show the ease of the strategy to immobilize biospecific ligands in patterns

50

and may be extended to generate co-culture and dynamic surfaces for cell migration studies in the future.
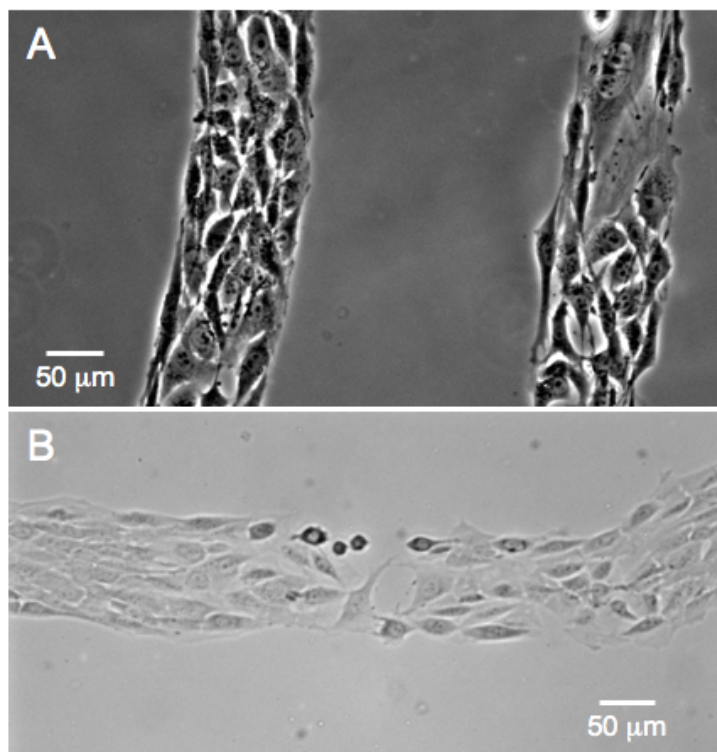
Figure 2.4. A micrograph of Swiss albino 3T3 fibroblasts attached biospecifically to a microfluidic/electrochemical activated surface presenting RGD immobilized ligands. A) A curved cell pattern. B) A linear cell pattern.

2.4 Conclusion

In this chapter, a straightforward and flexible method to pattern a variety of ligands and cells using a combination of electroactive SAM surfaces and microfluidics was developed. The spatial control over the surface was maintained with the PDMS microchip, which limited the electrolyte flow within the channels. The regions on the surface under the channels underwent activation by oxidation of hydroquinone to quinone. Once the surface is activated, an oxyamine containing ligand was bound selectively to the activated portions of the surface. The entire process was simultaneously activated and characterized quantitatively with electrochemistry. The synergistic approach is straightforward and is amenable to immobilizing a wide variety of

ligands to a surface for complex cell adhesion, co-culture and migration studies. The dynamic nature of the hydroquinone-quinone redox couple allows for the generation of a simple surface that can be easily manipulated to generate complex patterns of ligands for a variety of applications without the need for intricate photo-activation steps, serial microfabrication or the requirement of synthetically difficult molecules essential for other strategies. Unlike other electrochemical strategies, this methodology does not pattern cells by destroying the integrity of the surface for non-specific cell binding, but allows for the precise control of surface density for a variety of ligands and is compatible with biospecific cell assays for the generation of a new class of cell based biotechnologies[18,19] and for fundamental studies of cell behavior.[20] The ability to combine microfluidics and potentially nanofluidics to position ligands and electrochemistry to activate selective regions provides new opportunities for patterning sequential series of molecules on a variety of materials for applications ranging from cell biology to molecular electronics.

2.5 References

1. Chen, C. S.; Mrksich, M.; Huang, S.; Whitesides, G. M.; Ingber, D. E. *Science* **1997**, 276, 1425-1428.

2. Yousaf, M. N.; Houseman, B. T.; Mrksich, M. *Angew. Chem. Int. Ed.* **2001**, 40, 1093-1096.

3. Falconnet, D.; Csucs, G.; Grandin, M.; Textor, M. *Biomaterials.* **2006**, 27, 3044-3063.

4. Mrksich, M.; Dike, L. E.; Tien, J.; Ingber, D. E.; Whitesides, G. M. *Exp. Cell Res*. **1997**, 235, 305-313.

5. Chiu, D. T.; Jeon, J. L.; Huang, S.; Kane, R. S.; Wargo, C. J.; Choi, I. S.; Ingber, D. E.; Whitesides, G. M. *Proc. Nat. Acad. Sci.* **2000**, 97, 2408-2413.

6. Delamarche, E.; Bernard, A.; Schmid, H.; Bruno, M.; Biebuyck, H. *Science*. **1997**, 276, 779-781.

7. Dillmore, W. S.; Yousaf, M. N.; Mrksich, M. *Langmuir.* **2004**, 20, 7223-7231.

8. Demers, L. M.; Ginger, D. S.; Park, S.-J.; Li, Z.; Chung, S.-W.; Mirkin, C. A. *Science*. **2002**, 296, 1836-1838.

9. Liu, G. Y.; Gu, S.; Qain, Y.; *Acc. Chem. Res.* **2000**, 33, 457-466.

10. Hoover, D. K.; Lee, E. J.; Chan, E. W. L.; Yousaf, M. N. *ChemBioChem*. **2007**, in press.

11. Hinder, S. J.; Connell, S. D.; Davies, M. C.; Roberts, C. J.; Tendler, S. J. B.; Williams, P. W. *Langmuir.* **2002**, 18, 3151-3158.

12. Li, Y.; Yuan, B.; Ji, H.; Han, D.; Chen, S.; Tian, F.; Jiang, X. *Angew. Chem. Int. Ed.* **2007**, 46, 1094-1096.

13. Jiang, X.; Ferrigno, R.; Mrksich, M. *J. Am. Chem Soc.* **2003**, 125, 2366-2367.

14. Chan, E. W. L.; Yousaf, M. N. *J. Am. Chem. Soc*. **2006**, 128, 15542-15546.

15. Chan, E. W. L.; Yousaf, M. N. *ChemPhysChem*. **2007**, 8, 1469-1472.

16. Ostuni, E.; Chapman, R. C.; Liang, M. N.; Meluleni, G.; Pier, G.; Ingber, D. E.; Whitesides, G. M. *Langmuir*. **2001**, 17, 6336-6343.

17. Pierschbacher, M. D.; Ruoslahti, E. *Nature.* **1984,** 309, 30-33.

18. Chan, E. W. L.; Yousaf, M. N. *Angew. Chem. Int. Ed*. **2007,** 46, 3881-3884.

19. Hodgson, L. O.; Chan, E. W. L.; Hahn, K. M.; Yousaf, M. N. *J. Am. Chem. Soc*. **2007,** 129, 9264-9265.

20. Weibel, D. G.; DiLuzio, W. R.; Whitesides, G. M. *Nature Reviews*. **2007,** 5, 209-218.

Reproduced with permission from the American Chemical Society

Westcott, N. P.; Yousaf, M. N. *Langmuir* **2008**, *24*, 2261-2265.

Chapter III: Chemically and

Electrochemically Etched Gold Substrates for Cell Adhesion and Migration Studies
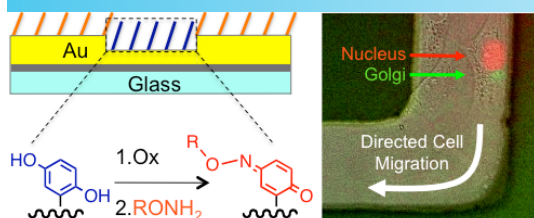
3.1 Introduction

Cell adhesion and migration is important for a number of fundamental processes ranging from differentiation, growth to development.[1] Cells migrate in a dynamic, complex environment that includes soluble factors, mechano-physical forces as well as hydrodynamic forces all in an evolving nanotopology based environment. The migrating cell experiences varying soluble nanostructures and immobilized nanotopology features on the extracellular matrix due to different 3-dimensional conformations of the constituent proteins. These external factors influence how the cell responds to its environment and can lead to morphology changes and directed migration.[2,3] Internally, many of the key proteins and signaling molecules involved in cell adhesion and migration have been discovered.[4] However, the environment's effects on these internal signaling processes is complex and an intense area of current research.[5,6] A systems biology level evaluation of the interconnecting signaling cascades and internal/external forces is needed in conjunction with new types of materials to generate model surfaces to position and control cell behavior. [7-10]

Gold has been the metal of choice for generating model substrates for cell biological studies, which utilize self-assembled monolayers (SAMs). These types of surfaces are useful due to

there resistance to oxidation, biocompatibility, synthetic flexibility to tailor its properties, conductivity and its ability to be inert to non-specific protein adsorption and cell attachment.[11] SAMs on gold present a well-defined surface which is ideally suited to study cell migration. Ligands can be chemoselectively immobilized to the surface in patterns to probe the subtle effects of ligand affinity and density on cell migration. However, a SAM surface generally is planar and does not replicate the complex nanotopology of the extracellular matrix. To study cells sampling a 3D environment, a number of modifications to the SAM substrate have been reported. For example, silicon substrates have been contoured using photolithographic techniques. Gold was then evaporated on the modified silicon wafers to generate SAM substrates to study cell adhesion. Another approach evaporated gold onto glass slides at an angle to the gold source resulting in different slopes of gold deposition thickness.[12,13] To understand the complex effects of nanotopology on cell migration and adhesion, a multidisciplinary effort that integrates surface chemistry, microfluidics, and electrochemistry may be utilized to simultaneously pattern surfaces while generating different surface topologies.

Fluorescence microscopy is a major research tool in cell biological investigations.[14] It has been used to image organelles, protein dynamics, and study protein-protein interactions. However, integrating SAMs of alkanethiolates on gold with live-cell fluorescence studies has been difficult due to the fact that gold surfaces efficiently quench fluorescence thus limiting access to important tools in cell biology research (such as fluorescently labeled cell lines, fluorescence resonance energy transfer (FRET) techniques, and fluorescent dyes). In a series of experiments, we recently overcame this limitation for FRET analysis by examining actin assembly at cell protrusions with a customized microscopy setup on gold SAM surfaces.[15] Another major limitation of SAM gold surfaces is the inability to visualize ligand patterns on the substrate

during cell adhesion or directed migration experiments. Although patterning gold with different chemistries is straightforward, observing the patterns on a flat 2 dimensional surface simultaneously while using compatible microscopies to observe live cell fluorescent behavior is currently unavailable. One solution to these challenges is to pattern the gold directly to generate gold/glass hybrid surfaces.[16,17] However, this methodology functions as a binary system and cannot generate topologies such as gradients.

Microfluidics has been shown to achieve spatial and temporal control over a variety of reactants and surfaces.[18,19] For reactions that interact with the surface, the high surface area to volume ratio in microchannels creates reactant depletion zones.[20] This leads to gradients of reaction progress in the microchannels and has been used to generate gradients of biomolecules.[21] If a strategy could be developed to easily generate gold surfaces with different surface topologies, a wide range of studies into the effects of nanotopology on cell adhesion and migration could be performed.

Herein, a combined strategy to generate various glass and gold patterns on gold substrates is described. Both electrochemical and chemical triiodide etching conditions within microfluidic channels are used to produce patterns in gold to provide spatial control over the surface. The variety of gold surfaces produced will be useful for a range of cell adhesion and cell migration studies. Furthermore, we also show the SAM surface chemistry can be used to enhance or inhibit gold etching. These substrates were then used to study cell migration around a corner.

3.2 Experimental

3.2.1 Synthesis of Alkanethiols. The undecane thiols terminated with tetra(ethylene glycol), and hydroquinone tetra(ethylene glycol) were synthesized as reported previously.[22,23]

3.2.2 Solid Phase Peptide Synthesis. Peptide synthesis of RGD-oxyamine was performed as previously reported.[24,25,26]

3.2.3 Microfabrication. The polydimethylsiloxane (PDMS) microchips were fabricated using soft lithography.[27] Patterns were fabricated using masks drawn in Adobe Illustrator CS3 and photoplotted by Pageworks onto transparencies. SU-8 50 (Microchem) was patterned using the manufacturer's directions to obtain 100 µm channel depth. Slygard 184 (Dow Corning) was cast onto the mold in a 1:10 curing agent to elastomer w/w. The prepolymer was degassed for 15 minutes and then poured over the mold. The prepolymer was cured for 1 hr at 75 °C. The PDMS was removed from the master and access holes were punched into the PDMS.

3.2.4 Preperation of Monolayers. Gold substrates were prepared by electron beam deposition of titanium (6 nm) and gold (12 nm - 18 nm) on 24 mm x 100 mm glass microscope slides. The slides were cut into 1 x 2 cm^2 pieces and washed with absolute ethanol before use.

3.2.5 Electrochemical Gold Etch. A microfluidic cassette was reversibly sealed to a gold substrate. To generate the gold depth gradients, a solution containing 1 M KI and 0.1 M $NaSO_3$ in water was flowed into the channels. Using a Mastech HY1803D power supply, one electrode was applied to the solution and the other was applied to the gold surface. 2.3V was then applied to etch the gold. The titanium was removed with a solution of 1:1:5 $NH_4OH:H_2O_2:H_2O$ (v/v/v). The PDMS microchip was removed and the patterned gold substrates were immersed in ethanolic 1mM tetra (ethylene glycol) undecane thiol for 12h.

3.2.6 Chemical Gold Etch. A microfluidic cassette was reversibly sealed to a gold substrate. To chemically etch the gold surface, a solution containing 5.8 M of KI and 1.3 M of I_2 in PBS was flowed into microchannels to remove the gold layer. The titanium layer was etched with 1:1:5 $NH_4OH:H_2O_2:H_2O$ (v/v/v). To etch the surface partially, the etch solution was diluted to 1/320 (v/v) with water. The dilute etching solution was flowed into the microchannels for 10s. The PDMS microchip was removed and the patterned gold substrates were immersed in ethanolic 1 mM tetra (ethylene glycol) undecane thiol for 12h.

3.2.7 Formation of SAMs in Microfluidic Channels. Once the substrates had been etched either electrochemically or chemically, the microchannels were cleaned with DI water then ethanol for 10s each. 0.1 mM of hexadecane thiol in ethanol was vacuumed into the microchannels and allowed to react for 10s to form a partial SAM on the gold regions of the microchannels. The PDMS microchip was removed and the gold substrates were immersed in tetra (ethylene glycol) undecane thiol for 12h. *For cell biological studies:* a mixed SAM containing 10% hydroquinone- tetra(ethylene)glycol alkanethiol and 90% tetra(ethylene)glycol alkanethiol was flowed through the microchannels (1mM total, 1 min), the microfluidic cassette was then removed and the remaining bare gold regions backfilled with tetra(ethylene)glycol alkanethiol (1mM) for 8 hrs. The surface was electrochemically oxidized and RGD-oxyamine (1mM, 2 hrs) reacted with the quinone surface to install the peptide on the surface for subsequent biospecific cell adhesion and migration studies.

3.2.8 Electrochemistry. All electrochemical measurements were made using a Bioanalytical Systems Epsilon potentiostat. An Ag/AgCl electrode served as the reference, the gold monlayer acted as the working electrode, and a Pt wire served as the counter electrode. The electrolyte was 1 M $HClO_4$ and the scan rate was 100 mV/s. All measurements were made in a standard electrochemical cell.

3.2.9 Oxyamine coupling reaction. The surface was activated with an application of 750 mV for 10s to oxidize the hydroquinone to the reactive quinone. For surface characterization 250 mM oxyamine acetic acid was added to the surface for 2 hrs. For cell biological surfaces the same activating conditions were used but RGD-oxyamine peptide was immobilized to the surface (1 mM, 2 hrs).

3.2.10 Microscopy. Fluorescent and brightfield microscopy was performed using a Nikon TE2000-E inverted microscope. Image acquisition and processing was done using Metamorph

software. Scanning electron microscopy was performed using a Hitach S-4700. Live cell fluorescence microscopy was performed as reported previously.[15]

3.2.11 Cell Culture. Swiss Albino 3T3 mouse fibroblasts (ATCC) were cultured in Dulbecco's Modified Eagle Medium (Gibco) containing 10% calf bovine serum and 1% penicillin/streptomycin. Rat2 fibroblasts with coronin labeled actin were cultured in Dulbecco's Modified Eagle Medium (Gibco) containing 5% fetal bovine serum and 1% penicillin/streptomycin. Cells were removed with a solution of 0.05% trypsin in 0.53 mM EDTA and re-suspended in serum-free medium (100,000 cells/mL). The cells were seeded with 1 mL of this solution to surfaces for 2 h. After 2 h, the appropriate serum containing media was added for cell growth. In a 5% CO_2 atmosphere at 37 °C, cells were allowed to grow 2-3d and become confluent. Imaging was then performed at room temperature. Histone-2B-mCherry and GFP-α-Tubulin expressing Rat2 fibroblasts were cultured in Dulbecco's modified eagle's medium supplemented with 5% fetal bovine serum and 1x penicillin/streptavidin antibiotics. Cells were removed from tissue culture plastic with Trypsin EDTA, added to serum containing media and pelleted. Cells were resuspended in serum-free media and plated to the partially etched SAM patterned substrates for 1.5 hrs. After a gentle rinse with PBS, cell plated substrates were placed in culture media for 2 hours prior to imaging.

3.2.12 X-Ray Photoelectron Spectroscopy (XPS). Partially etched gold surfaces were generated with $EG_4C_{11}SH$ SAMs installed as previously described. XPS measurements were then preformed on these surfaces with a Kratos Axis Ultra DLD. A mono Al anode source was used with specific excitation energy of 1486.6 eV and a 20 eV pass energy was used for the high resolution scans. All binding energies are reference to the C 1s of a saturated hydrocarbon at 284.7 eV.

3.2.13 Atomic Force Microscopy (AFM). Atomic force microscopy (AFM) images were obtained by using a MFP-3D Stand Alone atomic force microscope (Asylum Research, Santa Barbara, CA) with optical alignment system. Lateral force images were acquired in contact mode, using a silicon tip (0.03-0.08 N/m, MikroMasch USA, Wilsonville, OR), at a scan rate of 1 Hz, under ambient conditions.

3.3 Results and Discussion

3.3.1 Explanation of Procedure. To etch gold with spatial control, a microfluidic cassette was used to generate patterns with a variety of gold etching chemistry conditions. Our surfaces consisted of a glass substrate over which a 6 nm titanium adhesion layer was evaporated followed by a 12-18 nm layer of gold. To generate the gold/glass hybrids, both the gold and the titanium adhesion layer were completely etched. A strategy to chemically or electrochemically etch gold in patterns is outlined below (Figure 1). To establish microchannels, a polydimethylsiloxane (PDMS) microfluidic cassette was reversibly sealed to the gold substrate. A triiodide solution containing 5.8 M of KI and 1.3 M of I_2 in PBS was flowed for 3s into the microchannels to chemically etch the gold layer. The solution only etched the gold from the surface in the microchannels, which resulted in a 2D projection of the microfluidic pattern onto the substrate. Once the gold layer had been removed, a solution of 1:1:5 $NH_4OH:H_2O_2:H_2O$ (v/v/v) was flowed for 10s into the channels to strip the titanium adhesion layer and leave only a patterned glass/gold surface.
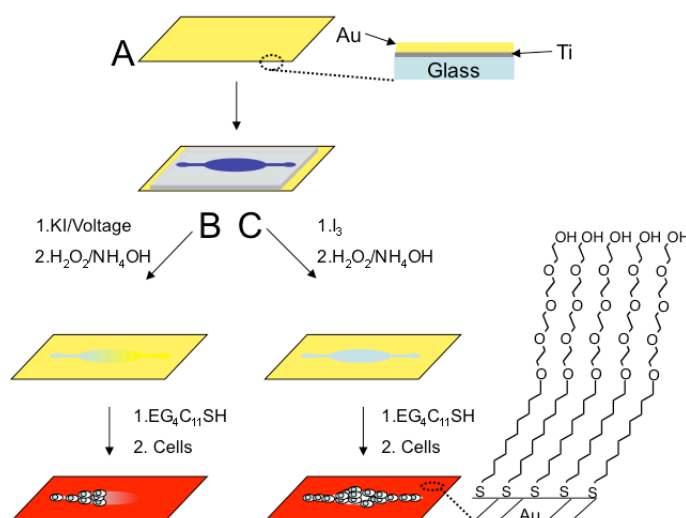
Figure 3.1. A scheme outlining the strategy to electrochemically and chemically generate gold/glass hybrid substrates for cell culture. (A) A PDMS microfluidic chip was reversibly sealed to a bare gold surface. (B) To electrochemically etch the gold, a potassium iodide (KI) electrolyte solution was flowed into the channels with the simultaneous application of 2.3 V. A 1:1:5 solution of $NH_4OH:H_2O_2:H_2O$ was then flowed into the microchannels to remove the Ti adhesion layer. (C) For chemical etching of gold using microchannels, a solution of I_2 and KI was flowed into the channels. After the gold was etched, the same titanium etching solution was used to remove the adhesion layer. After both these surfaces were etched, they were immersed in an ethanolic solution containing $EG_4C_{11}SH$ (1mM) to form SAMs on the remaining gold surface. The resulting hybrid surface is composed of a SAM surface region that resists non-specific protein adsorption and cell adhesion and a glass region that allows protein and cells attachment.

To electrochemically etch a gold surface, a solution containing 1 M KI and 0.1 M $NaSO_3$ in PBS was flowed into the channels. The gold surface was grounded and a voltage of 2.3V was applied to a bubble of electrolyte solution above one of the cassette's access holes using a power supply (Mastech HY1803D) to etch the gold. Again, the I⁻ acted as a gold complexing agent and the voltage served to oxidize the gold. The titanium adhesion layer was removed as described above to complete the removal of the metal layers. At the boundary of the reaction, a gradient of gold was formed due to local reactant depletion of I⁻ in the microchannels. After removal of the two layers by chemical or electrochemical means, a SAM surface was formed by immersing the surface in a 1 mM ethanolic solution containing tetra (ethylene glycol) undecane thiol

(EG$_4$C$_{11}$SH). The resulting gold surfaces were resistant to non-specific protein adsorption and cell adhesion.

3.3.2 *SEM Study of the Chemically Etched Surface.* To study the *chemically* etched surface, scanning electron microscopy (SEM) was used to image the gold/glass hybrids (Figure 2). The surface consisted of a 6 nm titanium adhesion layer with a 100 nm sputtered gold layer. The thicker layer of gold (12 nm vs. 100 nm) was to aid in visualization of the etch boundaries at the microchannels. Also, only the gold layer was removed so the etched regions would be conductive to aid in visualization with SEM. The image taken at lower magnification demonstrates that no gold remains on the surface of the glass after the triiodide etch process and the reaction was localized to the regions of the microchannels. Using imaging processing software, the fidelity of the etch pattern was verified. The PDMS channels were 110 μm in width and the brightfield microscopy of completely etched surfaces reveals etched widths of 112 μm. The SEM image at the higher magnification shows the boundary between the etched and remaining regions of gold. The image further confirmed that no gold remains after the chemical etching process. Furthermore, the gold/glass boundary was sharp, showing no undercutting with 100 nm gold. Once the titanium etching was complete, brightfield microscopy was used to verify no titanium remained on the surface. The etched gold substrates have two different surface properties, allowing for the patterning of several different alkanethiol molecules.

3.3.2 *Cell Seeding to Chemically Etched Surfaces.* Several gold/glass hybrids were immersed in a 1 mM ethanolic solution of EG$_4$C$_{11}$SH to form a SAM that would render the gold surface inert to non-specific cell attachment and protein adsorption for cell studies. The exposed glass remains capable of binding cells through non-specific interactions. Swiss Albino 3T3 fibroblasts (cells) were seeded to the surface (Figure 3) in order to study cell adhesion to these hybrid

surfaces. To image the cells and demonstrate the power of the gold/glass hybrids, cells bound

to the surface were treated with CellTracker™ Green 5-chloromethylfluorescein diacetate

(CMFDA) dye (Molecular Probes) which the cells uptake and cleave internally to generate a

fluorescent molecule. Fluorescence micrographs were then taken and show that the cells

adhered to the glass surface and became confluent.
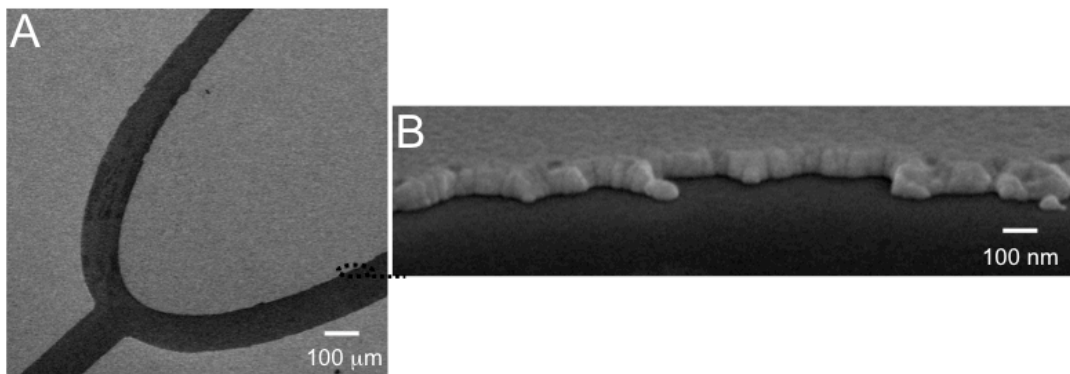
Figure 3.2. Etched gold surfaces imaged by scanning electron microscopy (SEM). (A) A microfluidc patterned etch of a gold surface. (B) A high-resolution image of the gold layer at the etched boundary region. These images show the fidelity of the patterning method and the complete removal of the gold layer.
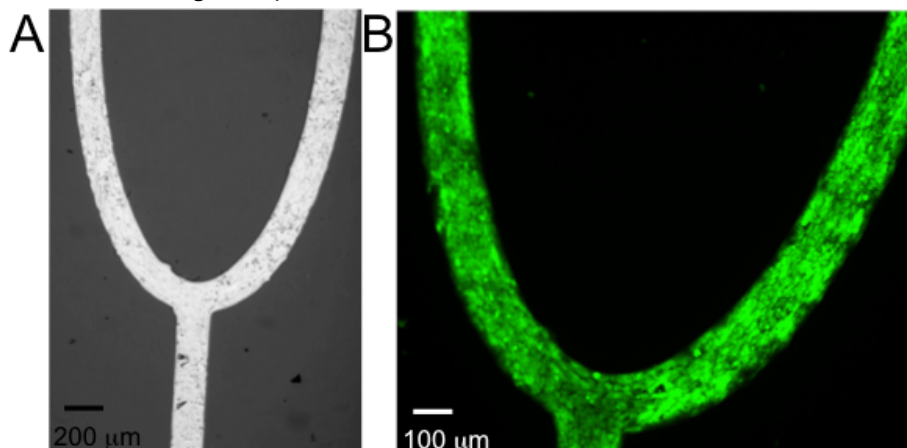
Figure 3.3. Swiss Albino 3T3 mouse fibroblasts seeded on chemically etched gold surfaces with subsequent installation of inert $EG_4C_{11}SH$ SAMs. The cells adhered only to the exposed non-inert glass region. (A) A phase contrast image of cells seeded to an elliptical microfluidic pattern. (B) Fluorescent image showing cells stained with CellTracker green dye on the chemically etched pattern.

3.3.4 SAM effects on Etch Rates. To examine the role of surface chemistry on electrochemical

or chemical etch rates a patterned SAM was made with both hexadecanethiol (HDT) and

EG$_4$C$_{11}$SH present on the surface in localized regions. HDT was microcontact printed on approximately half the gold surface and then EG$_4$C$_{11}$SH was used to backfill the remaining bare gold surface. Both surface thiol densities were 4x10^{14} molecules/cm^2.[11] At the boundary of the two different SAMs, a microchip was placed and filled with previously described triiodide etching solution diluted to 1/320 (v/v) with DI water for 10s. The surface was then imaged (Figure 4). In order to determine the amount of etching, plots were constructed by measuring the relative absorbance, using image processing software, of the remaining gold on the surface versus a completely etched surface. The plots demonstrate the HDT SAM was approximately etched twice as much as the EG$_4$C$_{11}$SH SAM (6 nm vs 12 nm) where the initial gold thickness was 18 nm in depth determined by quartz crystal microbalance during gold evaporation. The different head groups of EG$_4$C$_{11}$SH and HDT SAMs caused the disparity in the etch rates. The ethylene glycol head group oxidized instead of the gold thereby reducing the amount of I$_2$ in solution, thus slowing the oxidation of the gold. The sacrificial oxygen was observed by analyzing the oxygen present on the surface by XPS. The oxygen 1s binding energy increases when treated with the triiodide and the peak area was also reduced demonstrating the destructive oxidation of the monolayer. It is interesting to note that the HDT SAM did not provide any protection from the etching solution. In fact, it was etched at roughly the same rate as bare gold under the same conditions. This result is completely reversed for the classic cyanide gold etching chemistry where HDT inhibits the cyanide gold etch process.[28]
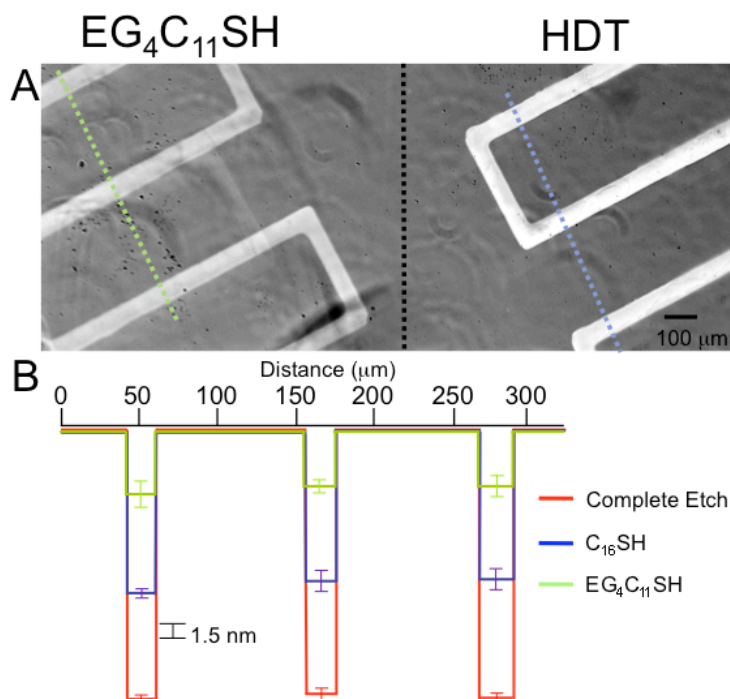
Figure 3.4. The type of SAMs on gold influence the depth of chemical etch. For example, gold is chemically etched differently through patterned EG$_4$C$_{11}$SH and HDT SAMs. (A) A brightfield image of the etched SAM surface. The SAM on the left side was composed of EG$_4$C$_{11}$SH and the SAM on the right side was composed of HDT. The dashed colored lines represent the measured areas. (B) A comparison of the depth of etch plots for EG$_4$C$_{11}$SH SAM, HDT SAM, and bare gold. The y-axis is the etch depth. The x-axis is distance. The difference in etch depths was caused by the terminal ethylene glycol groups serving as sacrificial oxidants slowing the oxidation of the gold on these SAM surfaces.

3.3.5 Partial and Electrochemical Gold Etch. To generate different gold topologies on the surface, gold was both partially and electrochemically etched. Electrochemically etched surfaces present an interesting topology when the patterns are not completely etched. A gradient of gold was formed at the boundary between the etched and unetched portions of the gold surface in the microchannel. The position of the gradient in the microchannel can be controlled by the length of time the voltage is applied (Figure 5). In the microchannels, the gold was etched and formed a gradient based on its distance from the access hole. The gradient was caused by local reactant depletion of I$^-$ in the microchannels with increased voltage application time leading to greater gold etching. To visualize ligand patterns on the gold surface, the gold was incompletely etched using a very dilute etching solution (Figure 5C). To partially etch the

gold surfaces, a 1:320 v/v in distilled water was prepared from the triiodide etching solution. The solution was flowed through microchannels sealed to a gold surface for 10s. The resulting surface had incompletely etched regions of gold whose patterns corresponded to the microchannels.
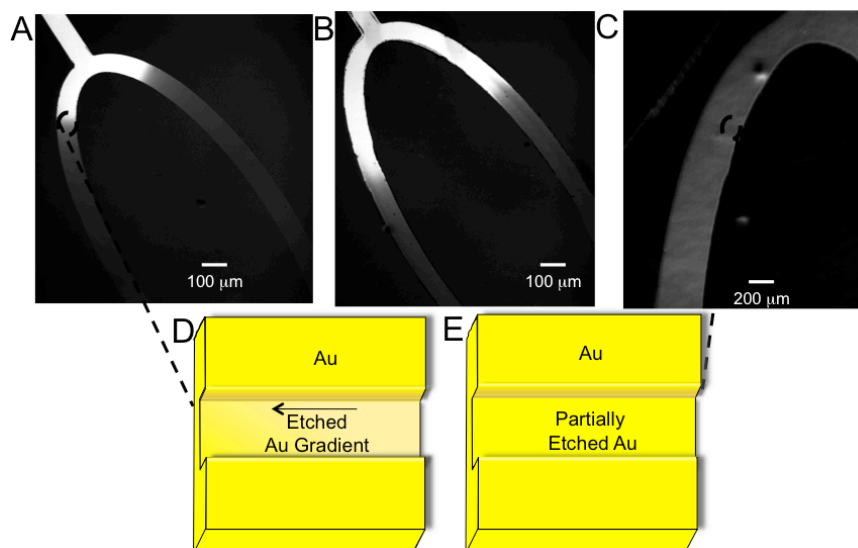
Figure 3.5. Images of partially etched and gradient etched gold surfaces. Brightfield images of the electrochemical gold etch run for (A) 3 sec and (B) 5 sec. The gold outside the patterns was not etched and the gold inside the pattern formed a gradient based on the reactant depletion of the complexing agent. (C) A brightfield image of a partially etched gold surface. The partially etched surface allows for pattern visualization but remains gold for subsequent SAM formation and ligand immobilization. (D) An illustrative representation of the electrochemically gradient etched surface. (E) A representation of the partially etched continuous flat surface.

3.3.6 Electrochemical Etch Slope Study. To study slopes generated by the electrochemical process a microchip containing 2 identical patterns was sealed to a gold surface. The gold was etched for 4s and 6s. Using imaging processing software, the slope of each gradient was determined (Figure 6).   The gradient slope was steeper with longer etch times and can be controlled by the position within the microchannel and the distance from the inlet access hole. By varying the voltage application time, a range of different slopes can be generated over distances relevant for cell migration studies. To observe the etched gold at higher resolution, a SEM image of the gradient was analyzed (Figure 6D).
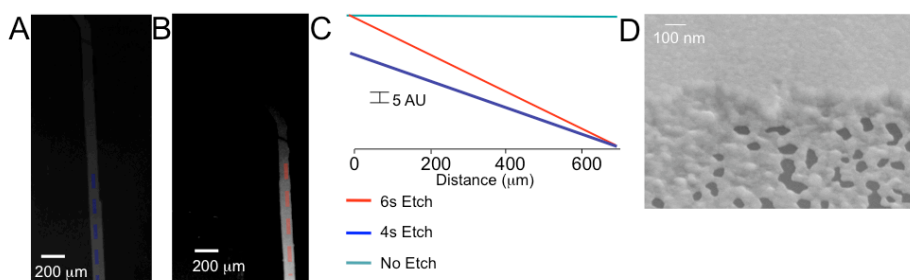
Figure 3.6. Controlled differential gradient slopes obtained with different voltage application times. Brightfield micrographs of (A) 4 second application time (B) 6 second application time. (C) A plot of the etch obtained with the differential etching conditions. The y-axis is absorbance units and the x-axis is distance. (D) A SEM of the gradient surface showing the interface between the gold surface and the electrochemically etched regions.

3.3.7 Visualization of SAM Patterns. To visualize ligand patterns for cell adhesion the gold surfaces were first partially etched and then functionalized with SAMs on the partially etched region selectively (Figure 7). After a partial gold etch and without removing the microfluidic cassette, the channels were then rinsed with ethanol and water for 10s. A HDT SAM was formed on the surface by flowing ethanolic 0.1 mM HDT in the microchannels and then letting it self-assemble on the gold surface for 10s. This resulted in a SAM forming on the partially etched regions capable of cell adhesion through non-specific hydrophobic interactions. The microfluidic cassette is then removed and the remaining gold surface was backfilled with $EG_4C_{11}SH$ to form an inert SAM. Swiss Albino 3T3 mouse fibroblasts were then seeded to these surfaces to demonstrate cell adhesion only to the partially etched regions. Figure 8 shows stably transfected fluorescent Rat2 fibroblasts with green-fluorescent-protein tagged (GFP)-coronin-bound actin seeded to the partially etched surfaces to study cell adhesion and migration utilizing fluorescent live cell microscopy. In order to overcome the inherent quenching of fluorescence by the gold surface we used an optimized inverted microscope.[26] The combination of microfluidic etching, SAM installation and live cell fluorescence microscopy allows for the control of cell position, motility direction and fluorescence characterization on tailored surfaces.
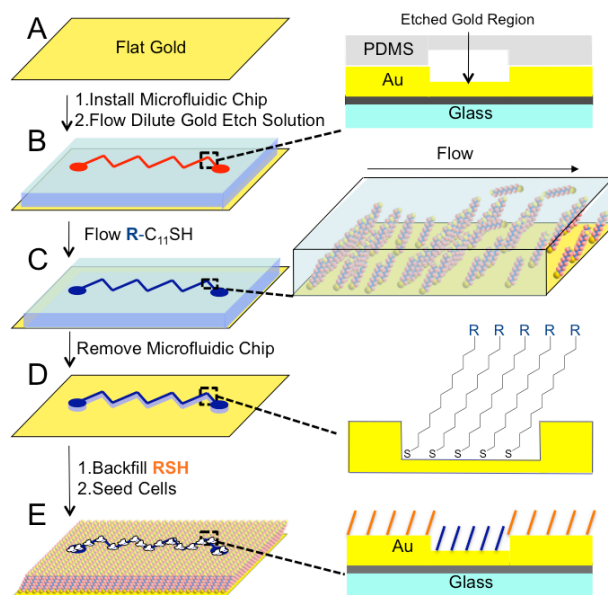
Figure 3.7. A two-step process to generate partially etched and patterned alkanethiol surfaces. (A) A PDMS microfluidic cassette was reversibly sealed to a flat bare gold surface. (B) A dilute triiodide etch solution was flowed into the microfluidic cassette for 10s to create a recessed patterned gold surface. (C) Without removing the PDMS cassette a rinsing solution of absolute ethanol (20 µL) and then water was flowed through the channel followed by the addition of 0.1 mM hexadecanethiol (HDT) in EtOH for 10s. This generated a SAM on the partially etched gold regions. (D) Removal of the cassette from the gold surface exposed the partially etched SAM patterned regions and the bare gold regions. (E) The entire substrate was then immersed in 1 mM $EG_4C_{11}SH$ solution for 8 h to create an inert SAM background resistant to protein and cell adhesion in the non-etched regions. Cells only adhered to the hydrophobic (non-inert) presenting gold etch regions. Directional cell migration can be predicted and tracked by visualizing the cells and the path trajectory with standard live-cell fluorescence microscopy.

3.3.8 Cell Seeding to Partially Etched Surfaces. To verify that gold was still present in the partially etched regions and able to form SAMs, a number of control experiments were performed. Instead of patterning ligands on the etched region of the surface, the PDMS microchip was removed and the entire surface was used to form an $EG_4C_{11}SH$ SAM. Cells were seeded to the surface and did not adhere to the surface including the etched regions. The ability to resist non-specific cell attachment demonstrates that well-ordered SAMs were formed in the partially etched regions. Furthermore, an electroactive molecule, hydroquinone alkanethiol, was immobilized to the partially etched region using microfluidics. Electrochemical

69

analysis showed the characteristic hydroquinone alkanethiol peaks. The integrated area of the peaks was used to quantify the amount of molecules immobilized on the surface and determined to correspond to a full SAM formed in the partially etched regions.[16e]
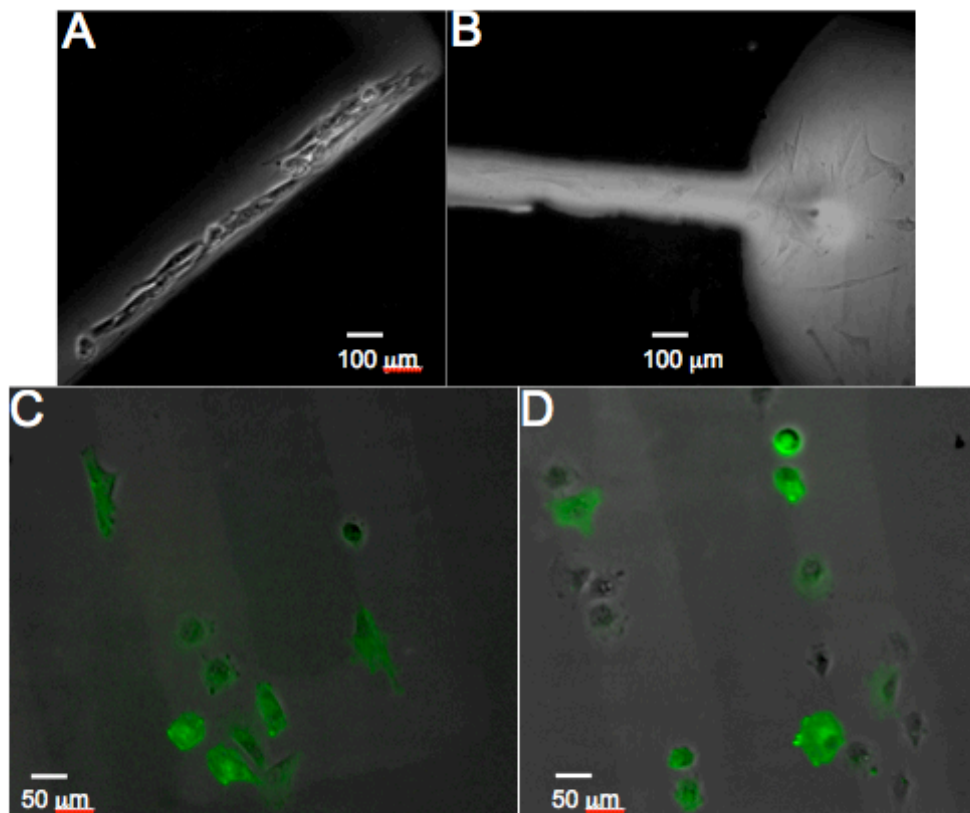
Figure 3.8. Cell attachment to microfluidic generated partially etched and functionalized gold substrates. (A) Cells adhered specifically to the etched line pattern presenting HDT. (B) Cells adhered to a circular pattern. (C) Stably transfected Rat2 fibroblasts expressing GFP-coronin attached to the partially etched pattern. (D) The same fluorescent cells bound to a line pattern. The cells only adhere to partially etched regions of the gold allowing for live-cell visualization of cells on patterned surfaces.

3.3.9 Cells Seeded to Electrochemically Etched Surfaces. To demonstrate cell adhesion and migration on microfluidic/electrochemically etched *gradient* topology gold surfaces, gradient gold substrates were generated and immersed in an ethanolic solutions of different alkanethiols (Figure 9). The gradient gold surfaces were generated as described above but patterned with two different alkanethiols in the microfluidic etched regions. For the case where $EG_4C_{11}SH$ was installed on the gradient gold topology, Swiss Albino 3T3 fibroblasts

attached to the glass region only. This gold gradient region, despite being partially etched, resists non-specific protein adsorption showing the gradient gold topology is able to form competent SAMs. Cells attached to the etched glass/gold gradient pattern were treated with CMFDA dye and imaged using a fluorescence microscope. The resulting image shows that the cells adhered only to the glass region. In the second case, we used a hydrophobic HDT to pattern the gold gradient toplogy pattern. Cells were seeded to the resulting surface and adhered to both the glass and electrochemically etched gold/gradient regions. This demonstrates that the etched gold was able to support SAMs for cell adhesion. Using this strategy, gradients of gold height can be generated with a variety of different slopes with control over the surface chemistry present in the gradient regions to influence cell adhesion to the substrate.

3.3.10 Electrochemical Characterization. In order to characterize the quality of the SAMs on the patterned partially etched regions by microfluidic lithography, a hydroquinone tetra (ethylene glycol) undecane thiol ($H_2QEG_4C_{11}SH$) was assembled onto the surface on the partially etched regions of gold (1 mM, 30 s) and backfilled with the inert tetra(ethylene)glycol alkanethiol ($EG_4C_{11}SH$) (1 mM, 10 min). The hydroquinone group is electroactive and can be reversibly oxidized to the quinone which can subsequently react chemoselectively with oxyamine tethered ligands to generate an interfacial oxime conjugate (Figure 3.10). Cyclic voltammograms (CV) were taken of the partially etched surface and show two distinct redox peaks at 570 and 290 mV characteristic of the hydroquinone-quinone redox couple. To demonstrate the chemoselective reaction, an oxyamine acetic acid was immobilized to the surface (250 mM, 2 hrs). The two redox peaks shifted to 483 mV for the oxidation and 342 mV for the reduction peak corresponding to the oxime product. The resulting redox peak shift and

peak integration allows for a diagnostic and quantitative evaluation of the yield of reaction and therefore density of immobilized ligand.[22,24,31]
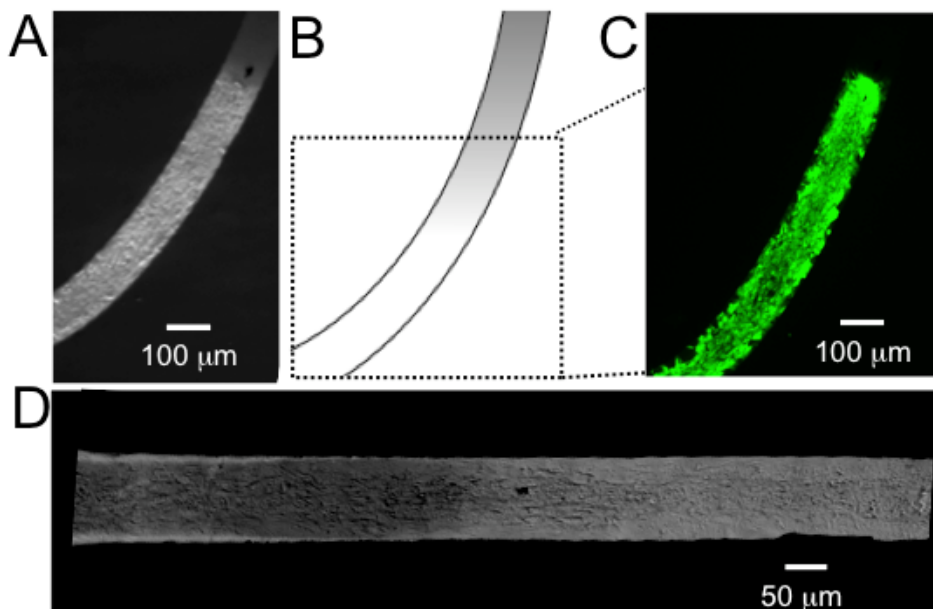
Figure 3.9. Cells seeded to an electrochemically etched glass/gold gradient surface. (A) Swiss Albino 3T3 fibroblasts seeded to an electrochemically etched glass/gold surface with an $EG_4C_{11}SH$ SAM. (B) Representation of the gradient of glass/gold created by electrochemical etching. The gray region of the pattern corresponds to increasing gold height from a bare glass region where the gold is completely etched. (C) Cells seeded to an $EG_4C_{11}SH$ SAM with an elliptical pattern and then fluorescently labeled with CellTracker green dye. Cells only attached to the glass region and a short distance of gradient gold. (D) Fibroblasts seeded to an etched gold surface with HDT patterned on the etched gold gradient and backfilled with $EG_4C_{11}SH$. The images demonstrate the ability of the gradient topology gold left in the channel regions to generate SAMs that both resist non-specific adhesion ($EG_4C_{11}SH$) and bind cells (HDT) depending on the properties of the alkanethiol presented on the gold surface.

To verify the quality of the SAM and amount of electroactive molecule on the partially etched region, we used cyclic voltammetry to calculate and confirm the amount of electroactive molecules with the corresponding patterned etch area.[24] For example, the total area etched using the microfluidic cassette and therefore total area of installed electroactive hydroquinone or oxime ligand conjugate was 0.375 cm^2 and the gold surface was 2 cm^2. The peak area for the hydroquinone was calculated to be 4.05 μC with the equation $Q = nFA\Gamma$ (Q represents total charge, n = mols of electrons (2), F = Faraday's constant, Γ = molecules per

surface area). From the peak area data, theoretically our 0.375 cm^2 surfaces should have a total of 3.75 x 10^{13} electroactive molecules on the surface if a full monolayer was present on the surface. We found experimentally the hydroquinone molecule was 3.38 x 10^{13} molecules on the etched surface which closely approximates the theoretical calculation and demonstrates that an electroactive SAM can be installed rapidly by μFL and the density of the molecules/ligands on the patterned surface can be precisely determined.

      3.3.11 Directed Cell Migration on Etched Surface. To observe directed cell migration on the partially etched surface, an RGD oxyamine peptide, the minimum adhesion peptide found in the extracellular matrix protein fibronectin, was synthesized and chemoselectively immobilized to the etched and patterned quinone-alkanethiol surfaces. For cell biological studies, a mixed SAM containing 10% H$_2$QEG$_4$C$_{11}$SH and 90% EG$_4$C$_{11}$SH was flowed through the microchannels (1mM total, 1 min), the microfluidic cassette was then removed and the remaining bare gold regions backfilled with tetra(ethylene)glycol alkanethiol (1mM) for 8 hrs. The surface was activated with an application of 750 mV for 10s to oxidize the hydroquinone to the reactive quinone to which RGD-oxyamine was immobilized (1mM, 2 hrs). A stable transfected fluorescent Rat2 cell line that contains a GFP labeled golgi and mCherry labeled nuclei was then seeded onto the surface (Figure 3.11). As the cell polarizes and migrates the relative positional vector of the concentrated golgi and nucleus can be determined to measure the role of cell polarity on directed cell migration, a fundamental question in cell motility.[32]
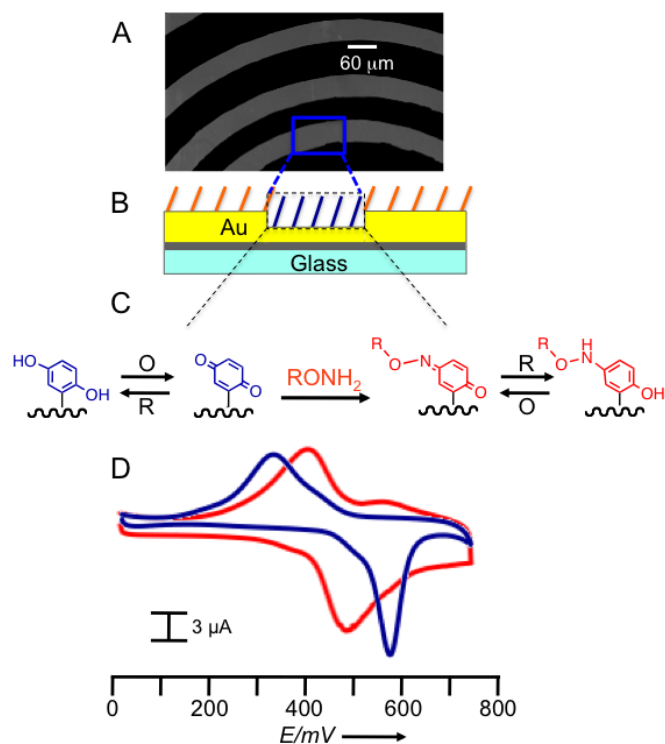
Figure 3.10. Electrochemical characterization of a chemoselective ligand immobilization strategy on a patterned partially etched gold surface. (A) Brightfield micrograph of a partially etched surface. (B) Sideview representation of a partially etched patterned SAM. In the etched regions, a hydroquinone alkanethiol SAM was patterned using microfluidic lithography. (C) The hydroquinone was activated by electrochemical oxidation to the quinone and subsequently reacted chemoselectively with oxyamine tethered ligands to generate a stable interfacial oxime linkage. (D) Cyclic voltammetry of the surface showed diagnostic redox signals for the hydroquinone-quinone and the oxime product. Integrating the waves provided a quantitative measure of the amount of oxime product on the partially etched regions.

We were interested in studying the relative orientation of the golgi and nucleus when the cell changes direction and migrates around corners. It is unclear how and why the nucleus to golgi vector orients during directed cell migration through a turn. A number of different experimental observation and theories have been proposed: 1. The vector always points in the direction of migration; 2. The vector is random and does not consistently point in the direction of migration; and 3. The golgi remains concentrated but moves to the rear of the nucleus during a turn and then becomes diffuse and re-concentrates and re-orients to the front of the nucleus in the direction of migration after the turn is completed.[25,33-37] With the biospecific and etched

patterned surfaces a clear determination of the nucleus to golgi vector can be measured as cells predictably change their direction of migration. Upon cell seeding, the cells adhered only to the partially etched regions of gold because the RGD-ligands were localized in these areas only and appear lighter than the thicker gold regions clearly showing the etch pattern and therefore ligand pattern and cell path trajectory. Over a period of 12 hours, cell migration was observed on the partially etched surface. The cells stayed confined to the etched regions and clearly showed the golgi was concentrated toward the leading edge of migration. Our results suggest that the polarity vector (nucleus to golgi) re-orients after completion of a directional turn around corners (supplemental movie of an example of directed migration around corners). As controls, no cells adhered to surfaces that were not reacted with RGD-oxyamine or reacted with a scrambled RDG-oxyamine peptide.
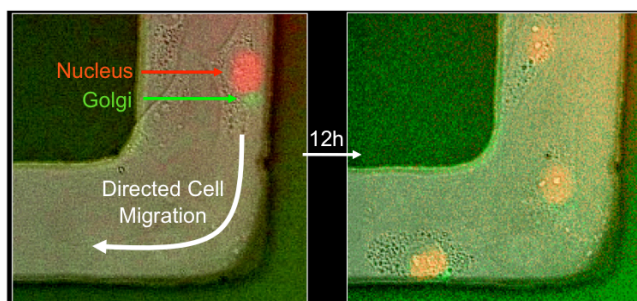
Figure 3.11. Multiwavelength time-lapse live-cell fluorescence microscopy of transfected Rat2 fibroblast cells undergoing directed migration on partially etched electroactive RGD presenting SAM gold surfaces. The partially etched regions appear lighter in the micrographs. (A) Initial position of cells on the etched region of the gold. Red = Nucleus. Green = Golgi. (B) An image taken 12 hrs later after cell migration had occurred in the etched regions of the gold.

3.4 Conclusion

In this chapter, a straightforward methodology to generate a variety of different topologies and surface chemistries on gold surfaces was developed. Gold was etched using both electrochemical and chemical methods under spatial control with PDMS microfluidic cassettes. The chemically etched surfaces had no remaining gold on the etched portion of the

surface. Cells were seeded to these surfaces with an $EG_4C_{11}SH$ monolayer on the gold and only adhered to the glass regions of the hybrid surfaces. Additionally, it was observed that the SAM could serve as a protecting layer from the etch solution with the $EG_4C_{11}SH$ serving as a sacrificial oxidant. Using dilute triiodide solution, the gold was partially etched and the surface chemistry present in the microchannels was controlled to influence cell adhesion. The electrochemically etched surfaces generated a boundary layer which consisted of a gradient of gold height. The position and slope of the gold gradient was determined by the voltage application time and was due to local reactant depletion in the microchannels. Cells were seeded to these surfaces with an $EG_4C_{11}SH$ monolayer on the surface and interestingly, did not bind to the gold gradient region. However, once HDT was added to the gold in the microchannel, the cells bound the gold gradient. The combination of microfluidics and the electrochemical and chemical etching methods allow for the creation of gold/glass hybrids surfaces for numerous biointerfacial studies. The gradients will allow for the study of cell migration on slopes of gold height with tailored surface chemistry. Additionally, cell migration was tracked using these substrates to determine organelle organization during cell migration around a corner. In the future, these studies will be followed up to study organelle organization with number of different features.

References

1. Ridley, A. J.; Schwratz, M. A.; Burridge, K.; Firtel, R. A.; Ginsberg, M. H.; Borisy, G.; Parsons, J. T.; Horwitz, A. R. *Science*. **2003**, 302, 1704-1709.

2. Lo, C.-H.; Wang, H.-B.; Dembo, M.; Wang, Y.-l.. *Biophy. Journ.* **2000**, 79, 144-152.

3. Pelham, R. Jr.; Wang, Y.-l. *Proc. Nat'l Acad. Sci.* **1997**, 94, 13661-13665.

4. Giancotti, F.; Ruoslahti, E. *Science*. **1999**, 285, 1028-1033.

5. Holly, S. P.; Larson, M. K.; Parise, L. V. *Biomat.* **2000,** 261, 69-74.

6. Hoch, H.C.; Staples, R.C.; Whitehead, B.; Comeau, J.; Wolf, E.D.; *Science.* **1987**, 235, 1659 – 1662.

7. Mrksich, M.; Chen, C. S.; Xia, Y.;Dike, L. E.; Ingber, D. E.; Whitesides, G. M. *Proc. Natl. Acad. Sci.* **1996,** 93, 10775-10778.

8. Bhat, R.R.;Chaney, B.N.; Rowley, J.; Liebmann,-Vinson, A.; Genzer, J. *Adv. Mat.* **2005**, 17, 2802-2807. c) Bhat, R.R.; Genzer, J. *Langmuir*. **2008**, 2294-2317.

9. Washburn, N.R.; Yamada, K.M.; Simon, C.G.; Kennedy, S.B.; Amis, E.J. *Boiomat.* **2005**, 25, 1215-1224.

10. Arnold, M.; Cavalcanti-Adam, E.A.; Glass, R.; Blummel, J.; Eck, W.; Kantehler, M.; Kessler, H.; Spatz, J.P. *ChemPhysChem*. **2004,** 5, 383-388.

11. Love, J. C.; Estroff, L. A.; Kriebel, J. K.; Nuzzo, R. G.; Whitesides, G. M. *Chem. Reviews*. **2005**, 105, 1103-1169.

12. Simon, K. A.; Burton, E. A.; Han, Y.; Li, J.; Huang, A.; Luk, Y. *J. Am. Chem. Soc.* **2007**, 129, 4892-4893.

13. Zhang, J.; Campbell, R.E.; Ting, A. Y.; Tsien, R.Y. *Nat. Rev.* **2002,** 3, 906-918.

14. Misteli, T.; Spector, D.L. *Nat. Bio Tech.* **1997,** 15, 961-964. c) Axelrod, D. *Traffic*, 2, 764-774.

15. Hodgson, L.; Chan, E. W. L.; Hahn, K. M.;Yousaf, M. N. *J. Am. Chem. Soc.* **2007**, 129, 9264-9265.

16. Kandere-Grzybowska, K.; Campbell, C.; Komarova, Y.; Grzybowski, B. A.; Borisy, G. G. *Nat. Meth.* **2005,** 2, 739-741.

17. Hu, Z.; Ritzdorf. T. *J. Echem. Soc.* **2007,** D543-D549

18. Delamarche, E.; Bernard, A.; Schmid, H.; Bruno, M.; Biebuyck, H. *Science.* **1997**, *276*, 779-781.

19. Hinder, S. J.; Connell, S. D.; Davies, M. C.; Roberts, C. J.; Tendler, S. J. B.; Williams, P. W. *Langmuir.* **2002**, *18*, 3151-3158.

20. Delamarche, E.; Bernard, A.; Schmid, H.; Bietsch, A.; Michel, B.; Biebuyck, H. *J. Am. Chem. Soc.* **1998**, 120, 500-508.

21. Kari, A.; Fosser, K. A.; Nuzzo, R. G. *Anal. Chem.* **2003,** 75, 5775-5782.

22. Chan, E. W. L.; Yousaf, M. N. *J. Am. Chem. Soc.* **2006,** 128, 15542-15546.

23. Chan, E.W.L.; Park, S.; Yousaf, M.N. *Angew. Chem. Int. Ed.* **2008,** *47*, 6267-6271.

24. Chan, E.W.L.; Yousaf, M.N.; *ChemPhysChem* **2007,** *8*, 1469-1472.

25. Hoover, D.K.; Chan, E.W.L.; Yousaf, M.N. *J. Am. Chem. Soc.* **2008,** *130*, 3280-3281

26. Lamb, B. M.; Westcott, N.P.; Yousaf, M.N. *ChemBioChem* **2008,** 9, 2220-2224.

27. Weibel, D. G.; DiLuzio, W. R.; Whitesides, G. M. *Nature Reviews*. **2007**, 5, 209-218.

28. Xia, Y.; Zhao, X.; Kim, E.;Whitesides, G. M. *Chem. Mat.* **1995,** 7, 2332-2337.

29. Kumar, A.;Whitesides, G. M. *App. Phys. Lett.* **1993**, 63, 2002-2004.

30. C. Pale-Grosdemange, E. S. Simon, K. L. Prime, G. M. Whitesides *J. Am. Chem. Soc.* **1991**, *113*, 12-20.

31. Westcott, N.P.; Yousaf, M.N. *Langmuir* **2008**, 6, 2261–2265.

32. Hong, H-G.; Park, W. *Electrochimica Acta* **2005**, *51*, 579-587.

33. Ueda, M.; Graf, R.; MacWilliams, H.K.; Schliwa, M.; Euteneuer, U. *Proc. Nat. Acad. Sci. USA* **1997**, *94*, 9674-9678;

34. Gomes, E.R.; Jani, S.; Gundersen, G.G. *Cell* **2005**, *121*, 451-463.

35. Théry, M. ; Racine, V. ; Piel, M. ; Pépin, A. ; Dimitrov, A.; Chen, Y.; Sibarita, J.-P. *Proc. Natl. Acad. Sci. U.S.A.* **2006,** *103*(52), 19771-19776.

36. Etienne-Manneville, S.; Hall, A. *Cell*, **2001**, *106*, 489–498.

37. Czuchra, A.; Wu, X.; Meyer, H.; van Hengel, J. ; Schroeder, T.; Geffers, R.; Rottner, K.; Brakebusch, C. *Mol. Bio. Cell* **2005**, *16(10)*, 4473-4484.

Reproduced with permission from the American Chemical Society and Wiley

Westcott, N. P.; Lamb, B. M.; Yousaf, M. N. *Anal. Chem.* **2009**, *81*, 3297-3303.

Lamb, B. M.; Westcott, N. P.; Yousaf, M. N. *ChemBioChem* **2008**, *9*, 2220-2224.

Chapter IV: Alcohol Oxidation of SAMs
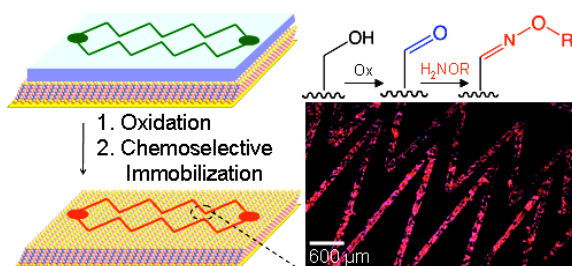
4.1 Introduction

Self-assembled monolayers (SAMs) of alkanethiolates on gold represent a class of well-defined surfaces that can be synthetically functionalized and patterned to tailor the surface properties for a variety of applications ranging from molecular electronics to biotechnology.[1-3] Generally, tailoring these surfaces requires laborious and expensive synthesis of thiol containing ligands, polymers or biomolecules. As a result, there have been numerous chemoselective immobilization strategies for conjugation to SAM surfaces including Staudinger ligation[4], Click chemistry,[5] maleimide,[6] amide,[7] Diels-Alder[8-10] and oxime chemistry.[11-15] In combination with patterning strategies and surface characterization techniques, this allows for spatial control on the surface. Most direct and convergent strategies to tailor surfaces require the multistep synthesis of molecules and/or co-catalysts that either limits their accessibility to the broad research community or are not affordable.[16-18] A more expedient and inexpensive method to generate patterns of chemoselective ligands on a surface using simple starting materials would be of tremendous practical utility to the surface chemistry, biosurface and materials research communities. However, there are limitations to the use of this model platform. The thiol-gold bond is thermally unstable and upon long

durations of air exposure may oxidize, destroying the monolayer.[19] Gold also quenches

fluorescence and has limited optical transparency, properties that reduce its use for biosensor

technologies.[20]

To overcome the limitations of gold as a substrate, an alternate model system of SAMs

of alkanephosphonates on indium tin oxide (ITO) has been explored.[21,22] ITO is a common

material widely used for applications in optoelectronics, such as the transparent conductive

coatings found in plasma, touch, and liquid crystal displays, as well as solar cells and organic

light emitting diode (OLED) devices.[23,24] Its high conductivity permits the use of ITO for a

variety of analytical techniques.[25,26] Unlike gold, the optical transparency of ITO presents

opportunity for studies involving fluorescence and, in particular, research in cell biology

conducted by *live-cell* fluorescence microscopy.[27] The major limitation of alkanephosphonates

on ITO is the lack of synthetic routes available to different terminal functionalities reducing the

immobilization strategies primarily to amide formation to carboxylic acids.[28] However, a

methodology that could chemically alter a single phosphonate SAM on ITO to multiple

functionalities for subsequent orthogonal ligand immobilization would be useful. Not only

would this strategy circumvent the difficulties encountered in synthesis, but it would also have

a wide range of applications in different research communities. This platform would have the

versatility to tailor surfaces essential for the production of electronic devices and biosensors, in

addition to the design of ideal materials to carry out biological assays.

Carbonyls in the form of aldehydes or ketones presented on surfaces have been shown to be

synthetically versatile conjugation partners that react chemoselectively with multiple

functional groups.[8-15] To exploit this conjugation strategy, synthesis of aldehyde terminated

alkanethiols,[29] generation of aldehydes from vicinal diols by oxidation,[16-18] and ketones under

oxidative control have all had varying degrees of success.[7] However, the synthetic routes to the

precursors are multi-step, low-yield, and expensive which limits their overall feasibility. If the aldehyde could be generated on the surface from inexpensive, commercially available materials, it would allow for easy access to carbonyl immobilization strategies. Furthermore, combining this strategy with a simple method to precisely control the density of aldehydes under spatial control would be of enormous practical utility.

An expedient, inexpensive and broadly applicable strategy to pattern and control the density of aldehydes on a SAM for subsequent ligand immobilization was developed for SAMs on gold. All materials are commercially available with little to no synthetic route. Utilizing microfluidic cassettes, primary alcohol oxidation was performed on both hydroxy and ethylene (glycol) terminated SAMs to generate terminal aldehyde groups with pyridinium chlorochromate (PCC)[30] for subsequent chemoselective ligand immobilization with precise density and spatial control. These surfaces were characterized with electrochemistry, contact angle, and XPS and shown to be compatible with biospecific cell adhesion and migration.

Additionally, the method was extended to generate spatially controlled aldehyde and carboxylic acid functionalized SAMs on ITO using microfluidic oxidation from self-assembled monolayers (SAMs) on ITO. This system allows for ligand immobilization by two orthogonal strategies originating from an alcohol-terminated alkanephosphonate. Microfluidic patterning provides spatial control of the aldehydes and acids formed by oxidation directly on the surface. Through chemoselective conjugation of oxyamine-containing ligands to aldehydes and of amine-containing ligands to acids, a variety of electroactive and fluorescent molecules were immobilized. The resulting oxime and amide linkages were characterized by electrochemistry, X-ray photoelectron spectroscopy (XPS), fluorescence microscopy, and contact angle measurements.

4.2 Experimental Section

4.2.1 Synthesis of Alkanethiols and Peptides. Undecane thiol terminated with tetra(ethylene glycol) and peptides were synthesized as reported previously or purchased.[11]

4.2.2 Microfabrication. The microchips were fabricated using soft lithography. Patterns were achieved using masks drawn in Adobe Illustrator CS3 and photoplotted by Pageworks onto mylar sheets. SU-8 50 (Microchem) was patterned using the manufacturer's directions to obtain 100 μm channel depth using the masks. The Slygard 184 (Dow Corning) was prepared in a 1:10 curing agent:elastomer w/w then degassed for 15 min. The prepolymer was cast over the mold and cured for 1h at 75 °C. The PDMS was then removed from the master and access holes were added to the PDMS to allow fluid flow.

4.2.3 Preperation of Monolayers. Gold substrates were prepared by electron beam deposition of titanium (6 nm) and gold (24 nm) on 24 mm x 100 mm glass microscope slides. The slides were cut into 1 x 2 cm^2 pieces and washed with absolute ethanol. The slides were then immersed in an ethanolic solution containing either 1 mM tetra (ethylene glycol) undecane thiol or 1-mercapto-11-undecanol (Sigma). After 12-16h, the slides were removed from solution. They were rinsed with ethanol and dried before use. All slides were used within a week of fabrication to minimize oxidation of the surface.

4.2.4 Preparation of ITO and SAM Formation. Indium tin oxide-coated (10 nm) slides (1" x 3" x 1.1 mm, 10 Ohm/sq) were obtained from Nanocs (NY, USA). The slides were cut into 1 x 2 cm^2 pieces and sonicated in deionized water, ethanol, and acetone each for 20 minutes. Surfaces were then rinsed with ethanol and dried. In order to form SAMs on ITO, the slides were immersed in a 1 mM solution of 11-hydroxyundecylphosphonic acid in water for at least 16 hours. Once removed from solution, the surfaces were rinsed with ethanol and dried before use.

4.2.5 Electrochemistry. All electrochemical measurements were made using the Bioanalytical Systems Epsilon potentiostat. An Ag/AgCl electrode (Bioanalytical systems) was the reference, the gold monlayer or ITO SAM acted as the working electrode, and a Pt wire served as the counter electrode. The electrolyte was 1 M $HClO_4$ and the scan rate was 100 mV/s. All measurements were made in a standard electrochemical cell.

4.2.6 Ferrocene Immobilization. Either SAMs of tetra (ethylene glycol) undecane thiol or 1-mercaptoundecanol were oxidized using 300 μM PCC for up to 1h. Once the surfaces were oxidized to the corresponding aldehyde, the reaction was quenched with ethanol and ferrocene oxyamine was immobilized to the surface by adding 50 μL of 30 mM ferrocene oxyamine in ethanol (1 hr). Once the immobilization was complete, the surfaces were cleaned with acetone then ethanol. Cyclic voltammagrams were taken of the surface to determine the amount of ferrocene immobilized.

4.2.7 Patterned Oxidation of Alcohols to Aldehydes. A PDMS microchip was cleaned with ethanol and dried. It was then sealed reversibly to a SAM of 1-mercapto undecanol or 1-phosphono undecanol. The exposed alcohol groups were oxidized to aldehyde groups by flowing 300 μM PCC in acetonitrile and letting the solution react for up to 1h. Once the PCC had reacted with the surface, the reaction was quenched by flowing ethanol into the channels. The PDMS microchip was removed from the surface and the surface was cleaned with ethanol. 50 μL of 10 mM Alexa 488 oxyamine (Invitrogen) in ethanol was immobilized to the aldehyde groups by evaporating the ethanol from the surface.

4.2.8 Patterned Oxidation of Tetra (ethylene glycol) undecane thiol to Aldehydes. A PDMS microchip was cleaned with ethanol and dried. It was then sealed reversibly to a SAM of tetra (ethylene glycol) undecane thiol. The exposed alcohol groups were oxidized to aldehyde groups by flowing 100 μM PCC in acetonitrile for 5s. Once the PCC had reacted with the surface, the

reaction was quenched by flowing ethanol into the channels for another 5s. The PDMS microchip was removed from the surface and 40 μL of 10 mM GRGDS oxyamine in water was immobilized for 3h to the surface.

4.2.8 Patterned Mixed Surface by Microfluidic Oxidation of Alcohol-terminated SAMs. A PDMS microfluidic cassette was reversibly placed on an ITO surface containing a SAM of 11-hydroxyundecylphosphonic acid. A 300 mM solution of PCC in acetonitrile was flowed through the channels and allowed to react for 45 min. Without removing the cassette, the reaction was quenched, and the surface and cassette were cleaned by flowing ethanol through the channels. A solution of 4 mM Alexa 488-oxyamine (Invitrogen), 150 mM NHS, 150 mM DCC, and 7 mM Rhodamine (Invitrogen) in DMSO was allowed to react with the surface for 3h at 75°C. The reaction was then quenched by submerging the surface in DMSO and was rinsed with ethanol and dried.

4.2.9 Dual-Patterned Surface by Microfluidic Oxidation of Alcohol-terminated SAMs. A PDMS microfluidic cassette was reversibly placed on an ITO surface containing a SAM of 11-hydroxyundecylphosphonic acid. A 300 mM solution of PCC in acetonitrile was flowed through the channels and allowed to react for 45 min. Without removing the cassette, the reaction was quenched, and the surface and cassette were cleaned by flowing ethanol through the channels. With the cassette still in place, a solution of 4 mM Alexa 488-oxyamine in DMSO was flowed through the channels and allowed to react for 1h at 75°C. The reaction was quenched as previously stated, and the PDMS microfluidic cassette was removed. A different PDMS microfluidic cassette was reversibly sealed to the same ITO surface containing patterned Alexa 488-oxyamine and remaining SAM of 11-hydroxyundecylphosphonic acid. The immobilization procedure was repeated as stated, with the exception of PCC oxidation for 65 min followed by

reaction with a solution of 150 mM NHS, 150 mM DCC, and 7 mM Rhodamine in DMSO for 3h at 75°C.

4.2.10 Ferrocene-Oxyamine and Dopamine Immobilization on ITO. Surfaces containing SAMs of 11-hydroxyundecylphosphonic acid were oxidized using a 300 mM solution of PCC in acetonitrile for either 15 min to generate aldehyde head-groups or 65 min to generate carboxylic acid head-groups. Surfaces were then rinsed with ethanol and dried. A 30 mM solution of ferrocene-oxyamine in ethanol was allowed to react on the aldehyde surface for 20 min at 40°C. To immobilize dopamine, a solution of 150 mM N-hydroxysuccinimide (NHS), 150 mM dicyclohexyl carbodiimide (DCC), and 300 mM dopamine in DMSO was left to react on the surface for 16h at room temperature. Once the immobilization was complete, the surfaces were rinsed with ethanol and dried before verification by cyclic voltammetry.

4.2.11 Microscopy of Surface Immobilized Alexa 488 and Cells. Scotch tape (3M) was adhered to the monolayer and then cured at 70 °C for 20 min. The tape was peeled from the substrate, resulting in transfer of the monolayer from the gold substrate to the tape and visualized. Fluorescent and brightfield microscopy was performed using a Nikon TE2000E inverted microscope. Image acquisition and processing was done using Metamorph software.

4.2.12 Contact Angle Measurement. Both $HOC_{11}SH$ and $EG_4C_{11}SH$ SAMs were oxidized for 1h with 300µM PCC in acetonitrile. ITO surfaces containing SAMs of 11-hydroxyundecylphosphonic acid were oxidized with 300 mM PCC in acetonitrile ranging from 0 to 65 min. Along with untreated $HOC_{11}SH$ and $EG_4C_{11}SH$ SAMs, the static contact angle was measured using 10 µL drops of H2O with KSV CAM 200.

4.2.13 X-Ray Photoelectron Spectroscopy (XPS). HOC11SH and EG4C11SH SAMs were oxidized for 1h with 300 µM PCC in acetonitrile. To immobilize ligands on the surface, 50 µL of 30 mM ferrocene oxyamine in ethanol was allowed to react at 40 °C for 1 hr. Ferrocene-oxyamine,

dopamine, and mixed functionalized ITO SAMs were prepared as previously described. XPS measurements were taken with a Kratos Axis Ultra DLD of the oxidized $HOC_{11}SH$ and $EG_4C_{11}SH$ SAMs with and without immobilized ferrocene oxyamine. A mono Al anode source was used with a specific excitation energy of 1486.6 eV and a 80 eV pass energy was used for the high resolution scans. All binding energies are reference to the C 1s of a saturated hydrocarbon at 284.7 eV.

4.2.14 11-hydroxyundecylphosphonic acid $(H_2O_3PC_{11}OH$, **1**)*:2-(11-bromoundecyloxy)tetrahydro-2H-pyran (3)* To a solution of **2** (4.00 g, 15.9 mmol) in THF (40 mL) was added dihydropuran (6.54 mL, 71.1 mmol) and HCl (3 drops). The reaction was stirred under inert atmosphere (N_2) for 12h and was then washed with sodium bicarbonate (3x25mL) and brine (1x25mL). The mixture was purified by flash chromatography (9:1 Hex:EtOAc) and concentrated to afford a colorless oil **3** (4.84 g, 91%). ^1H NMR (400 Hz, $CDCl_3$, δ): 4.58 (t, 1H, J=8; CH), 3.86-3.75 (m, 2H, J=7; CH_2), 3.52 (m, 1H, J=8; CH), 3.41-3.38 (m, 3H, J=7; CH, CH_2), 1.87-1.84 (m, 3H, J=7; CH, CH_2), 1.58 (m, 1H, J=8; CH), 1.55 (m, 6H, J=7; CH_2), 1.43-1.40 (m, 2H, J=7; CH_2), 1.29 (m, 12H, J=7; CH_2).

4.2.15 diethyl 11-(tetrahydro-2H-pyran-2-yloxy)undecylphosphonate (4) To a solution of **3** (3.24 g, 9.66 mmol) in neat triethylphosphite (9.85 mL, 53.1 mmol) was refluxed at 110°C under inert atmosphere (N2) for 12h. The mixture was concentrated and purified by flash chromatography (1:1 Hex:EtOAc, eluted 3 with 100% MeOH) to afford a colorless oil **4** (2.98 g, 74%). ^1H NMR (400 Hz, $CDCl_3$, δ): 4.57 (t, 1H, J=7; CH), 3.83-3.81, (q, 4H, J=9; CH_2), 3.72-3.68 (m, 2H, CH_2), 3.48-3.39 (m, 2H, J=7; CH_2), 1.81 (m, 1H, J=9; CH), 1.68-1.59 (m, 3H, J=8; CH, CH_2), 1.53-1.52 (m, 7H, J=11, J=7; CH, CH_2), 1.32-1.30 (m, 18H, J=7; CH_2, CH_3).

4.2.16 diethyl 11-hydroxyundecylphosphonate (5) To solution of acetic acid, water, and THF (3:1:1 30mL, 10mL, 10mL) was added **4** (0.800 g, 2.00 mmol). The mixture was stirred under inert atmosphere (N_2) for 16h. After completion, the mixture was concentrated, diluted with

EtOAc, and washed with 0.01 M NaOH (3x25mL) to afford a colorless oil **5** (0.379 g, 61%). ^{1}H

NMR (400 Hz, CDCl$_3$, δ): 4.09-4.05 (q, 4H, J=9; CH$_2$), 3.62-3.59 (t, 2H, J=7; CH$_2$), 2.55 (s, 1H; O-H),

1.70-1.66 (m, 2H, J=8; CH$_2$), 1.56-1.53 (m, 4H, J=7; CH$_2$), 1.32-1.26 (m, 18H, J=7, J=7; CH$_2$, CH$_3$).

*11-hydroxyundecylphosphonic acid (1)*To a solution of **5** (0.379 g, 0.12 mmol) in dry CH2Cl2

(15mL) was added trimethylbromosilane (0.50 mL, 3.6 mmol). The mixture was stirred under

inert atmosphere (N$_2$) for 6h. After completion, the mixture was concentrated and stirred with

MeOH (20mL) under N$_2$ for 2h. The mixture was then concentrated to a colorless oil and

recrystallized with acetone to afford a white solid **1** (0.288 g, 93%). ^{1}H NMR (400 Hz, MeOD, δ):

3.51 (t, 2H, J=7; CH$_2$), 1.82-1.80 (m, 2H, J=7; CH$_2$), 1.58-1.48 (m, 6H, J=8; CH$_2$), 1.30 (m, 12H, J=7;

CH$_2$); HRMS (ESI, m/z): [M-H] calcd for C$_{11}$H$_{25}$O$_4$P, 252.2876; found, 251.1.
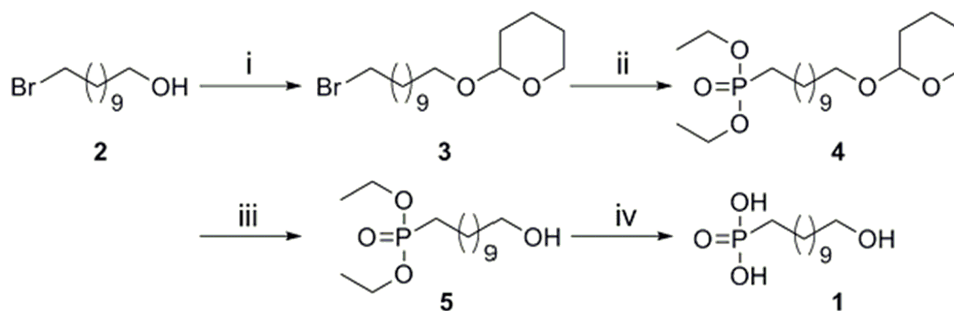
Scheme 4.1. Synthesis of 11-hydroxyundecylphosphonic acid. Reagents and conditions:(i)
dihydropuran, HCl, THF, rt, 12 h; (ii) triethylphosphite, 110°C, 12 h; (iii) 3:1:1 AcOH:THF:H$_2$O, rt,
16 h; (iv) bromotrimethylsilane, DCM, rt, 6 h.

4.3 Results and Discussion

4.3.1 Procedure Outline. The strategy to oxidize alcohol terminated SAMs on gold to generate

terminal aldehyde groups with spatial and density control is outlined below (Figure 4.1). A

polydimethylsiloxane (PDMS) microfluidic cassette was reversibly sealed to a gold surface with

a SAM of tetra (ethyleneglycol) undecane thiol (EG$_4$C$_{11}$SH) or 11-mercapto-1-undecanol

(HOC$_{11}$SH) to achieve spatial control. PCC (300 μM in acetonitrile) was flowed into the

microfluidic cassette and allowed to react with the surface for up to 1h to generate aldehydes in

the microchannels. The resulting aldehyde pattern was a 2D projection of the microchannels on the SAM surface. To tailor the surface with a variety of functional groups and ligands, a number of different oxyamine ligands were chemoselectively reacted with the aldehydes to generate covalent oxime linkage surfaces.
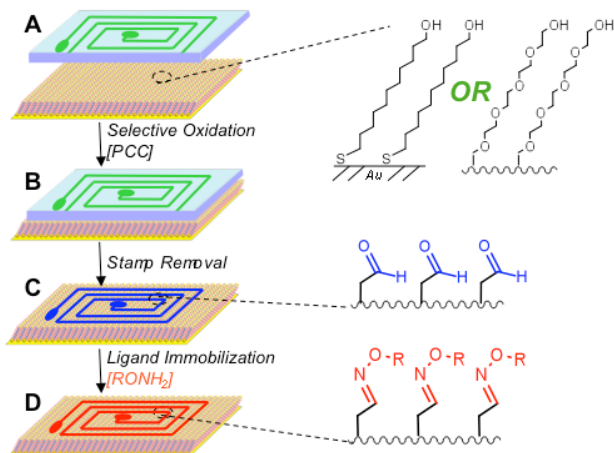
Figure 4.1. Schematic for the generation of patterned aldehydes by microfluidic oxidation of $C_{11}OH$ and $EG_4C_{11}SH$ SAMs. (A) A PDMS microchip was reversibly sealed to an alcohol terminated self- assembled monolayer. (B) To selectively and rapidly oxidize the exposed terminal alcohol groups in the microchannels to aldehydes, a mild oxidant PCC in acetonitrile was flowed through the channels. (C) The PDMS microchip was removed and the resulting aldehyde pattern represented the 2D projection of the microchannels on the surface. (D) To functionalize the surface, oxyamine-terminated ligands (R-ONH$_2$) were reacted to the exposed aldehyde groups to generate an interfacial oxime conjugate.

4.3.2 Contact angle Measurements. Alcohol oxidation was investigated by measuring the static contact angle of water on the surface. (Table 4.1) Conditions favoring aldehyde generation correspond to higher contact angles for both $HOC_{11}SH$ and $EG_4C_{11}SH$, indicating that there was a uniform increase in hydrophobicity on the surface. This result was expected as the aldehyde group is more hydrophobic than the alcohol group.

4.3.3 XPS Measurements. XPS was also performed to examine the amide and oxime nitrogen bound to the SAM on the surface. Alcohol-terminated SAMs were oxidized for 1h, ferrocene-oxyamine. (Figure 4.2) The nitrogen 1s peak representing the oxime linkage between ferrocene-oxyamine and aldehydes was observed at 398 eV. Controls including unoxidized

SAMs of mercaptoundecanol and $EG_4C_{11}SH$. Oxidized SAMs without ferrocene immobilization were scanned and no nitrogen was observed.
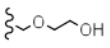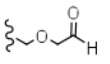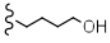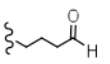
SAM	Ave.Contact Angle (°)	Std. Dev. (±°)
(1)	31.6	1.30
(2)	43.6	1.84
(3)	26.1	3.70
(4)	54.7	2.67

Table 4.1. Contact angle data for the oxidation of alcohol to aldehyde for both $HOC_{11}SH$ and $EG_4C_{11}SH$ SAMs. The blue box indicates the unoxidized and oxidized $EG_4C_{11}SH$ and the red box indicates the unoxidized and oxidized $HOC_{11}SH$. The contact angle increased with the oxidation of the alcohol to aldehyde indicating an increase in hydrophobicity. For $EG_4C_{11}SH$, the change was 12 degrees and for $HOC_{11}SH$, the angle change was 28.6 degrees. n=5 for each measurement. Parenthesis refer to structure number of molecule in the above structure list.
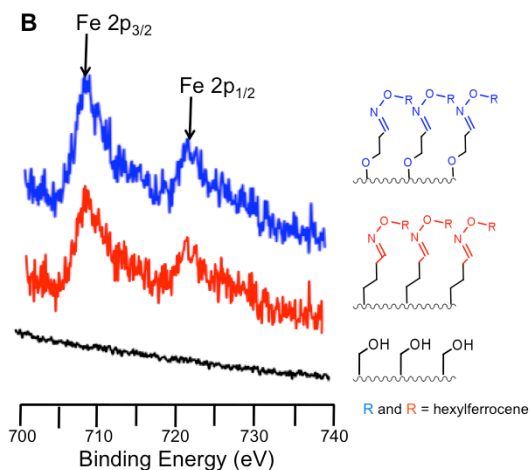
Figure 4.2. X-ray Photoelectron Spectroscopy (XPS) data of ferrocene oxyamine immobilized to oxidized $HOC_{11}SH$ and $EG_4C_{11}SH$ SAMs. A) The characteristic nitrogen peak appears only after immobilization of the oxyamine to the surface of both $HOC_{11}SH$ (red) and $EG_4C_{11}SH$ (blue) and does not appear in either $HOC_{11}SH$ or $EG_4C_{11}SH$ (black). B) The iron in ferrocene appears only after ferrocene immobilization (red and blue) and is not present in oxidized monolayer for either surface (black).

4.3.4 Electrochemical Measurements. To characterize and quantify the surface conversion from hydroxy to aldehyde-terminated surfaces, we used cyclic voltammetry (CV). A redox active ferrocene oxyamine was synthesized (**4**) and reacted with newly formed aldehyde

surfaces generated from hydroxy surfaces exposed to different oxidative durations. When the ferrocene oxyamine reacted with the oxidized $EG_4C_{11}SH$ and $HOC_{11}SH$ surfaces, CV characterization reveals distinct redox peaks at 221 and 210 mV (Figure 4.3). With increasing oxidative reaction times, the ferrocene signal increased due to more aldehyde groups generated on the surface. By integrating the area under the redox peaks, the precise amount of ferrocene, and therefore aldehyde generated on the surface could be determined. First, the theoretical charge (Q) generated from a 100% converted surface was calculated using $Q = nFA\Gamma$ (Q represents total charge, n = mols of electrons (1), F = Faraday's constant, Γ = molecules per surface area) and determined to be 16.1 $\mu C/cm^2$ for a 1 cm^2 surface (1×10^{14} molecules/cm^2) for a complete SAM. Next, the SAM area exposed to electrolyte solution and subsequent ferrocene immobilization was measured at different PCC exposure durations.

By determining the amount of charge for complete conversion from theory and actual charge measured, the yield of the surface reaction (aldehyde production) versus PCC exposure time could be calculated. The data was fitted to a pseudo first order rate profile and the rate constant (k') was calculated to be 0.032 min^{-1} for the $EG_4C_{11}SH$ surface and 0.046 min^{-1} for the HOC11SH surface. By varying the reaction times, the density of aldehydes and therefore ligands on the surface could be precisely controlled. Both hydroxy terminated surfaces could be converted completely to the aldehyde within 1h.

4.3.5 Cell and Ligand Patterning. To demonstrate ligand patterning, a spiral microchip was used to control oxidative PCC fluid flow to a $HOC_{11}SH$ surface for 45 min. The resulting patterned aldehyde surface was reacted with a fluorescent Alexa 488 oxyamine dye and imaged by fluorescence microscopy (Figure 4.4A). The fluorescent pattern shows no line width broadening and replicates with high fidelity the microchannel patterns
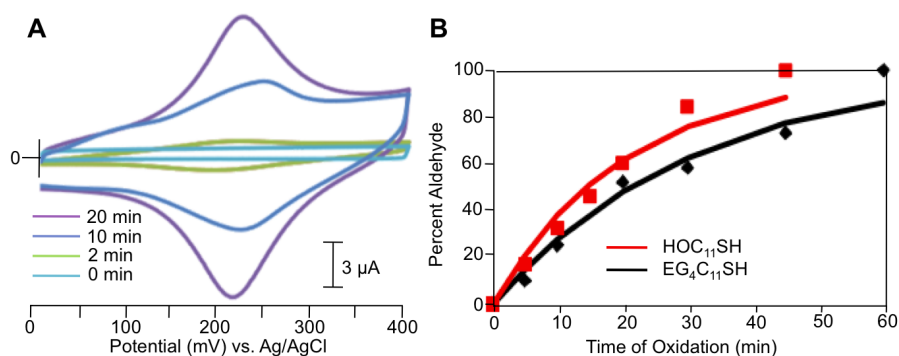
Figure 4.3. Characterization of aldehyde generation on $EG_4C_{11}SH$ and $HOC_{11}SH$ surfaces. (A) Cyclic voltammagrams of ferrocene oxyamine immobilized to a $EG_4C_{11}SH$ surface. Increasing PCC reaction times generated more aldehyde groups and resulted in more ferrocene oxyamine immobilization to the surface. (B) Aldehyde conversion vs. Oxidation time plot for both $EG_4C_{11}SH$ and $HOC_{11}SH$ surfaces. The percent aldehyde was determined by taking the area under the CV peaks for the ferrocene immobilization. The data was fit to a pseudo first order rate profile and the rate constant for aldehyde generation was 0.032 min^{-1} for the $EG_4C_{11}SH$ and 0.046 min^{-1} for the $HOC_{11}SH$.
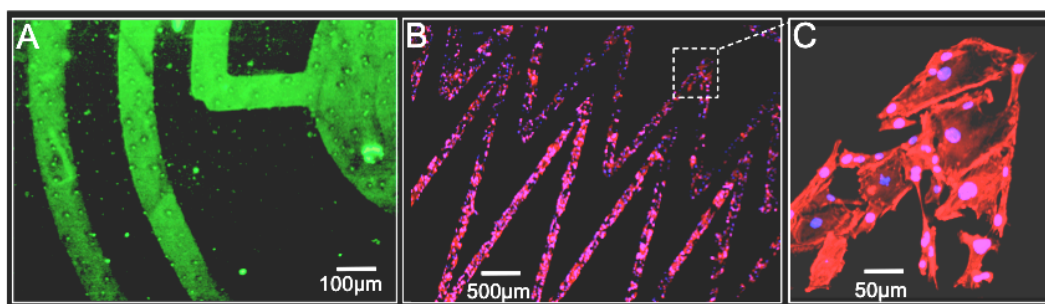
Figure 4.4. Fluorescent micrographs of patterned ligands and cells from microfluidic oxidation of $HOC_{11}SH$ and $EG_4C_{11}SH$ surfaces to generate aldehydes for chemoselective immobilization. (A) A $HOC_{11}SH$ surface was oxidized via a spiral pattern microchip and reacted with Alexa 488 oxyamine. (B) $EG_4C_{11}SH$ SAMs were oxidized with a triangle wave pattern microchip and subsequently reacted with the biospecific cell adhesive peptide RGD oxyamine. Fibroblast cells adhered specifically to the RGD patterns. The cells were visualized by staining the nucleus (DAPI) and actin (Phalloidin). (C) A higher magnification image of the cells present on the oxidized $EG_4C_{11}SH$ surface.

For biological applications, we used hydroxy terminated $EG_4C_{11}SH$ surfaces, which prevent non-specific protein adsorption. A microchip was sealed to the $EG_4C_{11}SH$ surface and 100 µM PCC in acetonitrile was flowed into the channels for 5s. These conditions caused only a small fraction of the exposed alcohol groups to be oxidized to the aldehydes in order for the surfaces to retain their ability to resist non-specific protein adsorption. For biospecific cell adhesion, we

immobilized a RGD-oxyamine peptide[11] to the surface and seeded Swiss 3T3 fibroblasts. The cells adhered to the oxidized regions where the RGD was present and became confluent. Cells were visualized by staining for nucleus and actin (Figure 4.4B and 4.4C). As controls, non-oxidized surfaces and scrambled RDG peptide immobilization showed no cell attachment.

4.3.6 Alcohol Oxidation Procedure on ITO. After, characterizing the oxidation on gold SAMs, the procedure was extended to SAM on ITO. The general schematic illustrating the oxidative activation of SAMs on ITO with controlled generation of aldehyde and carboxylic acid head-groups for subsequent chemoselective ligation is displayed in Figure 4.5. Following SAM formation of 11-hydroxyundecylphosphonic acid ($H_2O_3PC_{11}OH$,1), Scheme 4.1, on ITO, a polydimethylsiloxane (PDMS) microfluidic cassette was reversibly sealed to the substrate. PCC (300 mM in acetonitrile) was then flowed through the microchannels and allowed to oxidize the alcohol-terminated SAM. Dependent on the oxidative duration, surface alcohols could either be converted to aldehydes (15 min) or carboxylic acids (65 min). After aldehyde generation, oxyamine-containing ligands were chemoselectively immobilized to the surface resulting in a covalent oxime bond. When exposed to PCC for 65 min, amide linkages were formed from reaction of acid head-groups with amine-containing ligands in the presence of N-hydroxysuccinimide (NHS) and dicyclohexyl carbodiimide (DCC). Thus, a single alcohol SAM composition could be chemically altered with the same oxidant and concentration to generate two different orthogonal chemoseletive strategies followed by ligand immobilization.

4.3.7 Contact Angle Measurements of ITO SAMs. Alcohol oxidation was investigated by measuring the static contact angle of water on the surface. (Table 4.2) Conditions favoring aldehyde generation correspond to larger contact angles than conditions forming acids, as well as starting $H_2O_3PC_{11}OH$ SAMs, indicating that there was a uniform increase in hydrophobicity on the surface. On ITO, acids can be formed by the harsher oxidation conditions required for

transformation from starting alcohols without monolayer desorption. A similar oxidation method was performed on gold surfaces containing SAMs of 11-mercapto-1-undecanol using PCC concentrations lower by 1000-fold, resulting solely in aldehydes. Higher concentrations or oxidizing durations longer than 70 min appeared to etch the gold and destroy the monolayer. Therefore, carboxylic acid formation is compatible with alcohol-terminated SAMs on ITO but not SAMs of alkanethiols on gold, presumably due to the greater stability of the ITO-phosphonate bond.
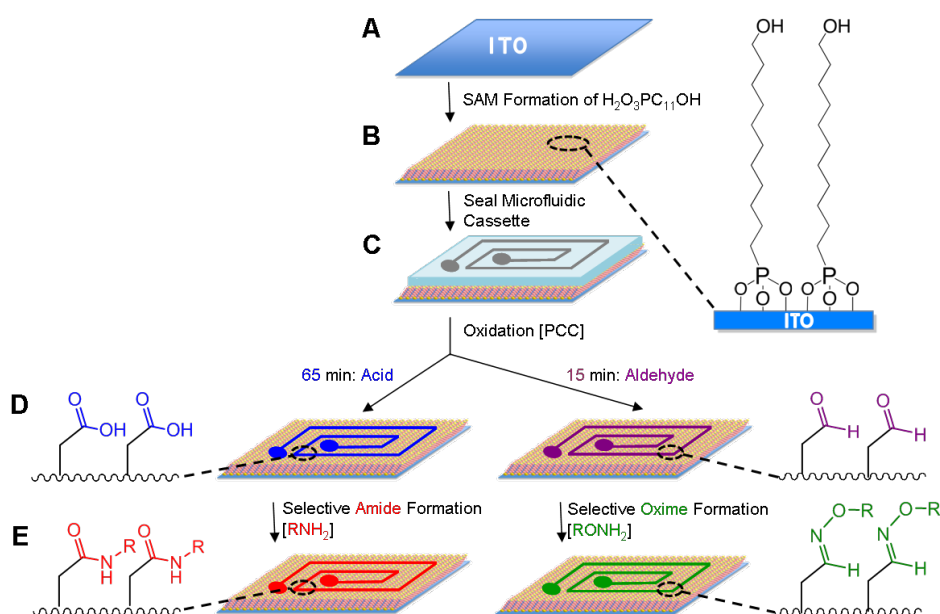
Figure 4.5. Schematic for the oxidative activation of $H_2O_3PC_{11}OH$ SAMs on ITO with controlled generation of aldehyde and carboxylic acid head-groups for subsequent chemoselective ligation. (A) An ITO substrate was sonicated in water, ethanol, and acetone. (B) In order to form a self-assembled monolayer, the substrate was submerged in a solution of $H_2O_3PC_{11}OH$ in water (16h). (C) A microfluidic cassette was reversibly sealed to the surface, and PCC, a mild oxidant, in acetonitrile was flowed through the microchannels in order to convert the alcohol-terminated SAM to aldehyde (15 min) or carboxylic acid head-groups (65 min). (D) After stamp removal, the patterned microchannels represented a 2D projection of aldehydes or acids on the surface. (E) For chemoselecitve immobilization of ligands to aldehyde- or acid-terminated surfaces, oxyamine- ($RONH_2$) or amine- (RNH_2) containing ligands, respectively, were allowed to react on the surface and immobilized only to the oxidized regions. The resulting oxime and amide conjugates represented as a 2D projection of the microchannels.
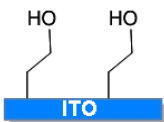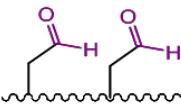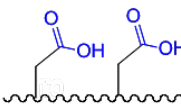
Surface Group			
Contact Angle (°)	33.9 ± 0.40	52.9 ± 0.80	22.0 ± 2.0

Table 4.2. Contact angle measurements of alcohol-, aldehyde-, and carboxylic acid-terminated surface-groups on ITO.

4.3.8 Electrochemical Measurement of ITO SAMs. To verify that both aldehydes and acids were being generated from the same alcohol-terminated SAM on ITO, cyclic voltammetry (CV) was performed. Figure 4.6 shows CV data from surfaces that have been oxidized with conditions for aldehyde (300 mM PCC, 15 min) and acid (300 mM PCC, 65 min) generation, as well as a mixed aldehyde and acid surface (300 mM PCC, 45 min). Electroactive ferrocene-oxyamine (30 mM in ethanol, 40°C, 20 min) and dopamine (300 mM in DMSO, 16h) with NHS/DCC (150 mM) were immobilized to substrates following oxidation. Distinctive redox peaks at 230 and 270 mV for ferrocene-oxyamine, and 360 and 730 mV for dopamine were seen from the resultant covalent oxime and amide linkages, respectfully. As a control, dopamine was immobilized to surfaces oxidized for 15 min, and ferrocene-oxyamine was reacted on substrates that had been exposed to PCC for 65 min. Redox peaks were not present when scanned, indicating that no ligand immobilization occurred. Therefore, oxidation over the substrate can be controlled to generate aldehydes, acids, as well as a mixture of the two. Also, immobilization of oxyamine- and amine-containing ligands can be carried out independently or on the same surface.

Figure 4.6. Electrochemical characterization of ferrocene-oxyamine and dopamine immobilized to aldehydes and acids generated on SAMs of $H_2O_3PC_{11}OH$. (A) A CV of ferrocene-oxyamine (green) with distinctive redox peaks of 230 and 270 mV chemoselectively immobilized to aldehyde head-groups generated from oxidation of $H_2O_3PC_{11}OH$ on ITO. (B) A CV of dopamine (red) with distinctive redox peaks of 360 and 730 mV chemoselectively immobilized to acid head-groups generated from oxidation of $H_2O_3PC_{11}OH$ on ITO. (C) A mixed surface containing both electroactive ligands immobilized to both aldehyde and acid head-groups after oxidation of $H_2O_3PC_{11}OH$ on ITO.

4.3.9 XPS Measurements on ITO SAMs. XPS was also performed to examine the amide and oxime nitrogen bound to the SAM on the surface. Alcohol-terminated SAMs on ITO were oxidized for 15, 45, and 65 min, followed by subsequent selective immobilization of ferrocene-oxyamine and dopamine. (Figure 4.7) The nitrogen 1s peak representing the oxime linkage between ferrocene-oxyamine and aldehydes was observed at 398 eV, corresponding to data as seen with gold SAMs.[15] Likewise, the nitrogen 1s peak of the amide resultant from conjugation of dopamine to acid was observed at 400 eV. This peak was compared with the XPS data produced by dopamine immobilization to SAMs of carboxylic acid-terminated phosphonate (Fluka) on ITO and was found to be the same. Also, substrates were oxidized for 45 min,

generating mixed aldehyde and acid surfaces, followed by immobilization of ferrocene-oxyamine and dompamine ligands. Again, the nitrogen 1s peaks appeared at 398 and 400 eV, respectively, verifying that both ligands were immobilized on the same substrate. Controls including unoxidized SAMs of $H_2O_3PC_{11}OH$ on ITO, dopamine immobilization onto surfaces that had been oxidized for 15 min, and ferrocene-oxyamine onto substrates with exposure to PCC for 65 min, showed no nitrogen present.
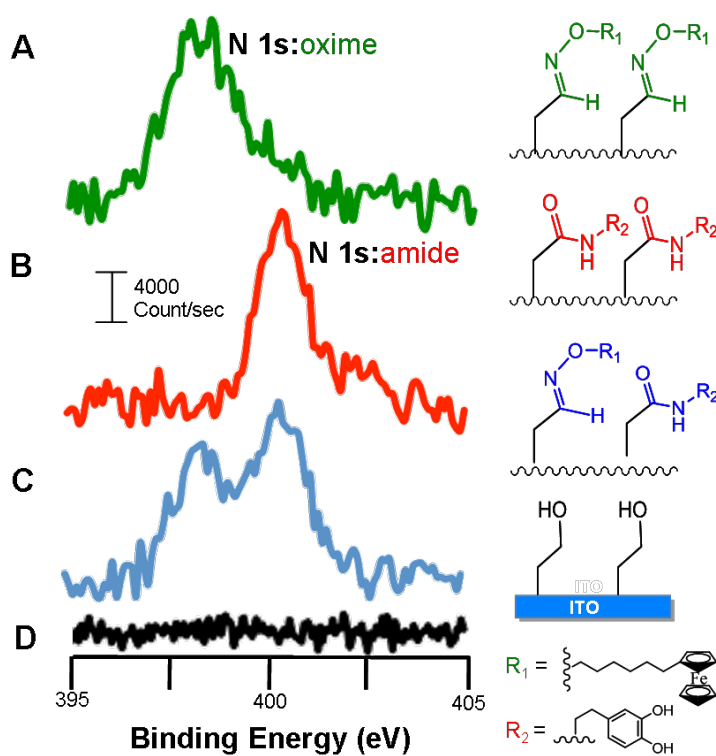
Figure 4.7. XPS characterization of oxime and amide bonds on ITO. Surfaces containing SAMs of $H_2O_3PC_{11}OH$ were oxidized with controlled generation of aldehyde or carboxylic acid head-groups for subsequent chemoselective ligation, and XPS measurements were performed. (A) The nitrogen 1s peak observed at 398 eV which corresponds to the oxime nitrogen of ferrocene-oxyamine immobilized on ITO. (B) The nitrogen peak observed at 400 eV which corresponds to the amide nitrogen of dopamine immobilized on ITO. (C) A mixed surface of ferrocene-oxyamine and dopamine ligands, showing both nitrogen peaks of oxime and amide bonds, respectively. (D) An unoxidized ITO surface containing a SAM of $H_2O_3PC_{11}OH$ showing no nitrogen present.

97

4.3.10 Dual Immobilization to ITO SAMs. To exhibit the diversity in performing this dual-orthogonal strategy to spatially control the immobilization of the oxyamine- and amine-containing ligands on ITO, fluorescent compounds were patterned by microfluidics and then visualized by fluorescence microscopy (Figure 4.8). A microfluidic cassette with separate channels was reversibly sealed to an ITO surface containing SAMs of $H_2O_3PC_{11}OH$, and oxidation with PCC was carried out as previously described. (Figure 4.9) Following oxidation, a mixture of Alexa 488-oxyamine and Rhodamine were allowed to react on the surface. When imaged, the immobilized fluorescent dyes produced a 2D-projection of the microchannels, and patterns of oxime (green), amide (red), and a mixture of oxime and amide (yellow) conjugates were seen. More specifically, both carboxylic acids and aldehydes were generated with spatial control on an ITO substrate. PCC was allowed to react in the microchannels for 45 min resulting in mixture of acids and aldehydes projected from the surface. Rhodamine (7 mM in DMSO, 3h, 75°C) followed by Alexa 488-oxyamine (4 mM in DMSO, 1h) were immobilized. In addition, a single substrate displayed in Figure 5 with a pattern of two dyes: Alexa 488-oxyamine (A, green), rhodamine (B, red), with a superimposed image showing the same mixed region (C, yellow).
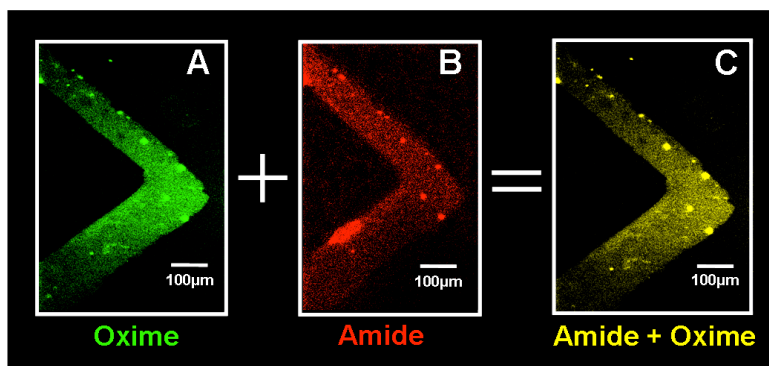
Figure 4.8. Fluorescent micrographs of a mixed aldehyde and acid surface patterned by microfluidic oxidation followed by chemoselective oxime and amide immobilization. Ligands were imaged directly on the surface. (A) Alexa 488-oxyamine immobilized to aldehyde surface-groups proceeding microfluidic oxidation with PCC in acetonitrile. (B) Rhodamine immobilized to acid surface-groups proceeding microfluidic oxidation of the same pattern. (C) A combined image of the pattern visualizing a mixed surface containing both oxime and amide conjugates.
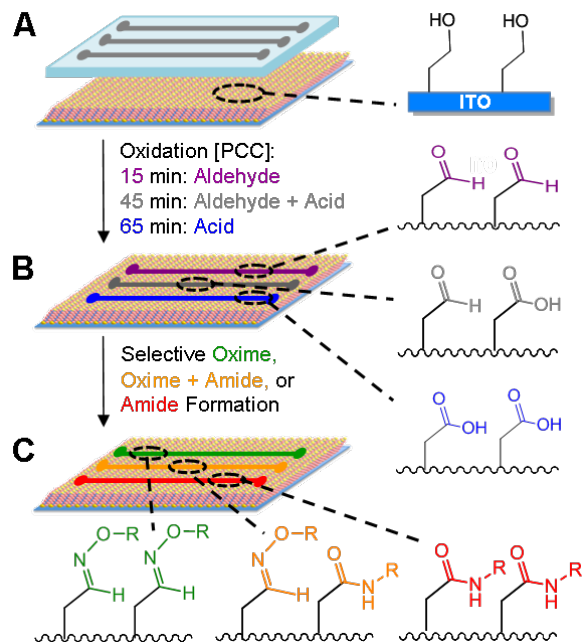
Figure 4.9. Schematic for the oxidative activation of $H_2O_3PC_{11}OH$ SAMs on ITO for controlled generation of aldehyde, carboxylic acid, and a mixed surface of both aldehyde and acid head-groups for subsequent chemoselective ligation. (A) A microfluidic cassette with separate channels was reversibly sealed to an ITO surface containing SAMS of $H_2O_3PC_{11}OH$. (B) PCC in acetonitrile was flowed through the microchannels in order to convert the alcohol-terminated SAM to aldehyde (15 min), mixed aldehyde and acid (45 min), or acid head-groups (65 min). (C) To functionalize the surface, oxyamine-, amine-, and a mixture of oxyamine- and amine-containing ligands were chemoselectively immobilized to regions presenting aldehyde, acid, or a mixture of aldehydes and acids on the surface.

4.3.11 Dual Ligand Patterning on ITO SAMs. Alternatively, spatially controlled generation of aldehydes and carboxylic acids independently is also compatible with using different microfluidic cassettes for patterning ligands on the same surface (Figure 4.10). Beginning with one cassette on a SAM of $H_2P_3OC_{11}OH$, substrates were oxidized for 45 min in order to generate both aldehydes and acids, followed by immobilization of Alexa 488-oxyamine within the microchannels (4 mM in DMSO, 1h, 75°C). The Alexa 488-oxyamine immobilized to aldehydes present, resulting in a clear projection of the pattern. After cleaning and removing the cassette, a different cassette was reversibly sealed to the surface, and PCC was left to react for 65 min in order to generate acids for subsequent rhodamine immobilization within the channels (7 mM in DMSO, 3h, 75°C). Rhodamine immobilized to the newly formed acids, in

addition to the acids patterned in overlapping regions that were generated by the first oxidation. When visualized using fluorescence microscopy, two distinct oxime (green, Figure 4.10A) and amide (red, Figure 4.10B) patterns were observed, with overlapping regions containing a mixture of both oxime and amide conjugated ligands (yellow, Figure 4.10C).
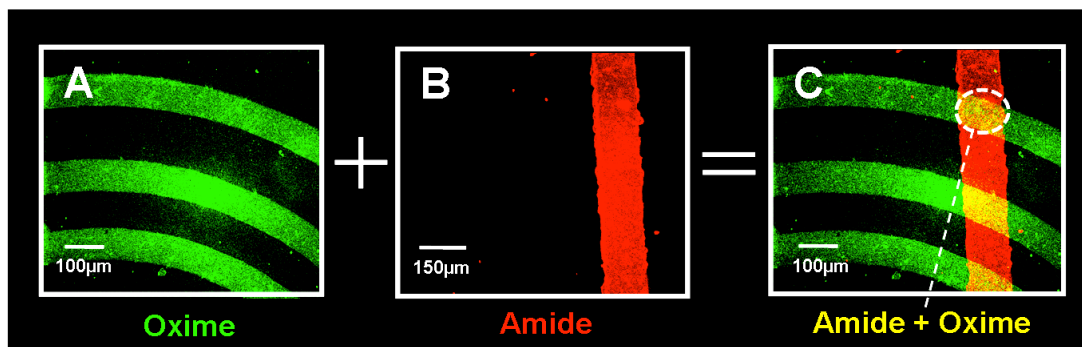

Figure 4.10. Fluorescent micrographs of an aldehyde and acid surface dually-patterned by microfluidic oxidation followed by chemoselective oxime and amide immobilization. (A) Immobilized Alexa 488-oxyamine after selective microfluidic oxidation conditions to generate aldehyde surface-groups in a spiral pattern. (B) Immobilized Rhodamine in a bar pattern after selective microfluidic oxidation to generate acid surface-groups in the same region. (C) A combined image of the region displaying a dual-patterned surface containing both oxime and amide conjugates, as well as the overlap upon mixing.

4.4 Conclusions

In conclusion, we show a flexible and inexpensive strategy to generate patterned aldehydes for subsequent chemoselective immobilization. Furthermore, varying the oxidative reaction time could control the density of terminal aldehydes. For biological applications, patterned aldehydes were generated from inert ethylene glycol alkanethiol SAMs on gold. Futhermore, the strategy was extended to SAMs on ITO. Aldehyde and carboxylic acid surface-groups were generated by oxidation of alcohol-terminated SAMs followed by immobilization and characterization of a variety of oxyamine- and amine-containing compounds. Microfluidic patterning provides spatial control of aldehydes and acids on the surface, as well as resulting oxime and amide conjugates, respectively. Taking advantage of the robust, conductive, and transparent nature of ITO and gold, oxime and amide linkages were characterized by CV, XPS,

and fluorescence microscopy. Having the ability to spatially control and pattern the generation of mixed acids and aldehydes for subsequent immobilization of ligands containing different functionalities would greatly benefit research fields such as cell biology and molecular electronics. Future works include exploring the means to pattern and study co-cultures of cells as well as enzymatic activity when encountering biomolecules such as peptides and carbohydrates.

4.5 References

1. Hoover, D.K.; Lee, E.-J. Chan, E.W.L.; Yousaf, M. N. *ChemBioChem*. **2007**, *16*, 1920-1923.

2. Hoover, D.K.; Chan, E.W.L.; Yousaf, M.N. *J. Am. Chem. Soc.* **2008**, *130*, 3280-3281.

3. Vuillaume, D.; Lenfant, S. *Microelec. Engin.* **2003**, *70*, 539-550.

4. Watzke, A.; Kohn, M.; Wacker, R.; Schroder, S.L.; Waldmann, H. *Angew. Chem. Int. Ed.* **2006**, *45*, 1408-1412.

5. Zhang, Y.; Wang, P.G. *Anal. Chem.* **2006**, *78*, 2001-2008.

6. Houseman, B.T.; Gawalt, E.S.; Mrksich, M. *Langmuir,* **2002**, *19,* 1522-1531.

7. Lahiri, J.; Isaacs, L.; Tien, J.; Whitesides, G. M. *Anal. Chem.* **1999**, *71*, 777.

8. Yousaf, M.N.; Houseman, B.T.; Mrksich, M. *Angew. Chem.* **2001**, *113*, 1127-1130.

9. Yousaf, M. N.; Mrksich, M. *J. Am. Chem. Soc.* **1999**, *121*, 4286.

10. Yousaf, M.N.; Houseman, B.T.; Mrksich, M. *Proc. Natl. Acad. Sci. USA*, **2001**, *98*, 5992-5996.

11. Chan, E.W.L.; Yousaf, M.N. *J. Am. Chem. Soc.* **2006**, *128,* 15542-15546.

12. Chan, E.W.L.; Yousaf, M.N. *ChemPhysChem* **2007**, *8*, 1469-1472.

13. Park, S.; Yousaf, M.N. *Langmuir* **2008**, *24*, 6201-6207.

14. Westcott, N.P.; Yousaf, M.N. Langmuir 2008, 24, 2261-2265.

15. Lamb, B.M.; Barette, D.G.; Westcott, N.P.; Yousaf, M.N. *Langmuir* **2008**, 16, 8885–8889.

16. Jang, C.-H.; Stevens, B.D.; Phillips, R.; Calter, M.A.; Ducker, W. A. *Nano Lett.* **2003**, *3*, 691-694.

17. Peelen, D.; Smith, L.C. *Langmuir.* **2005,** *21,* 266-271.

18. Hahn, C.D.; Holzl, M. *Bioconjugate Chem.* **2007,** *18*, 247-253.

19. Delamarche, E.; Michel, B.; Kang. H.; Gerber, C. *Langmuir.* **1994,** *10*, 4103-4108.

20. Kandere-Grzybowski, K.; Cambell, C.; Komarova, Y.; Grzybowski, B. A.; Borisy, G. G. *Nat. Meth.* **2005,** *2*, 739-741.

21. Tosatti, S.; Textor, M. M.; Spencer, N. D. *Langmuir*, **2002**, *18,* 3537-3548.

22. Hofer, R.; Textor, M.; Spencer, N. D. *Langmuir*, **2001,** *17*, 4014-4020.

23. Zhu, F.; Zhang, K.; Guenther, E.; Jin, C. S. *Thin Solid Films*, **2000**, *363*, 314-317.

24. Zhu, F.; Jennings, P.; Cornish, J.; Hefter, G.; Luczak, K. *Sol. Energy Mater. Sol. Cells.* 1997**,** *49*, 163-169.

25. Choi, C. K.; Margraves, C. H.; Jun, S. I.; English, A. E.; Rack, P. D.; Kihm, K. D. *Sensors*, **2008**, *8*, 3257-3270.

26. Curreli, M.; Li, C.; Sun, Y.; Lei, B.; Gundersen, M. A.; Thompson, M. E.; Zhou, C. *J. Am. Chem. Soc.* **2005**, *127*, 6922-6923.

27. Mrksich, M.; Whitesides, G. M. *Annu. Rev. Biophys. Biomol. Struct.* **1996**, *25*, 55-78.

28. Gnauck, M.; Jaehne, E.; Blaettler, T.; Tosatti, S.; Textor, M.; Alder, H.-J. P. *Langmuir*, **2007,** *23*, 377-3^{81}.

29. Horton Jr., R.C.; Herne, T.M.; Myles, D.C. *J. Am. Chem. Soc.* **1997,** *119,* 12980-12981.

30. M. Hunsen, *Synthesis*, **2005**, 2487-2490.

Reproduced with Permission from the American Chemical Society

Westcott, N. P.; Pulsipher, A.; Lamb, B. M.; Yousaf, M. N. *Langmuir* **2008**, *24*, 9237-9240.

Pulsipher, A.; Westcott, N. P.; Luo, W.; Yousaf, M. N. *J. Am. Chem. Soc.* **2009**, *131*, 7626-7632.

Chapter V: SAMs as an Affinity Platform for Mass Spectrometry
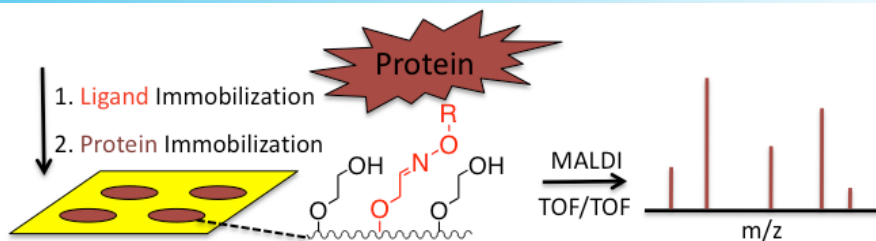
5.1 Introduction

Proteins are the engines of life, and emerging as one of the most important fields in biology.[1] After genomics, proteomics is the next great challenge and several hurdles confront researchers studying the proteome. One main hurdle is the complexity of the proteome due to the numerous protein modifications available to cells. Intron splicing, glycosylation, phosphorylation, and mrystilation are not only necessary for protein function, but multiply the number of possible proteins generated from a single gene.[2] Currently, an estimated 21,000 human genes encode for proteins, while the number of proteins is estimated to be up to 10 times that number.[3,4] The complexity of the proteome is not the only challenge facing scientists. Additionally, no readily available in vitro protein replication mechanism exists, so either *in vivo* protein replication or rabbit reticuluocyte methods are used to create enough protein for study. For these reasons, any instrument used to study proteomics should be able to distinguish between different protein modifications and utilize a small amount of protein.

Mass spectrometry (MS) has emerged as the instrument of choice for proteomics.[5,6] Small quantities of protein can be studied with its superior sensitivity and a tandem dimension can fragment the protein's constituent peptides for sequencing. Additionally, MS has been used to

study protein modifications such as glycosylation, ubiquination, and phosphorylation, and protein modifications can be localized to certain peptides within the proteins.[7] Also with isotopic labeling, proteins can be quantified. However, MS does not deal with mixtures of proteins effectively.[8] As a result, many different protein separation methodologies have been coupled to instruments to simplify protein mixtures prior to MS analysis.[9-12] Off line methodologies such as gel electrophoresis and affinity chromatography have been used along with on line methods such as HPLC and CE in order to simply the protein mixture.

Affinity chromatography specifically has proven useful for purifying a single protein quickly and efficiently.[13] Generally, a ligand recognizing an enzyme or tag is attached to a solid support, and the ligands then bind the protein and remove it from a mixture. The separating power of this technique relies on the specificity of the protein-ligand interaction. Typically proteins are tagged with His_6, FLAG, or strepavidin, and a matching solid support is used to perform the protein pull down.[14,15] The solid support does not bind a number of different proteins. Instead, the support is designed to pull down the protein tag, and the proteins are genetically manipulated to add the tag for separation. Ideally, a solid support should bind many different ligands, so if genetic manipulation is difficult, a ligand for the protein can be used. This flexible support would be capable of binding many different ligands, and consequently capable of binding many proteins in their natural state.

Self-assembled monolayers (SAMs) are a quick and easy way to generate flexible surfaces capable of binding many different ligands. SAMs of alkanethiolates in particular are well studied and present several advantages for this application.[16,17] They are synthetically flexible, well-defined, and electroactive. Furthermore, SAMs terminated in oligo (ethylene glycol) groups resist non-specific protein adsorption and adhesion.[18] With this background, proteins that do not bind specifically to a ligand presented on the surface will not adhere. So, proteins

only interact with the surface if they recognize the ligand, which enhances purification by reducing the background. However, these oligo (ethylene glycol) SAMs have no functional group capable of binding ligands. To solve this problem, we have developed a methodology to oxidize tetra (ethylene) glycol SAMs to aldehydes for cell patterning.[19,20] By using aldehyde chemistry, the SAMs can be functionalized with amines, hydrazines, and hydroxylamines to immobilize proteins. Once oxidized, the surface has the flexibility to bind many different ligands while still resisting non-specific protein adsorption.

Herein we have developed a procedure based on oxidizing tetra (ethylene) glycol (TEG) SAMs to aldehydes for protein pulldown. To fabricate the surfaces, we have adapted our previous methodology for oxidation of alcohol terminated SAMs. TEG SAMs are oxidized with pyridium chlorochromate to generate a low percentage of surface aldehydes. The low percentage of aldehydes on the surface allows the SAM to resist non-specific protein adsorbtion while gaining the capability of bind ligands. We use three different protein ligands: mannose, biotin, and FLAG peptide to pull down three different proteins. We were able to immobilize the proteins on the surface, cleave with trypsin, and identify them with a database search of NCBI with $p < 0.01$ from the MS data.

5.2 Experimental Section

5.2.1 Synthesis of Alkanethiols and Ligands. Undecane thiol terminated with tetra(ethylene glycol), peptides, and sugars were synthesized as reported previously.[20,21]

5.2.2 Preperation of Monolayers. Gold substrates were prepared by electron beam deposition of titanium (6 nm) and gold (24 nm) on 24 mm x 100 mm glass microscope slides. The slides were cut into 1 x 1 cm^2 pieces and washed with absolute ethanol. The slides were then immersed in an ethanolic solution containing either 1 mM tetra (ethylene glycol) undecane thiol. After 12-

16h, the slides were removed from solution. They were rinsed with ethanol and dried before use. All slides were used within a week of fabrication to minimize oxidation of the surface.

5.2.3 Patterned Oxidation of Tetra (ethylene glycol) undecane thiol to Aldehydes. A SAM of tetra (ethylene glycol) undecane thiol was cleaned with ethanol and dried with nitrogen. The exposed alcohol groups were oxidized to aldehydes by adding 60 μL of 10 mM PCC in acetonitrile to each surface for 1 min. Once the PCC had reacted with the surface, the reaction was quenched by submerging the surfaces in ethanol and drying with nitrogen.

5.2.4 Ligand Immobilization. For ligand immobilization, 60 μL of 10 mM ligand solution in 1:1 ethanol:water was added to the surface and allowed to react for 3h. The surfaces were washed with ethanol and dried.

5.2.5 Protein Immobilization. For protein immobilization, 60 μL of 0.05 mg/mL protein solution in Dulbecco's modified eagle's medium (DMEM) containing 5% calf bovine serum (CBS) was added to the surface and allowed to react for 3h. The surfaces were rinsed with water and dried.

5.2.6 Tryptic Protein Digest. Once protein was immobilized to the SAMs, 100 μL of 0.02 mg/mL trypsin in 50 mM ammonium bicarbonate was added to the SAM. The surfaces were heated at 37 °C for 4h after which the solution was transferred to an eppendorf tube and washed with 2x 60 μL of 0.1% TFA in 1:1 acetonitrile:water. The washes were transferred to an eppendorf tube and dried under vacuum. Finally, the peptides were redissolved with 10 μL of 0.1% TFA, then concentrated and desalted with a C_{18} ZipTip (Applied Biosystems) onto a 384 spot plate.

5.2.7 Mass Spectrometry. All MS spectra were acquired with an Applied Biosystems 3800 TOF/TOF. The protein masses were internally calibrated with trypsin auto-digest peaks of 870.5 and 1140.5 m/z. Tandem data was acquired by selecting the 25 strongest non-trypsin peaks for collision induced dissocation by air.

5.2.8 Database Search. Once the MS data was acquired, the data was searched against the all entries in the NCBI database using Protein Pilot with 200 ppm mass tolerance, a trypsin digest, and 2 missed cleavages.

5.3 Results and Discussion

5.3.1 Explanation of Procedure. The procedure to pull down proteins is outlined in figure 5.1. Gold substrates were immersed in 1 mM tetra (ethylene glycol) undecane thiol to generate TEG SAMs. These SAMs naturally resist non-specific protein and cell adhesion, but are incapable of binding ligands to the surface. However, when a small percentage of the alcohols are converted to aldehydes, the surface will still retain its ability to resist non-specific protein adhesion, and be able bind oxyamine, amine, and hydrazine ligands. The oxidation was accomplished by first placing a TEG SAM in 10 mM pyridinium chlorochromate (PCC) for 1 min. The PCC oxidized the primary alcohol of the tetra (ethylene glycol) to an aldehyde, but the low concentration and short time generated only a small percentage of surface aldehydes. From our previous work, we have determined these conditions yield an overall aldehyde percentage of roughly 3%.[12] Next, a protein ligand was immobilized onto the surface by adding 10 mM of an oxyamine or hydrazine terminated ligand to the surface to create an affinity platform for protein immobilization. Due to flexibility of aldehyde chemistry, both oxyamines and hydrazides can be directly immobilized. Also, amines can be immobilized with reductive amination. Next, proteins dissolved at 0.05 mg/mL in 5% calf bovine serum in DMEM were added to the surface. The surface resisted non-specific protein adsorption from the proteins in the calf bovine serum while the ligands bound the protein of interest to pull it down from solution. Once the proteins were immobilized on the surface, the peptides were digested with trypsin and washed from the surface into an eppendorf tube. The peptides were concentrated with a C_{18} ZipTip and MS data

was taken. The MS/MS data was used to determine the weight of the tryptic peptides, and then fragment them to help determine their sequence. Additionally, a NCBI database search could be used to identify the proteins based on their similarity to previously discovered proteins.
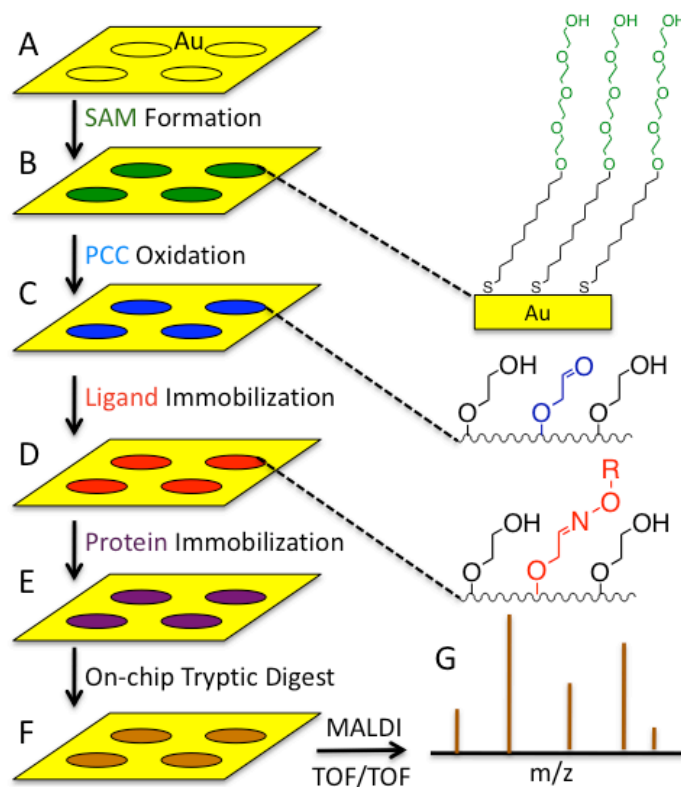
Figure 5.1. Outline of the affinity pulldown methodology. A) A gold surface used as the substrate for alkanethiolate SAMs. B) A TEG SAM was formed in order to provide an inert background against protein adsorption. C) A small percentage of the terminal alcohols were oxidized to aldehydes. The aldehydes provided a chemical handle to immobilize ligands to the surface. D) Oxyamine or hydrazine terminated ligands were immobilized to the surface. E) Proteins recognizing the ligand on the surface were immobilized. F) The proteins were then digested using trypsin for MS analysis. G) The peptides were concentrated, desalted, and a mass spectrum was used to identify the proteins.

5.3.2 Streptavidin Pull Down. For our first experiment, biotin-streptavidin complex was explored. The biotin-streptavidin pairing has one of the highest K_d (10^{-15}) in nature making the pulldown process easier and it is also a common protein tag used in other pull down assays.[23,24] Biotin hydrazide is a commercially available small molecule and reacts with our aldehyde

surface quickly and completely. After streptavidin was immobilized to the biotin on the SAM, MS analysis followed by a NCBI database search was able to identify strepavidin on the surface with confidence level of p< 0.01. (figure 5.2) For a control, oxidized TEG SAMs without ligands were used as affinity platforms for MS, and no proteins were observed on the surface. Also, DMEM with 5% CBS was added to an oxidized surface without streptavidin and no protein was observed in the MS data, demonstrating the non-specific protein resistance of the surface. A peptide fragment with a MW 708 was further fragmented by gas collision induced dissociation and the constituent peptide sequences were observed. The tandem data can be useful tool to identify the peptides, and provide data about the location of protein modifications.
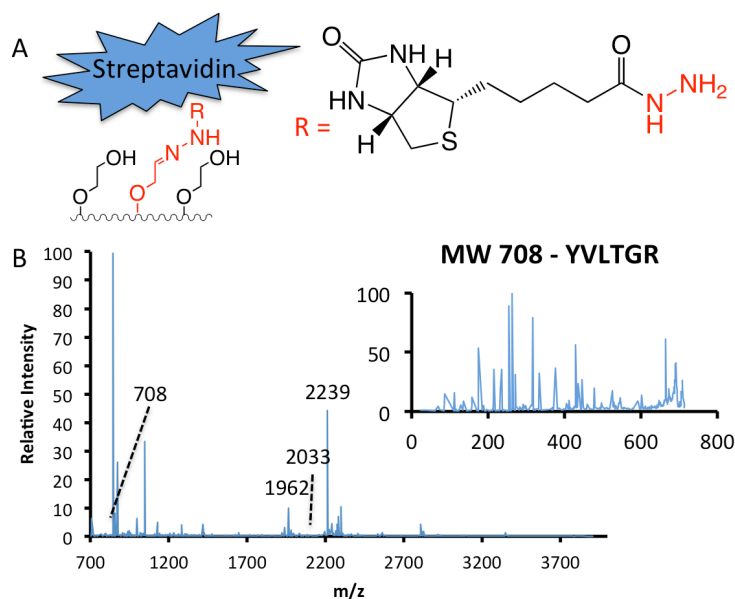
Figure 5.2. Affinity pulldown of streptavidin. A) Streptavidin immobilized to biotin hydrazide attached to a TEG SAM. The hydrazide reacts chemoselectively aldehydes present on the surface to immobilize the biotin to the surface. B) Mass spectrum of the immobilized streptavidin. The key peptides used for the identification are highlighted. The inset is the fragmentation of the MW 708 peptide sequence YVLTGR.

5.3.3 ConA Pull Down. Next, the lectin-carbohydrate interaction was explored. Carbohydrates are an important energy source in biology, and serve as recognition moieties.[25] Lectins bind their target sugars with a high affinity, and have many different biological functions.[26] They can

serve as adhesion sites for viral entry into a cell, cell adhesion sites, and glycoprotein regulators, among other functions. For our experiments, mannose oxyamine was immobilized to the oxidized TEG SAM. Concanivilin A recognizes the mannose with high affinity ($K_d \sim 10^{-9}$) and was pulled down from solution. MS analysis of the protein followed by a search against the NCBI database was able to identify the protein with a $p < 0.01$. (figure 5.3) A subspectrum of a MW 868 polypeptide was fragmented by collision induced dissociation, and the different peptide sequences were observed along with 2 phosphorylations. The tandem data helped localize the phosphylations to that specific peptide sequence, providing useful information about the protein.
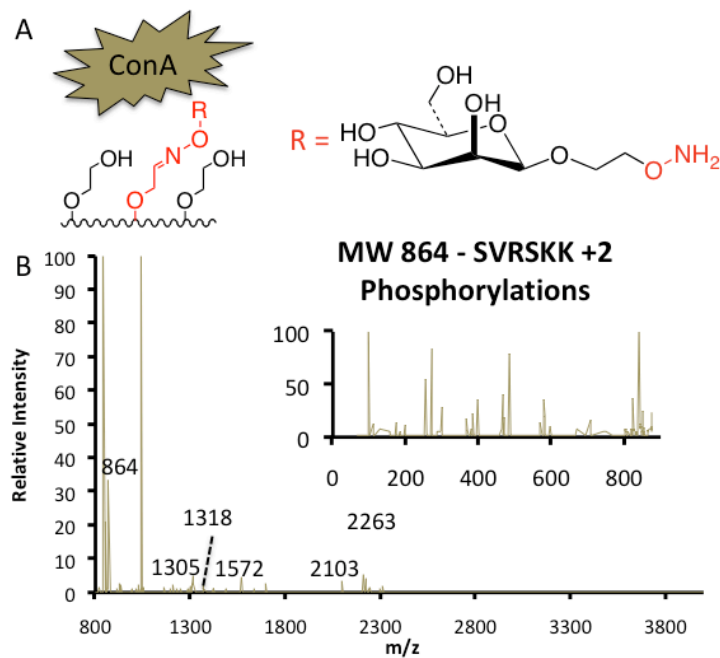
Figure 5.3. Concanavilin A (ConA) affintiy pulldown. A) ConA immobilized to an mannose oxyamine attached to an oxidized TEG SAM. B) Mass spectrum of the immobilized concanavilin A. The key peptides used for the identification are listed. The inset is the fragmentation of the MW 868 peptide sequence SVRKK with 2 phosphorylations.

5.3.4 Anti-Flag Pull Down. For the final ligand-protein pair, the FLAG peptide epitope and antibody was chosen. The FLAG peptide and antibody are commonly utilized as an antibody-

peptide tag for protein pulldown assays.[27,28] Additionally, small polypeptides have been used to successfully mimic proteins to influence cellular and protein function.[29] For example, cell surface integrin receptors recognize the RGD sequence, and bind to materials presenting that peptide sequence.[30] With the FLAG peptide bound to the surface, the FLAG antibody was captured from solution. After trypsin digestion, MS spectra were taken and database search was able to identify the heavy chain on a mouse antibody with a $p<0.01$. (figure 5.4) The variable regions were not identified, but the FLAG antibody was of mouse origin and the other proteins were of bovine origin. A subspectra at MW 1869 was taken and some peptide fragmentation was observed.
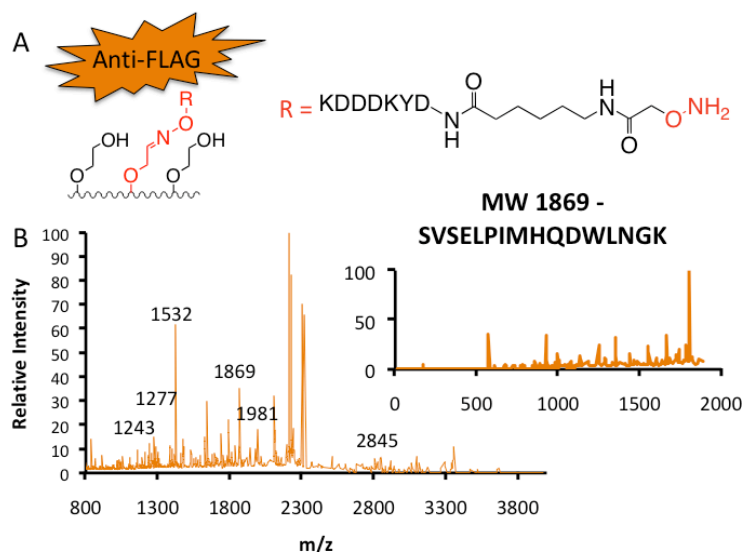
Figure 5.4. Affintiy pulldown of the FLAG antibody. A) FLAG antibody immobilized to a FLAG peptide attached to a TEG SAM. B) Mass spectrum of the immobilized streptavidin. The key peptides used for the identification are numbered. The inset is the fragmentation of the MW 1869 peptide with the sequence SVSELPIMHQDWLNGK.

5.4 Conclusions

For protein purification, we have generated inert SAMs capable of binding many different bioligands to the surface for protein pulldown assays. To generate the flexible SAMs, PCC was used to oxidize a TEG SAM. The terminal alcohols were oxidized to aldehydes, which provided a

functional group to immobilize ligands to the SAM. However, the low aldehyde density maintained the resistance to the non-specific protein adsorption to keep background low. After oxidation, a peptide, a carbohydrate, and small molecule were bound to the surface. Next, proteins were immobilized to the surface-bound ligands. After mass spectrometry of the proteins, a subsequent database search identified the proteins with $p<0.01$. In the future, we hope to transition this methodology to other protein-ligand interactions, protein-protein interactions, and further optimize the procedure.

5.5 References

1. Bhavsar, A. P.; Auweter, S. D.; Finlay, B. B. *Future Microbiol.* **2010**, *5*, 253-265.

2. Southan, C. *Proteomics* **2004**, *4*, 1712-1726.

3. Gingras, A.; Gstaiger, M.; Raught, B.; Aebersold, R. *Nat. Rev. Mol. Cell Biol.* **2007**, *8*, 645-654.

4. Domon, B.; Aebersold, R. *Science* **2006**, *312*, 212-217.

5. Siuti, N.; Kelleher, N. L. *Nat Methods* **2007**, *4*, 817-821.

6. Suzuki, T.; Ito, M.; Ezure, T.; Shikata, M.; Ando, E.; Utsumi, T.; Tsunasawa, S.; Nishimura, O. *Proteomics* **2006**, *6*, 4486-4495.

7. Tedford, N. C.; Hall, A. B.; Graham, J. R.; Murphy, C. E.; Gordon, N. F.; Radding, J. A. *Proteomics* **2009**, *9*, 1469-1487.

8. Gingras, A.; Gstaiger, M.; Raught, B.; Aebersold, R. *Nat. Rev. Mol. Cell Biol.* **2007**, *8*, 645-654.

9. Guillarme, D.; Schappler, J.; Rudaz, S.; Veuthey, J. *Trends in Analytical Chemistry* **2010**, *29*, 15-27.

10. Hu, S.; Xie, Y.; Ramachandran, P.; Loo, R. R. O.; Li, Y.; Loo, J. A.; Wong, D. T. *Proteomics* **2005**, *5*, 1714-1728.

11. Jonker, N.; Kool, J.; Krabbe, J. G.; Retra, K.; Lingeman, H.; Irth, H. *Journal of Chromatography A* **2008**, *1205*, 71-77.

12. Simpson, D. C.; Smith, R. D. *Electrophoresis* **2005**, *26*, 1291-1305.

13. Arnau, J.; Lauritzen, C.; Petersen, G. E.; Pedersen, J. *Protein Expr. Purif.* **2006**, *48*, 1-13.

14. Kubota, K.; Sato, Y.; Suzuki, Y.; Goto-Inoue, N.; Toda, T.; Suzuki, M.; Hisanaga, S.; Suzuki, A.; Endo, T. *Anal. Chem.* **2008**, *80*, 3693-3698.

15. Waugh, D. S. *Trends Biotechnol.* **2005**, *23*, 316-320.

16. Love, J. C.; Estroff, L. A.; Kriebel, J. K.; Nuzzo, R. G.; Whitesides, G. M. *Chem. Rev.* **2005**, *105*, 1103-1170.

17. Ulman, A. *Chem. Rev.* **1996**, *96*, 1533-1554.

18. Mrksich, M. *Curr. Opin. Colloid Interface Sci.* **1997**, *2*, 83.

19. Westcott, N. P.; Yousaf, M. N. *Electrophoresis* **2009**, *30*, 3381-3385.

20. Westcott, N. P.; Pulsipher, A.; Lamb, B.M.; Yousaf, M. N. *Langmuir* **2008**, *24*, 9237-9240.

21. Chan, E. W. L.; Yousaf, M. N. *J. Am. Chem. Soc.* **2006**, *128*, 15542-15546.

22. Dutta, D.; Pulsipher, A.; Yousaf, M.N. *Langmuir* **2010**, 12, 9835–9841.

23. Deng, W.; Zhu, Y.; Montero, A.; Wu, K. K. *Anal. Biochem.* **2003**, *323*, 12-18.

24. Zheng, L.; Roeder, R. G.; Luo, Y. *Cell* **2003**, *114*, 255-266.

25. Jiménez-Barbero, J.; Asensio, J. L.; Cañada, F. J.; Poveda, A. *Curr. Opin. Struct. Biol.* **1999**, *9*, 549-555.

26. Sharon, N. *Journal of Biological Chemistry* **2007**, *282*, 2753-2764.

27. Futatsumori-Sugai, M.; Abe, R.; Watanabe, M.; Kudou, M.; Yamamoto, T.; Ejima, D.; Arakawa, T.; Tsumoto, K. *Protein Expr. Purif.* **2009**, *67*, 148-155.

28. Papakostas, T. D.; Pieretti-Vanmarcke, R.; Nicolaou, F.; Thanos, A.; Trichonas, G.; Koufomichali, X.; Anago, K.; Donahoe, P. K.; Teixeira, J.; MacLaughlin, D. T.; Vavvas, D. *Protein Expr. Purif.* **2010**, *70*, 32-38.

29. Schulze, W. X.; Mann, M. *Journal of Biological Chemistry* **2004**, *279*, 10756-10764.

30. Humphries, J. D.; Byron, A.; Humphries, M. J. *J. Cell. Sci.* **2006**, *119*, 3901-3903.

Chapter VI: Controlling Cell Adhesion at the Nanoscale
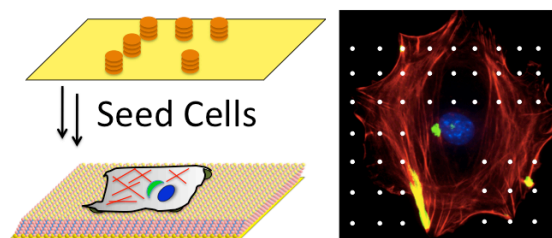
6.1 Introduction

The extracellular matrix is a very complex, heterogeneous mixture of proteins, peptides, and hormones, which has proven essential to cell survival. Mammalian cells adhered to the dynamic extracellular matrix interact with a range of proteins, growth factors and soluble signals that then shape and modulate internal cell machinery.[1-6] This outside-in signaling process is generally mediated by cell surface adhesion receptors (integrins) that recognize and bind ligands on large ECM proteins.[7] Additionally, spatial and temporal changes within the structure of the dynamic ECM, which reveal and hide ligands on extracellular matrix proteins, modulate cell behavior by altering integrin-ligand affinity, spatial distribution of ligands, and temporal availability of ligands.[8]

Currently, a number of model substrates and systems have been developed utilizing polymers, layer-by-layer methods, and self-assembled monolayers (SAMs).[9-15] SAMs of alkanethiolates on gold in particular, have proven to be useful model substrates with a number of key advantages;[16] SAMs are chemically well defined, synthetically flexible, conductive, compatible with live cell high resolution fluorescence microscopy techniques, can be patterned at the micro- and nanoscale, and most importantly they can be made to resist non-specific protein adsorption. These advantages allow for fabrication of complex, flexible substrates for

studies of cell phenomena at the molecular level. To tailor SAMs on gold with precise spatial control with quantification of ligand density, smart SAM surfaces have been developed to immobilize a variety of ligands by convergent synthetic approaches.[17,18,19] By installing the peptide ligand sequence RGD (an epitope for the ECM protein fibronectin) cells have been biospecifially adhered to SAMs to study cell behavior based on specific ligand-receptor interactions.[20] Additionally, SAMs on gold are amenable to a number of different surface patterning techniques to allow for spatial control over the surface, although only a few allow for nanometer scale control and are biocompatible.[21]

To study ligand-receptor interactions during cell adhesion and motility, many SAM patterning techniques have been developed ranging from dip pen nanolithography,[22,23] microcontact printing,[17] self-assembly,[9] and microfluidic lithography.[24] In particular, self assembly[6] has been used generate ligand spot sizes as small as 50 nm with ligand spacing in the 100s of nm, The small ligand size is important to study focal adhesions, but the small interligand distance means the cells can only experience a substrate with high ligand density. Although there has been much progress in generating patterned surfaces there have been few inexpensive methods that can control both the size of the adhesive area (at the nanometer scale) and the spacing between adhesive islands (at the micron scale) to study cell behavior.[25]

Dip pen nanolithography (DPN) has revolutionized nanoscience and is based on a scanning probe technique in which an atomic force microscopy (AFM) tip is used to pattern molecules on a surface with precise nanometer scale features.[26-30] A major under developed area of research in which DPN nanoarray technology will make a significant impact is in cell biology, only a small number of patterning methodologies can achieve nanometer control over cell adhesive areas. In particular, the number and size of biospecific interactions between extracellular ligands and cell surface receptors is critical for cell adhesion and migration. For example, the spatial

117

presentation of cell adhesive ligands influence the sub-cellular nanoarchitecture of adherent cells and affect their behavior.[31] These phenomena remain poorly understood and elusive due to the lack of easily available molecularly defined nanopatterned model substrates.

Previous DPN approaches to study cell behavior were performed on a standard AFM (i.e. designed specifically for imaging, not lithography), limiting the types of cell studies to serial pattern production using a single AFM tip, which restricted substrate throughput, pattern design, and pattern quantity.[22,23] These limitations have recently been overcome with the advent of parallel tip arrays and instrumentation designed specifically for large area, parallel nanolithography, instead of relying on AFM metrology tools that were designed with patterning secondary to image acquisition. Parallel DPN allows for printing multiple unique patterns onto a single substrate in a fraction of the time it would take with a single tip, which permits almost unlimited pattern design and feature sizes to combinatorially study cellular behavior.[32]

The polarity of a cell can be experimentally measured through the systematic reorientation and alignment of several organelles in the cell including the nucleus, centrosome and golgi apparatus, which can be visualized using fluorescent dyes to map the direction of polarity.[22,33] The orientation of cell division can be determined by observing the plane between the two resulting daughter cells immediately after division or where the chromosomes position themselves at the metaphase plate before the metaphase to anaphase transition followed by cytokinesis. The experiments described in this report are important to the nanoscience and cell motility research fields because previously no method to separate the dynamic processes of cell adhesion, cell polarity, and cell migration from each other without the use of genetic or small molecule manipulations. However, by using single cell nanoarrays, cells may first adhere to the nanoarray pattern, determine if the conditions are met for establishing polarity, then polarize

but not migrate. These surfaces would allow for the analysis of cell polarity and cell division orientation and determine how the underlying adhesive environment influences cell behavior.

Herein, parallel DPN to generate single cell patterns with control of spot size and distribution within each pattern was used to study their role in determining cell polarization direction and cell division orientation. Five asymmetric patterns were generated with different ligand densities in different regions. Due to advantages of parallel fabrication, substrates were generated with many different copies of each pattern on the surface (figure 6.1). The decreased fabrication time was critical for allowing multiplexed analysis of the asymmetric patterns as well as ligand effects on cell behavior. When combined with SAMs of alkanethiolates on gold and an electroactive immobilization strategy, surfaces can be rapidly generated that are capable of presenting many different ligands with the unique ability to resist non-specific protein adsorption. Finally, we observed the effects of ligand affinity, ligand area and ligand density on cell polarization direction and cell division orientation. We have also developed a flexible fabrication strategy to generate various hybrid gold/glass nanohole surfaces for studies of cell adhesion and cell migration.[8] The surfaces were fabricated with 500 nm ligand spot sizes and separated by 3 or 5 μm and characterized with scanning electron microscopy and optical microscopy (supporting information). For cell adhesion studies, cells were seeded to these substrates to study the effect of ligand spacing on cell spreading, stress fiber formation, and focal adhesion structure and size. Finally, cell migration rates were determined and compared on the various nanohole surfaces with the use of time-lapse microscopy.

6.2 Experimental

6.2.1 Peptide and alkanethiol synthesis. The RGD and PHSRN peptides, tetra (ethylene glycol), and hydroquinone terminated alkanethiols were synthesized as previously reported.[18]

6.2.2 Gold Preparation. Glass coverslips were cleaned by sonication in ethanol for 30 min. Then, an adhesion layer of titanium (4 nm) and a transparent layer of gold (10 nm) were thermally evaporated on them.

6.2.3 DPN Patterning. All DPN experiments were carried out using DPN 5000 system (NanoInk Inc, Skokie, IL) at 25 ˚C and 30% humidity. A 1-dimensional (1-D) tip array (6-tip, 280 μm pitch, Nanoink Inc., Skokie, IL) was used for patterning. This silicon nitride 1-D pen array was immersed in a hydroquinone-terminated alkanethiol ($HQEG_4C_{11}SH$, 5 mM in acetonitrile) for 10 s and then air-dried. The patterns of nanoarrays of dots in figure 3 were designed by InkCAD^{TM} software (NanoInk Inc, Skokie, IL) in a DPN 5000 system. An ink diffusion coefficient was repeatedly measured just before DPN printing of new patterns to optimize dwell-time for correct dot sizes. It took 5 min to 30 min to DPN print one set of patterns (5 patterns). All 5 patterns (Figure 3) were printed twice per each substrate.

6.2.4 Hybrid Substrate Fabrication. A glass slide was sonicated in acetone followed by cleaned in piranha for one hour. Next, a solution of polystyrene beads in water was drop-coated to the surface and allowed to dry in a humidity controlled environment (~70% humidity). The 5 μm beads were etched with O_2 plasma for 30 minutes to generate 500 nm holes with 5 μm spacing. The 3 μm beads were etched with O_2 plasma for 20 minutes to generate 500 nm holes with 3 μm spacing. Afterwards, the glass slide was coated with chromium then gold. Finally, the beads were removed by sonication with acetone.

6.2.5 SAM Formation and Fibronectin Absorption. After fabrication, the substrates were immersed in a 0.5 mM solution of tetra (ethylene glycol) undecane thiol for 12h. For fibronectin adsorption, the surfaces were placed on a 30 μL of 0.1 μg/μL fibronectin solution for 3 hr before cell seeding.

6.2.6 Lateral Force Microscopy. The patterns were printed on a marked substrate for registration purposes with a single tip. To provide further registration, a map of the tip relative to the surface was drawn. Each pattern was printed, and then the tip was changed for a non-inked a-type one for imaging. The images were scanned at 1 Hz with 256 lines of resolution for both the 60 µm x 60 µm and 6 µm x 6 µm windows.

6.2.7 Peptide Immobilization. A linear scan voltammagram was run with each substrate serving as the working electrode with a platinum counter and an Ag/AgCl reference from 0 to 850 mV for an Epsilon potentiostat (Bioanalytical systems). The substrates were cleaned in water and 60 µL of 10 mM solution of oxyamine-terminated peptide was added to parafilm in an evaporation proof petri dish. Patterned substrates were turned over such that SAM contacted the solution and left to react for 3h. After immobilization, the surfaces were cleaned and left in water overnight.

6.2.8 Cell Seeding. Swiss Albino 3T3 fibroblasts (ATCC) were cultured in Dulbecco's Modified Eagle Medium (Gibco) containing 10% calf bovine serum and 1% penicillin/streptomycin at 37 °C and 5% CO_2. Cells were removed with a solution of 0.05% trypsin in 0.53 mM EDTA and re-suspended in serum-free medium (20,000 cells/mL). The cells were seeded to surfaces for 2 h. After 2 h, the serum containing media was added for cell growth.

6.2.9 Cell Staining. 3T3 Swiss Albino mouse fibroblasts were seeded on the patterned substrates, incubated for 12h, 16h, or 26h in Dulbecco's modified Eagle's medium (Sigma) with 10% bovine calf serum and 1% penicillin/streptomycin, and then fixed with 3.2% formaldehyde in Dulbecco's PBS (Sigma). The cells were then permeated with PBS containing 0.1% Triton X-100 and stained with three fluorescent dyes and one antibody: DAPI (4',6-diamidino-2-phenylindole dihydrochloride; Sigma), anti-gigatin (BD Biosciences, San Jose, CA), phalloidin-tetramethylrhodamine B isothiocyanate (Sigma), and a secondary fluorescently labeled

antibody (FITC conjugated rabbit anti-mouse IgG, Jackson ImmunoResearch Laboratories, Inc., West Grove, PA). Cells were imaged with a Nikon TE2000E inverted microscope.

6.2.10 Microscopy of Surface Immobilized Cells. Fluorescent and brightfield microscopy was performed using a Nikon TE2000E inverted microscope. For time lapse microscopy, brightfield images were obtained at 10 minute intervals over a period of 24 hours. Image acquisition and processing was done using Metamorph software.

6.2.11 Environmental SEM. A FEI Quanta 200 FEG was used for environmental SEM. The imaging was done at 0.5 torr water pressure and 12 kV accelerating voltage.

6.3 Results and Discussion

6.3.1 DPN Patterning. To study how cell polarity and cell division orientation is influenced by nanoscale adhesive features, asymmetric nanopatterns were designed to observe the interplay between ligand density and total ligand area (figure 6.2). Until now, there has been no report that shows the fabrication or utilization of single cell biospecific nanopatterns where control of both the spot size and distribution of ligands can simultaneously be changed to study cell behavior. The overall 2500 μm^2 pattern consists of 2 different regions; the 1600 μm^2 L-shaped region 1 and the 400 μm^2 square region 2. Both spot diameter and pitch were varied within the regions to affect their adhesiveness that in turn control cell polarity and cell division orientation. Generally, region 1 ligand density decreased first by pitch then spot diameter and for region 2, ligand density increased with decreasing pitch. In order to quantitatively compare the densities in each region, the effective ligand density was determined by first calculating the total spot area for each region and dividing by its area. These calculations generated the absolute ligand densities for each region. For the effective ligand density in region 1, the absolute ligand density was used and for region 2, the effective ligand density was determined by dividing its absolute density by 4 (because region 1 has 4 times the area of region 2). For

example, both regions in pattern 3 have the same spot diameter but region 2 has half the pitch. The lower pitch means the absolute spot density in region 2 was 4 times higher than region 1. (0.081 vs. 0.022) Since region 2 had ¼ the area of region 1, the absolute density was divided by 4, so the two regions have roughly the same effective ligand density (0.02 vs. 0.022). For pattern 1, region 1 had 13 times higher effective density. In pattern 2, the regions had identical spot pitch and diameter, but because of the lower area in region 2, the effective density was 3.5 times higher in region 1. For patterns 4 and 5, the spot diameter and pitch are both lowered in region 1 while region 2 was held constant, which resulted in the same effective densities for patterns 4 and 5. Ideally, we should be able to observe cells initially polarized towards region 1, and as the effective ligand density decreases in region 1 and increases in region 2, the cells should polarize toward region 2.
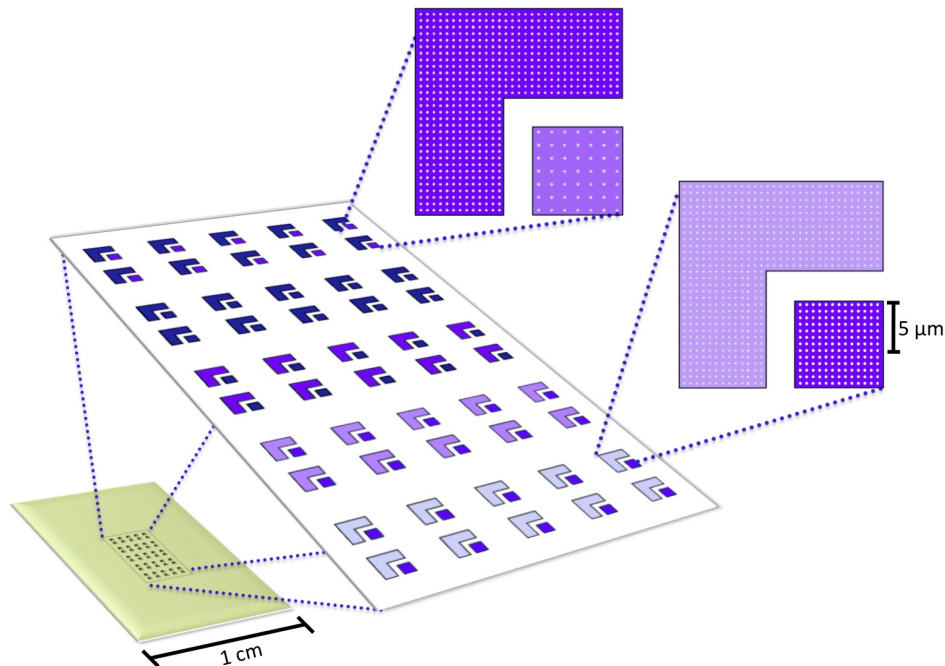

Figure 6.1. Schematic of the cell biochips and patterns used for evaluating cell behavior on Dippen nanolithography (DPN) patterned peptide nanoarrays. Gold surfaces (1 cm x 1 cm) contained around a hundred single cell patterned arrays with each single cell pattern consisting of different distributions of nanometer sized cell adhesive peptide spots.
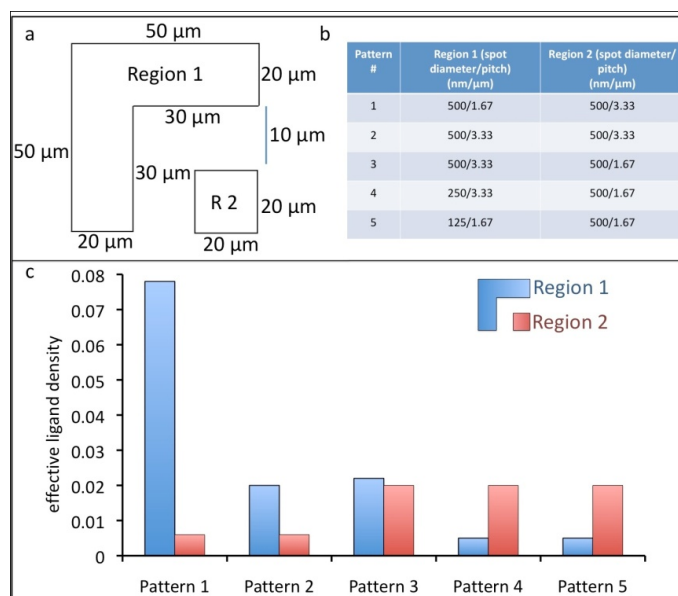
Figure 6.2. Dip-pen nanolithography (DPN) pattern design and dimensions. a) A schematic of the patterns used in the study. The total area for the pattern was 2500 μm² with each pattern divided into two regions. The larger region 1 was an L shape with an area of 1600 μm² and the smaller region 2 was a square with an area of 400 μm². b) A table of spot diameter (nm) and pitch (μm) used within each region for the 5 different patterns. c) A graph of effective ligand density vs. pattern number for both regions 1 and 2.

6.3.2 DPN Procedure. In order to generate biospecific peptide nanoarrays for cell behavior studies, we used parallel DPN to pattern an array of electroactive alkanethiols to gold surfaces (figure 6.3). First, a 5 mM Hydroquinone terminated thiol solution was coated on a 6-tip cantilever array with 280 μm pitch, and then used to generate nanoarrays on the surface. For one substrate, 96 copies of each pattern were spotted. Once DPN patterning was completed, the remaining bare gold regions were backfilled with tetra (ethylene glycol) terminated thiols for 12h to render the surface inert to non-specific protein adsorption and cell attachment. After SAM formation, the hydroquinones on the surface were electrochemically oxidized to the chemoselective quinones (essentially the redox unveling of a ketone group). To provide a cell adhesive surface, a 10 mM oxyamine terminated peptide (R-ONH$_2$) was immobilized to the

124

surface via an interfacial oxime linkage (R = RGD or PHSRN).   Cells were then seeded to these

substrates where they attached to a pattern, polarized, and then divided.
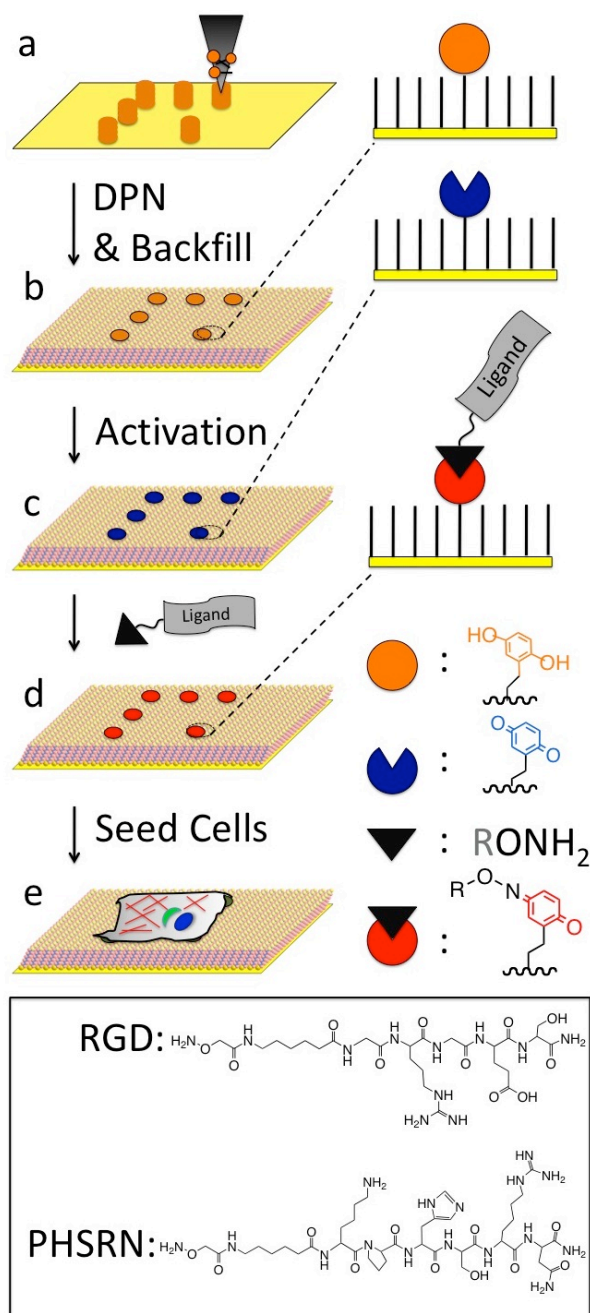
Figure 6.3. Schematic of the DPN methodology used to control cell polarity and cell division. a) An AFM tip was coated with hydroquinone alkanethiol and used to pattern the gold surface. b) A bio-inert surface was formed by backfilling with tetra(ethyleneglycol)undecanethiol. c) The hydroquinone molecule was oxidized to the quinone. d) A peptide-oxyamine was immobilized to the surface. e) Cells are seeded onto the biospecific peptide nanopatterns and modulate their behavior according to the interplay between spot size, pitch and ligand identity.

6.3.3 LFM of the Substrates. Once the hydroquinone nanoarrays were fabricated, the patterned surfaces were characterized by lateral force microscopy (LFM) (figure 6.4). Each pattern was spotted by DPN and afterwards, the tip was changed for optimal imaging from an array to a single AFM tip. The surfaces were scanned over a 60 μm x 60 μm area to capture the entire pattern in one window and on each image, with the hydroquinone spots visible as yellow dots. However, the smaller spots in patterns 4 and 5 (region 1) were not visible at that scale and a secondary 6 μm x 6 μm scan was therefore used to aid in visualization of the array. These scans are shown as insets in patterns' 4 and 5 LFMs. Overall, the fidelity of the patterns were excellent; the CAD (InkCAD™, NanoInk Inc) drawings were rendered on the surface rapidly with high precision and a low relative standard deviation for both the spot diameter and pitch.
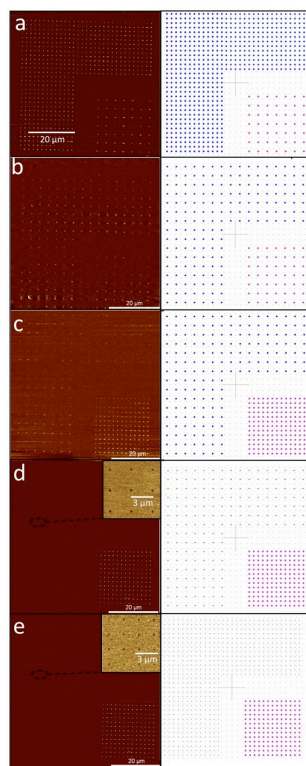
Figure 6.4. Lateral force microscope (LFM) images of the patterns used to control cell polarity and cell division. Left column: LFM images of the hydroquinone-alkanethiol patterned on the gold surface. Right column: InkCAD renderings of the patterns on the surface. LFMs of a) Pattern 1 b) Pattern 2 c) Pattern 3 d) Pattern 4. Inset - 250 nm spots not visible on the larger area LFM. e) Pattern 5. Inset – 125 nm spots not visible on the larger LFM.

126

6.3.4 Cell Polarization on DPN Patterns. To determine how the orientation of cell polarity is controlled at the nanoscale we immobilized the RGD peptide to the DPN fabricated asymmetric nanoarray patterns. Twelve hours after seeding, the cells were fixed and stained for nuclei (blue), golgi (green), and actin cytoskeleton (red). The polarity vector was determined by drawing a line from the center of the nucleus through the center of the concentrated golgi (figure 6.5). Overall, the cells polarized towards region 1 and as the effective ligand density decreased in region 1 and increased in region 2, the polarity vector switched to region 2 (n = 25). For patterns 1 and 2, the cells polarized towards the higher effective ligand density in region 1. Interestingly, no net cell polarity existed on pattern 3 as predicted by the effective ligand density being approximately the same for regions 1 and region 2 (fig. 6.2). For pattern 3, region 1 had 4 times the area but 1/4 of the 500 nm spots per unit area as region 2; the area and spot density appear to counterbalance one another and therefore the cell feels no net spatial difference or adhesive difference in the pattern. On patterns 4 and 5, the cells polarized towards region 2. Despite having different spot pitches and diameters in region 1, the patterns had the same effective ligand density and behaved accordingly. The data suggests that the effective ligand density was the overall controlling factor for cell polarity and not exclusively spot diameter or pitch.
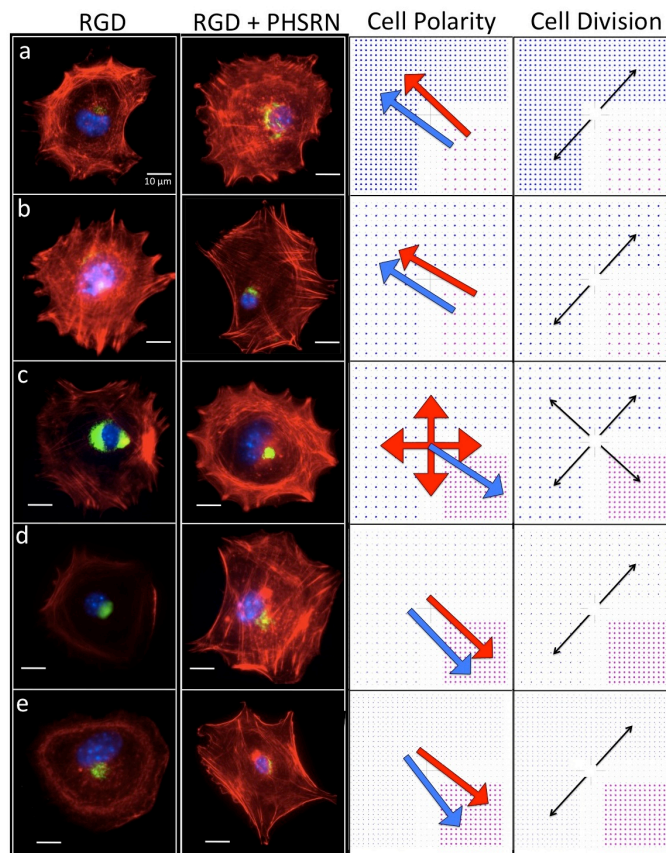
Figure 6.5. Cell images, polarity vectors, and division planes of cells adhered to the corresponding nanopatterns. First and Second columns: Fluorescent images of swiss 3T3 fibroblasts adhered to peptide nanoarrays. Green- golgi, blue-nuclei, red-actin. Third column: Cell polarity vectors superimposed on InkCAD renderings of the nanoarrays. Red arrows are summary polarity vectors for RGD only arrays. Blue arrows are summary polarity vectors for RGD and PHSRN arrays. Fourth column: Cell division planes for the various patterns. a)-e) patterns 1-5.

To study how cell division orientation is determined by the spatial presentation of nanopatterned RGD peptides, cells were allowed to first adhere and then proliferate on the substrates for 16h. The extra duration allowed the single adhered cell on the nanopattern to divide to two daughter cells. For cell division, it was observed that the cells divided along the plane of their polarity vectors (n = 25). All cells followed this rule, except for cells on pattern 3 which divided randomly due to no specific cell polarity orientation.

To study the interplay of ligand affinity and nanopattern distribution on cell polarity and cell division orientation, we immobilized a mixture of two cell adhesive peptides to the

nanoarrays. The peptide sequence PHSRN is an established synergy peptide located in the 10th domain of fibronectin.[34] The PHSRN ligand alone cannot support cell adhesion, however when combined with the RGD peptide, it has been shown to enhance cell binding, cell spreading, and increase cell migration rates.[35,36] To study PHSRN's and RGD's effects on cell polarity and cell division orientation, we immobilized a 1:1 mixture of 10 mM oxyamine terminated PHSRN and RGD peptides for 2h to the nanoarrays. Cells were seeded, allowed to grow for 12h, and it was observed that cells adopted the same polarity vector as the RGD only presenting nanoarrays (fig 6.5, PHSRN column) (n = 25). The only exception was for pattern 3 where on RGD only arrays, no polarity vector was observed, but when PHSRN was added (RGD + PHSRN (1:1)), the cells polarized towards region 2. We believe that the PHSRN ligand increased the overall adhesiveness of the nanoarray, and the greater absolute density of ligands in region 2 allowed the cells to polarize towards region 2. For cell division orientation studies, we observed all cells divided along the same polarity planes for the RGD arrays except for pattern 3; instead of having a variable division plane, it was fixed along the polarity vector.

6.3.5 Cell Division on DPN Patterns. To study the role of cell-cell contacts in determining cell polarity orientation on asymmetric nanoarrays we observed the polarity vector for two cells in the RGD nanoarrays. Previously, we have shown cells on symmetric or gradient presenting RGD surfaces consistently polarize away from one another and in opposite directions. For these experiments, we found cell-cell contacts overrode the symmetric or gradient surface cues.[10] To examine the effect of an asymmetric peptide surface on the cell polarity vectors for connected cells we seeded cells onto the RGD peptide nanoarrays. The cells were allowed to grow for 26h; the increased duration provided the single adhered cell to first polarize then divide and then re-establish cell polarity for the connected two daughter cells. After dividing to two daughter cells, the cells were fixed and stained for actin, nuclei, and golgi to determine their polarity vectors

(figure 6.6) (n = 38). Interestingly, from analysis of the polarity vectors the asymmetric surface

nanopatterns can override the cell-cell contacts and force the cells to polarize in the same

direction, whereas previous studies show cell-cell contacts are the main determinant of cell

polarity orientation and not the extracellular surface cues. This phenotype was observed for

patterns 1, 4, and 5 where the ratio in effective densities was greater than 3.6. However, when

regions 1 and 2 are within 3.6 times of one another, then cell-cell contacts override the surface

cues and the cells polarize away from one another as in patterns 2 and 3.
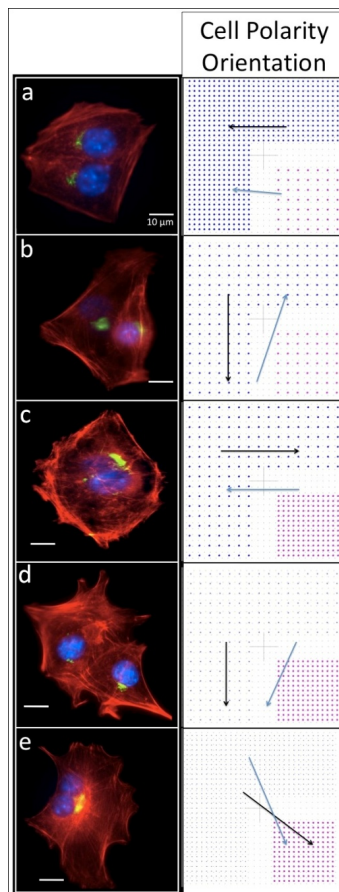
Figure 6.6. Cell images and polarity vectors of cells adhered to the corresponding nanopatterns after cell division. Left Column: Fluorescent images of swiss 3T3 fibroblasts adhered to RGD peptide nanoarrays. Green- golgi, blue-nuclei, red-actin. Right Column: Cell polarity vectors for both cells superimposed on InkCAD renderings of the nanoarrays. a) Cells on pattern 1 polarized towards region 1. b) Cells on pattern 2 were polarized away from each other. c) Cells on pattern 3 polarized away from one another. d) Both cells on pattern 4 were polarized to region 2. e) Both cells on pattern 5 polarized towards region 2.

6.3.6 Nanohole Substrate Procedure. The strategy to generate nanohole features is outlined in Figure 6.7. A glass microscope slide was sonicated in acetone and cleaned in pirhana solution. Then, a solution of either 5 or 3 µm polystyrene beads was drop coated onto the surface. The solvent (H_2O) was allowed to slowly evaporate in a humidified chamber (~70% humidity). During evaporation, the beads self-assembled into hexagonal patterns on the surface with spacings of 1-7 µm. To reduce the size of the beads and therefore control the size of the nanoholes, the beads were processed by reactive ion etching (RIE). For 500 nm holes the beads were exposed for 30 minutes with O_2 plasma, but by varying the reaction time the hole size could be varied from 50-500 nm. After the beads were etched, a layer of chromium (2 nm) then gold (15 nm) was evaporated onto the substrate. Sonication in acetone removed the beads leaving behind the corresponding glass nanohole features. It should be noted that no photoresist or complex soft lithography was used to generate these nanohole surfaces. The gold/glass nanohole substrate was then immersed in a solution (1mM for 12 hrs) of tetra(ethylene)glycol alkanethiol to render the gold regions inert to non-specific protein adsorption and cell attachment. For cell adhesion and migration studies, the substrate was then exposed to a solution of the extracellular matrix protein fibronectin (0.1µg/µL for 3 hrs), which selectively adsorbs only to the glass nanholes. This allows only adhesive interactions between the cell and the fibronectin coated nanoholes during the cell adhesion and migration processes.
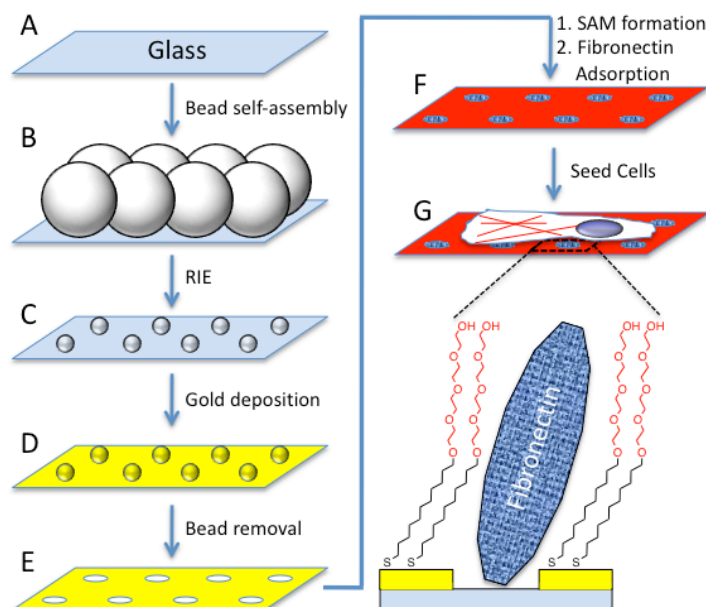
Figure 6.7. Strategy to generate patterned hybrid nanohole self-assembled monolayer surfaces for studies of cell adhesion and cell migration. (A) A glass slide was cleaned with piranha and acetone. (B) A solution of polystyrene beads was placed on the surface and self-assembles as the solvent (H_2O) slowly evaporates. (C) The spacing and size of the holes were controlled by selectively reducing the size of the beads with reactive ion etching (RIE) using O_2 plasma. (D) Chromium then gold was deposited on the surface. (E) To generate the nanoholes, the beads were removed from the surface with acetone. (F) The bare gold was exposed to a tetra (ethylene glycol) alkanethiol to form an inert SAM. The extracellular matrix protein fibronectin was then added and adsorbed only to the glass regions. (G) Cells were seeded to the surface to study adhesion and migration as a function of nanohole size and spacing.
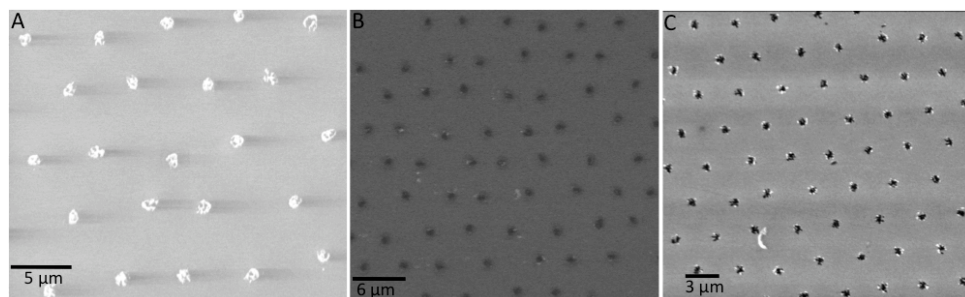
Figure 6.8. Environmental scanning electron microscopy (ESEM) of the hybrid nanohole surfaces. A) ESEM of silicon beads after the O_2 plasma etching. Hybrid surfaces made with B) 5 μm and C) 3 μm. beads after gold evaporation and bead removal.

6.3.8 Cell Adhesion on Nanohole Substrates. To study the role of ligand spacing on cell spreading, stress fiber formation and focal adhesion structure and size, Swiss 3T3 fibroblasts were seeded to the hybrid nanohole surfaces then fixed to observe internal structures after 24 hours (Figure 6.9). Cells were visualized by fluorescent microscopy and were stained with

132

markers for the nucleus (blue), actin (red), and focal adhesions (green). Figure 2B shows a table summarizing the cell characteristics on the various surfaces. Cells spread well on all the surfaces but focal adhesion structures were only found on surfaces with adsorbed fibronectin irrespective of nanohole spacing. Unlike the fibronectin coated glass surface, cells on the nanopatterns did not have actin stress fibers throughout the cell length. Larger and more focal adhesion structures were found on the 3 μm spacing of the 500 nm holes compared to the 5 μm spacing 500 nm holes. This observation is most likely due to the greater density of adhesive sites on the 3 μm nanohole array.

6.3.9 Cell Migration on DPN Patterns. For cell migration studies on the nanohole array surfaces, we used time-lapse microscopy (Figure 6.10). After cell seeding, brightfield images were taken every ten minutes over 24 hours and the migration rates were determined with Metamorph software for 10 cells. For fibronectin adsorbed on glass, the migration rate was 1.34 μm/hr and for cells migrating on the nanoholes (no fibronectin) with 5 μm spacing the migration rate was 1.20 μm/hr (nanohole size is 500 nm for all cell migration experiments). Once fibronectin was adsorbed to the glass nanoholes, the rate roughly doubled for the 5 μm spacing (2.88 μm/hr). When the cells were seeded to a surface with 3 μm spacing with fibronectin, the migration rate quadrupled to 11.32 μm/hr. Cells on the 3 and 5 μm array show characteristics of a motile cell with the lack of stress fibers but well-formed focal adhesions. The increase in ligand density on the 3 μm array resulted in a significant increase in migration rates. We observed on the series of fibronectin nanohole arrays that the cells had much greater lamellapodia and filopodia protrusions compared to the glass/fibronectin surface. Furthermore, we observed more focal adhesions on the 3 μm array than on the 5 μm array, which is most likely due to the higher ligand density on the surface. We believe there is a complex interplay between ligand density and spacing that contribute to the overall ability for

the cell to make focal adhesions which then allows for subsequent lamellapodia and filopodia protrusions for motility.
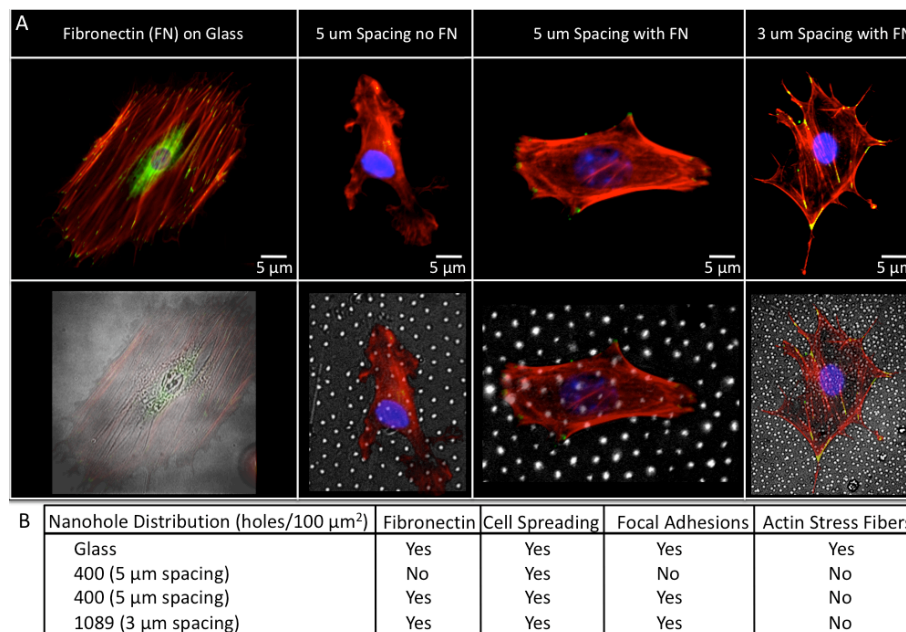
Figure 6.9. Representative micrographs of fibroblast cells adhered to various hybrid nanohole surfaces. Cells were fixed and stained for nucleus (blue), actin (red), and focal adhesions (green). (A) Top row. Fluorescent micrographs of cells immobilized on the different nanohole (500 nm) surfaces including fibronectin on glass, 5 μm spacing with and without fibronectin, and 3 μm spacing with fibronectin. Bottom row. The corresponding brightfield images with the fluorescent micrographs superimposed to aid in the visibility of the cells and nanohole spacing. (B) Comparison of cell adhesion characteristics on the various surfaces.

6.4 Conclusions

In summary, we have fabricated complex asymmetric peptide nanoarrays with DPN to study single cell and multi-cell polarization and cell division orientation. We examined the interplay between total region area, pitch, ligand affinity and spot size and found the effective ligand density controlled cell polarity orientation. On RGD nanoarrays, the key nanopattern for the study was pattern 3; both regions 1 and 2 had equivalent ligand density and cells did not polarize on these substrates. With the addition of the synergy peptide PHSRN, however, the cells on pattern 3 polarized towards region 2. Once cells had divided on RGD, the peptide

nanoarrays were able to override cell-cell contacts and force the cells to polarize to the same region. The results and methodology presented in this work show that DPN is a valuable and essential tool to study how the nano-environment influences cell behavior.
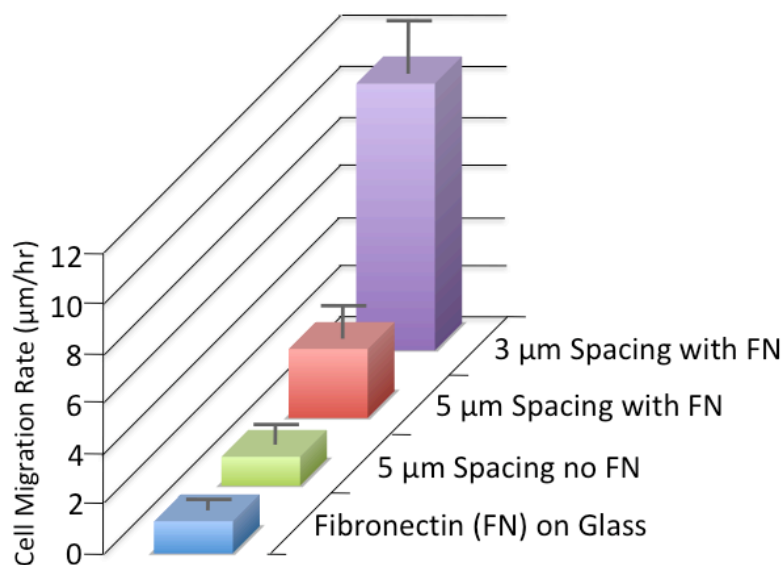
Figure 6.10. Comparison of cell migration rates on various surfaces. Swiss 3T3 fibroblast migration on the nanohole surfaces. Time-lapse microscopy was used to measure migration rates over 24 hrs. Cells migrated the fastest on hybrid nanohole surfaces (500 nm holes) with 3 μm spacing between nanoholes presenting fibronectin (FN).

Additionally, we have developed a novel hybrid nanohole array substrate to study cell adhesion and migration. The fabrication methodology relies on a straightforward bead self-assembly/reactive ion etching method to generate gold/glass hybrids with control over nanometer size holes and spacing between holes. These substrates were used to study cell adhesion characteristics by antibody staining. Cells spread on the different nanohole surfaces, but did not form long actin stress fibers. However, on fibronectin containing holes, the cells formed focal adhesions. Finally, cell migration rates were studied on the substrates with time-lapse microscopy. Migration rates increased on higher density surfaces containing fibronectin with increasing protrusions and focal adhesion. Future studies will aim to tailor the gold regions to present peptide ligands in patterns and gradients to study cell polarity and cell division. We

believe, the fabrication strategies combined with tailored surfaces and microfluidic lithography[9] techniques will allow for the generation of straightforward model systems to study a variety of fundamental cell behavior ranging from growth, differentiation to apoptosis.

6.5 References

1. Iden, S.; Collard, J. G. Nat. Rev. *Mol. Cell Biol*. **2008**, *9*, 846-859.

2. Lock, J. G.; Wehrle-Haller, B.; Strömblad, S. *Semin. Cancer Biol*. **2008**, *18*, 65-76.

3. Rhee, S.; Jiang, H.; Ho, C.; Grinnell, F. *Proc. of the Nat'l Acad, of Sci*. **2007**, *104*, 5425-5430.

4. Berrier, A. L.; Yamada, K. M. *J. Cell. Physiol*. **2007**, *213*, 565-573.

5. Aszódi, A.; Legate, K. R.; Nakchbandi, I.; Fässler, R. *Annu. Rev. Cell Dev. Biol*. **2006**, *22*, 591-621.

6. Canavan, H. E.; Cheng, X.; Graham, D. J.; Ratner, B. D.; Castner, D. G. *Langmuir* **2005**, *21*, 1949-1955.

7. Luo, B.; Carman, C. V.; Springer, T. A. *Annu. Rev. Immunol*. **2007**, *25*, 619-647.

8. Altroff, H.; Schlinkert, R.; van der Walle, C. F.; Bernini, A.; Campbell, I. D.; Werner, J. M.; Mardon, H. J. *J. Biol. Chem*. **2004**, *279*, 55995-56003.

9. Arnold, M.; Cavalcanti-Adam, E. A.; Glass, R.; Blümmel, J.; Eck, W.; Kantlehner, M.; Kessler, H.; Spatz, J. P. *ChemPhysChem* **2004**, *5*, 383-388.

10. Chan, E. W. L.; Yousaf, M. N. *Molecular BioSystems* **2008**, *4*, 746-753.

11. Thery, M.; Racine, V.; Pepin, A.; Piel, M.; Chen, Y.; Sibarita, J.; Bornens, M. *Nat. Cell Biol*. **2005**, *7*, 947-953.

12. Théry, M.; Racine, V.; Piel, M.; Pépin, A.; Dimitrov, A.; Chen, Y.; Sibarita, J.; Bornens, M. *Proc. of the Nat'l Acad. of Sci*. **2006**, *103*, 19771-19776.

13. Théry, M.; Pépin, A.; Dressaire, E.; Chen, Y.; Bornens, M. *Cell Motil. Cytoskeleton* **2006**, *63*, 341-355.

14. Hahn, C. D.; Tinazli, A.; Halzl, M.; Leitner, C.; Frederix, F.; Lackner, B.; Maller, N.; Klampfl, C.; Tampa, R.; Gruber, H. J. *Chemical Monthly* **2007**, *138*, 245-252.

15. Fukuda, J.; Khademhosseini, A.; Yeh, J.; Eng, G.; Cheng, J.; Farokhzad, O. C.; Langer, R. *Biomaterials* **2006**, *27*, 1479-1486.

16. Ulman, A. *Chem. Rev.* **1996**, *96*, 1533-1554.

17. Love, J. C.; Estroff, L. A.; Kriebel, J. K.; Nuzzo, R. G.; Whitesides, G. M. *Chem. Rev.* **2005**, *105*, 1103-1170.

18. Chan, E. W. L.; Yousaf, M. N. *J. Am. Chem. Soc.* **2006**, *128*, 15542-15546.

19. Westcott, N. P.; Yousaf, M. N. *Electrophoresis* **2009**, *30*, 3381-3385.

20. Huck, W. T. S. *Ange. Chem.* **2007**, *46*, 2754-2757.

21. Li, Y.; Yuan, B.; Ji, H.; Han, D.; Chen, S.; Tian, F.; Jiang, X. *Ange. Chem.* **2007**, *119*, 1112-1114.

22. Hoover, D. K.; Chan, E. W. L.; Yousaf, M. N. *J. Am. Chem. Soc.* **2008**, *130*, 3280-3281.

23. Hoover, D. K.; Lee, E.; Chan, E. W. L.; Yousaf, M. N. *ChemBioChem* **2007**, *8*, 1920-1923.

24. Lamb, B.M.; Westcott, N.P.; Yousaf, M.N. *ChemBioChem*, **2008**, *9*, 2628-2642.

25. Henzie, J.; Lee, J.; Lee, M.H.; Hasan, W.; Odom, T.W. *Annu. Rev. Phys. Chem.* **2009**, *60*, 147-65.

26. Piner, R. D.; Zhu, J.; Xu, F.; Hong, S.; Mirkin, C. A. *Science* **1999**, *283*, 661-663.

27. Salaita, K.; Wang, Y.; Mirkin, C. A. *Nat. Nano.* **2007**, *2*, 145-155.

28. Demers, L. M.; Ginger, D. S.; Park, S. -.; Li, Z.; Chung, S. -.; Mirkin, C. A. *Science* **2002**, *296*, 1836-1838.

29. Wilson, D. L.; Martin, R.; Hong, S.; Cronin-Golomb, M.; Mirkin, C. A.; Kaplan, D. L. *Proc. of the Nat'l Acad. of Sci.* **2001**, *98*, 13660-13664.

30. Huo, F.; Zheng, G.; Liao, X.; Giam, L. R.; Chai, J.; Chen, X.; Shim, W.; Mirkin, C. A. *Nat. Nano.* **2010**, advance online publication.

31. Arnold, M.; Hirschfeld-Warneken, V.; Lohmuller, T.; Heil, P.; Blummel, J.; Cavalcanti-Adam, E.; Lopez-Garcia, M.; Walther, P.; Kessler, H.; Geiger, B.; Spatz, J. P. *Nano Letters* **2008**, *8*, 2063-2069.

32. Salaita, K.; Wang, Y.; Fragala, J.; Vega, R. A.; Liu, C.; Mirkin, C. A. *Angew. Chem.* **2006**, *45*, 7220-7223.

33. Kupfer, A.; Louvard, D.; Singer, S. J. *Proc. Natl. Acad. Sci.* **1982**, *79*, 2603-2607.

34. Ochsenhirt, S. E.; Kokkoli, E.; McCarthy, J. B.; Tirrell, M. *Biomaterials* **2006**, *27*, 3863-3874.

35. Grant, R. P.; Spitzfaden, C.; Altroff, H.; Campbell, I. D.; Mardon, H. J. *J. Biol. Chem.* **1997**, *272*, 6159-6166.

36. Feng, Y.; Mrksich, M. *Biochemistry,* **2004,** *43*, 15811-15821.

Reproduced with Permission from the American Chemical Society

Westcott, N. P.; Lou, Y.; Muth, J. F.; Yousaf, M. N. *Langmuir* **2009**, *25*, 11236-11238.

1. Hydrogel Patterning
2. 3D Tissue Culture
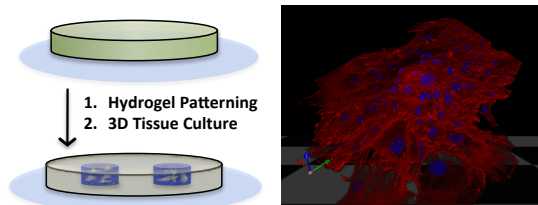
7.1 Introduction

The extracellular matrix (ECM) is a natural dynamic scaffold that consists of proteins, carbohydrates, and signaling molecules.[1] This environment provides a three-dimensional (3D) structure for cell proliferation and migration to occur.[2-4] Cells receive signals not only from the composition, but also the structure and stiffness of the ECM.[5,6] While the cells integrate these signals with several different proteins, integrins are the most ubiquitous.[7] This major class of transmembrane receptors mediate the cells' response not only based on the ECM components, but also the component's relative orientation.[8-11]

Traditionally, most cell-ECM component interaction studies have been performed on two-dimensional (2D) surfaces ranging from petri dishes and polymeric materials to self-assembled monolayers (SAMs).[12-16] These surfaces allow for the presentation of diverse ECM components with minimal consideration for steric effects, diffusion, and synergistic interactions. Due to these factors, it is also nearly impossible to properly mimic the *in vivo* presentation of ligands.[17,18]

Recently more research has been carried out on 3D substrates that better mimic the ECM, which cells experience *in vivo*. Proteins, tissues, and even synthetic polymers have been shown to form scaffolds for such use.[19,20] These 3D substrates have been utilized to study cell adhesion, migration, division, and tissue formation.[21,22] Some of the more widely adopted 3D

substrates are collagen and matrigel.[23] Although unnatural, synthetic polymers have proven to be biocompatible without the use of extraneous growth factors or signaling molecules that may affect matrigel- or collagen-based experiments.[24]

A class of synthetic polymers, hydrogels, has proven extremely useful for such studies. The hydrogel's structural and chemical characteristics are determined from its monomers, and through their variation, the gels can be tailored for different specifications.[25] Specifically, poly(ethylene glycol) (PEG) hydrogels have been used in a variety of experiments studying cell migration, tissue growth, and tissue implantation.[26,27] To facilitate cell adhesion to the gel, monomers containing PEG were modified with a tripeptide cell adhesive ligand, RGD, and then polymerized into the gels.[28,29] Currently, very little work has been conducted to modify hydrogels post-polymerization.

On 2D surfaces, photolithography has been widely used to pattern gradients and geometric shapes.[30] The basic principles have been utilized in a few methods for hydrogel experiments through photoinitiated polymerization, encapsulation, and photoinitiated degradation.[31-33] An alternative approach relies on photoprotecting an amino acid that is part of a polypeptide.[34,35] Previously, it has been shown that substitution of a photoprotected aspartic acid in RGD masks its cell recognition. Cell adhesion was not recovered until the aspartic acid was deprotected to reveal the RGD.

Herein, we develop a strategy to generate easily tunable hydrogels for 3D cell experiments. The gels were composed of a polymer solution containing PEG-diacrylate and PEG-ketone methacrylate monomers. Once polymerized, the gels were chemoselectively modified through the attachment of oxyamine-terminated ligands. Cells were seeded to the gels, and their proliferation and tissue formation were then imaged using confocal microscopy.

Furthermore, we generated dynamic 3D cell patterns within the hydrogel through the use of a photoprotected RGD.

7.2 Experimental

7.2.1 Methacrylation of Coverslips. 24.5mm #1.5 Glass coverslips were cleaned in boiling acetone for 20 minutes. 50 µL of 3-(trimethoxysilyl)-propyl methacrylate was pipetted on top of the coverslips. The coverslips were then placed in a vacuum chamber to react overnight. After the reaction, the excess 3-(trimethoxysilyl)-propyl methacrylate was rinsed off with ethanol, and the coverslips were dried under nitrogen.

7.2.2 Polymerization of Hydrogel. The hydrogels made were either 1:0, 95:5, or 90:10 PEGDA (MW 1623):KPEGMA (MW 1649). The hydrogel components were dissolved in twice their weight of ph 8.0 buffer (Potassium Phosphate Monobasic:Sodium Hydroxide 0.05 M in Water) to give a 1:2 wt%. Each gel was made from 100 µL of buffer and 50 mg total of precursor. APS and TEMED were used to initiate polymerization (1 µL of 10% w/w APS in water, 1 µL of TEMED). The precursor solution plus initiator was then immediately pipetted onto a teflon covered glass slide. The solution was then covered with a methacrylate presenting coverslip face down. The hydrogel was cured in vacuo for 45 mins.

7.2.3 Solid Phase Peptide Synthesis. Peptide synthesis of RGDS-oxyamine and photoprotected GRGDS-oxyamine was performed as previously reported.[37] Calculated [M+H$^+$] for $C_{37}H_{60}N_{12}O_{15}$ = 913.44 (photoprotected GRGDS-oxyamine), Actual [M+H$^+$] = 913.37. Calculated [M+H$^+$] for $C_{25}H_{45}N_{11}O_{11}$ = 676.33 (GRGDS-oxyamine), Actual [M+H$^+$] = 676.29.

7.2.4 Ligand Conjugation. Post polymerized hydrogels were placed gel side down on a 50µL aliquot of 10 mM ligand solutions and left overnight.

7.2.5 Hygrogel Patterning. Once the photoprotected peptide was immobilized to the gel, it was placed under a UV lamp and mask was placed on top of the substrate. The lamp was left on for

1h and the hydrogel was submerged in water for 2h before cell culture. For global deprotection, the hydrogel substrates in cell media were exposed to UV for 10 min and then replaced in the cell culture hood.

7.2.6 Cell Culture. Fibroblast cells were cultured in Dulbecco's modified Eagle medium with calf bovine serum (10%) and penicillin/streptomycin (1%). Cells were released with 0.05% trypsin in 0.53 mM EDTA.

7.2.7 Cell Spindown. 50 mL centrifuge tubes were filled with polydimethylsiloxane (PDMS) from an elastomer kit to create a flat surface. The gel substrates were placed in the centrifuge tubes face up. Cells were released from the flask with 0.05% trypsin in 0.53 mM EDTA and then resuspended in 5 mL of serum containing media. 1 mL of the resuspended cells was placed into a new cell culture flask with 5 mL of fresh serum-containing media. The rest of the unsuspended cells were pipetted into the spin down tubes. The cells were spun down for 2,000 *g*. The surfaces were then placed in evaporation proof petri dishes with serum-containing media and allowed to grow 1-4 days.

7.2.8 Cell Staining. The gel substrates were placed in Phosphate Buffered Saline (PBS) and allowed to clean for 10 minutes. The substrates were then placed into 3.2% formaldehyde in PBS for 1 hr. The substrate was then rinsed quickly in PBS and placed in Phosphate Buffered Saline with 1% triton-x 100 (PBS-T) for 1 hr. The substrate was then rinsed in PBS and placed face down on the cell staining solution. The cell staining solution was 475 μL Goat Serum, 20 μL phalloidin-tetramethylrhodamine B isothiocyanate, and 5 μL DAPI (4′,6-diamidino-2-phenylindole dihydrochloride) and the substrates were stained overnight.

7.2.9 Confocal Microscopy. Fixed and stained cells were imaged with a LeicaSP2 AOBS upright laser scanning confocal microscope. Images were taken at 1 μm step sizes and processed using Volocity image processing software.

7.2.10 Synthesis of PEG 1500 diacrylate. The synthesis was performed following the literature procedure with PEG 1500.[22]

7.2.11 Synthesis of α-methacrylic -ω-acetoacetate poly (ethylene glycol) (I, scheme 7.1):

Poly (ethylene glycol) methacrylate (2). To a stirred solution of PEG 1500 (1, 1 g, 0.67 mmol) in THF, methacrylic anhydride (113 mg, 0.73 mmol) and triethylamine (73 mg, 0.73 mmol) were added. The reaction was stirred overnight and the solvent was removed *in vacuo* and the product was precipitated in ethyl ether (0.6 mmol, 950 mg) with 90% yield. ^{1}H NMR (400 MHz, CDCl$_3$) d=2 (s, 1H; CH), 3.8 (m, J=16 Hz, ~140H; -OCH$_2$CH$_3$-), 3.95 (t, J=4 Hz, 2H; OCH$_2$), 5.6 (d, J= 2 Hz, 1H; =CH), 5.85 (d, J=2 Hz, 1H; =CH)

α-methacrylic -ω-acetoacetate poly (ethylene glycol) (I). To a stirred solution of poly (ethylene glycol) methacrylate (2, 0.7 mmol, 1.1 g) in toluene, tert-butyl acetoacetate (0.7 mmol, 111 mg) was added and was refluxed for 12h. The solvent was removed *in vacuo* and the product was precipitated in ethyl ether with a 98% yield. (1.15 g, 0.69 mmol) ^{1}H NMR (400 MHz, CDCl$_3$) d=2 (s, 1H; CH), 2.4 (s, 3H; CH$_3$), 3.7 (s, 1H; CH), 3.8 (m, J=16 Hz, ~140H; -OCH$_2$CH$_3$-), 4.15 (t, J=4 Hz, 2H; OCH$_2$), 5.6 (d, J= 2 Hz, 1H; =CH), 5.85 (d, J=2 Hz, 1H; =CH)

7.2.12 Synthesis of γ -3-(4,5-Dimethoxy-2-nitrophenyl)-2-butyl-l-aspartate (II, scheme 7.2):

3-(3,4-Dimethoxyphenyl)butan-2-one (3). 3,4-Dimethoxyphenylace- tone (3.78 cm^3, 21.7 mmol, 1 eq) was added to a NaH stirred suspension (625 mg, 26 mmol, 1.2 eq) in dry THF (50 mL). After 0.5 h at room temperature, the solution was cooled to 0 °C, and iodomethane (1.49 mL, 23.8 mmol, 1.1 eq) was added. After 0.5 h at 0 °C, the reaction mixture was slowly allowed to reach room temperature for 1 h, and was quenched by a saturated aqueous NaHCO$_3$ solution (150 mL). The aqueous layer was extracted with EtOAc (3 x 150 mL). The combined organic extracts were dried over anhydrous sodium sulfate, filtered, and concentrated *in vacuo* to give 3 (4.46 g, 21.4 mmol) as a yellow liquid in 98 % yield. ^{1}H NMR (400 MHz, CDCl$_3$) d=1.2 (d, J =8 Hz, 3H; CH$_3$),

1.8 (s, 3H; CH$_3$), 3.69 (q, J=8 Hz, 1H; CH), 3.82 (s, 6H; 2OCH$_3$), 6.55 (m, J=4 Hz, 2H; Ar H), 6.65 (d, 1H; Ar H)

3-(3,4-Dimethoxyphenyl)butan-2-ol (4). 3-(3,4-Dimethoxyphenyl)butan-2-one (717 mg, 3.44 mmol) was dissolved in 25 mL of methanol and NaBH$_4$ (6.88 mmol) was added. The reaction was stirred for 1.5 h and the solvent was removed *in vacuo*. The mixture was dissolved in 50 mL ethyl acetate and with with 3 x 100 mL of saturate aqueous NaHCO$_3$. The organic layer was dried over anhydrous magnesium sulfate concentrated *in vacuo* to give 4 (701 mg, 3.37 mmol) as a clear oil in 98% yield. ^{1}H NMR (400 MHz, CDCl$_3$) d=1.2 (d, J =8 Hz, 3H; CH$_3$), 1.45 (d, J=8 Hz, 3H; CH$_3$), 3.69 (q, J=8 Hz, 1H; CH), 3.75 (q, J=8 Hz, 1H; CH), 3.82 (s, 6H; 2OCH$_3$), 4.01 (t, J=4 Hz, 1H; OH), 6.67 (m, J=4 Hz, 2H; Ar H), 7.00 (d, 1H; Ar H)

3-(4,5-Dimethoxy-2-nitrophenyl)butan-2-ol (5). 4 (700 mg, 3.33 mmol) was dissolved in 20 mL of 1:1 acetic acid:water at 0 °C. 3 mL of 70% nitric acid was added slowly and allowed to stir for 4h. The reaction was diluted with 130 mL of water and extracted with 5x100 mL of DCM. The combined organic extracts were dried over anhydrous sodium sulfate, filtered, and concentrated *in vacuo* to give 5 (816 mg, 3.2 mmol) as a yellow liquid in 96% yield. ^{1}H NMR (400 MHz, CDCl$_3$) d=1.2 (d, J =8 Hz, 3H; CH$_3$), 1.5 (d, J=8 Hz, 3H; CH$_3$), 3.5 (q, J=6 Hz, 1H; CH), 3.85 (q, J=8 Hz, 1H; CH), 3.82 (s, 6H; 2OCH$_3$), 4.01 (t, J=4 Hz, 1H; OH), 6.9 (s, 1H; Ar H), 7.2 (s, 1H; Ar H)

α-tert-Butyl γ-3-(4,5-dimethoxy-2-nitrophenyl)-2-butyl N-BOC-l- aspartate (6). 3-(4,5-dimethoxy-2-nitrophenyl)butan-2-ol 5 (300 mg, 1.2 mmol) was dissolved in dry CH$_2$Cl$_2$ (30 mL) under argon. DCC (500 mg, 2.4 mmol), α -tert-butyl N-BOC-l-aspartic acid (740 mg, 1.8 mmol) and DMAP (5 mg, cat.) were added. After 12 h at room temperature, the reaction mixture was quenched with a saturated aqueous NaHCO$_3$ solution (100 mL). The aqueous layer was extracted with CH$_2$Cl$_2$ (3 x 150 mL). The combined organic extracts were dried over anhydrous sodium sulfate, filtered and concentrated *in vacuo*. The residue was purified by flash chromatography (hexane/EtOAc

145

50:50) to give the product (400 mg, 0.62 mmol) as a yellow solid in 35% yield. ^{1}H-NMR

(400MHz, CDCl3): δ/ppm = 1.27 (2H, m, J=16 Hz;CH2 β), 1.35 (9H, m, J= 12 Hz; -CH3 O*tBu*), 2.75

(2H, m, CH2 α), 3.89 (3H, s, OCH3 meta), 3.93 (3H, s, OCH3 para), 4.53 (4H, m, J=8 Hz,; CH benz,

CH Fmoc9, CH2 Fmoc), 5.19 (1H, m, J=2 Hz; CH), 5.64 (1H, m, J=5 Hz; CH α), 7.02 (1H, s, CH,

arom6), 7.38 (5H, m, J=8 Hz; CH arom3, CH Fmoc2,3,7,6), 7.59 (2H, d, J=6.9 Hz; CH Fmoc1,8),

7.76 (2H, d, J=8 Hz; CH Fmoc4,5)

γ-3-(4,5-Dimethoxy-2-nitrophenyl)-2-butyl-l-aspartate *(II).* tert-butyl g-3-(4,5-dimethoxy-2-

nitrophenyl)-2-butyl N-BOC-l-glutamate (400 mg, 0.62 mmol) was dissolved in dry CH_2Cl_2 (20

mL), trifluoroacetic acid (TFA) (12 mL) was added dropwise at room temperature. The reaction

mixture was diluted with H_2O (50 mL) after 5 h at room temperature, and the product was

extracted with EtOAc (3 x 100 mL). The combined organic extracts were dried over anhydrous

sodium sulfate, filtered and concentrated *in vacuo* to give IV (350 mg, 0.6 mmol, 97 %) as a

yellow solid. ^{1}H-NMR (400MHz, CDCl3): δ/ppm = 1.4 (2H, m, J=16 Hz;CH2 β), 1.8 (2H, m, CH2 α),

3.89 (3H, s, OCH3 meta), 3.93 (3H, s, OCH3 para), 4.53 (4H, m, J=8 Hz,; CH benz, CH Fmoc9, CH2

Fmoc), 5.19 (1H, m, J=2 Hz; CH), 5.64 (1H, m, J=5 Hz; CH α), 6.8 (1H, s, CH, arom6), 7.2 (5H, m,

J=8 Hz; CH arom3, CH Fmoc2,3,7,6), 7.4 (2H, d, J=6.9 Hz; CH Fmoc1,8), 7.76 (2H, d, J=8 Hz; CH

Fmoc4,5) Calculated [M+Na$^+$] for $C_{31}H_{32}N_2O_{10}$ = 615.21, Actual [M+Na$^+$] = 615.15.
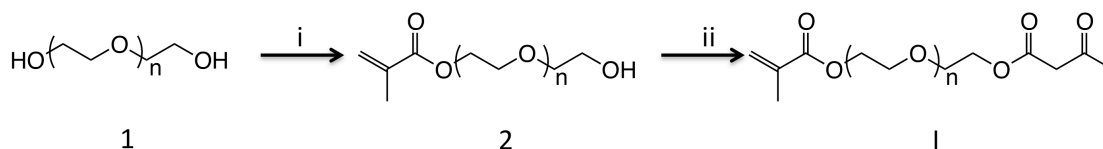
Scheme 7.1. Synthesis of α-methacrylic -ω-acetoacetate poly (ethylene glycol). Reagents and conditions i) TEA, methacrylic anhydride, DCM. rt, 12h, 91% ii) tert-butyl acetoacetate, toluene, reflux, 12h, 95%
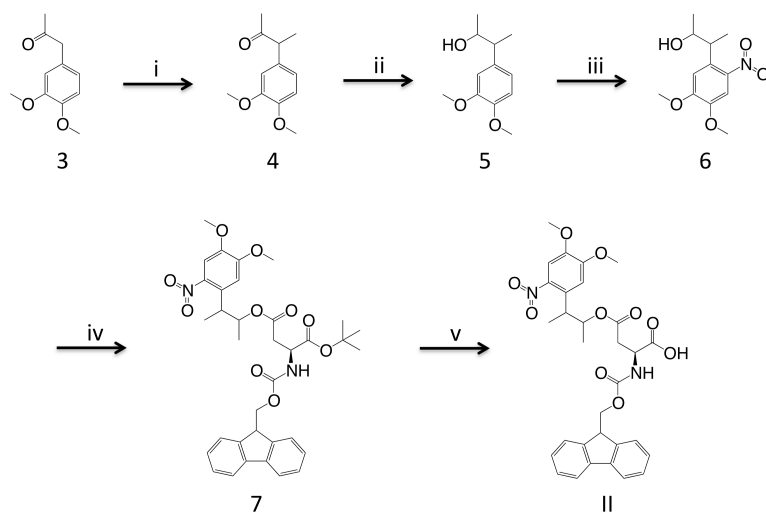
Scheme 7.2 Synthesis of γ -3-(4,5-Dimethoxy-2-nitrophenyl)-2-butyl-l-aspartate: Reagents and conditions i) NaH, MeI, 0 C, rt, THF, 2h, 98% ii) NaBH4, MeOH, 2h, 98% iii) HNO3, 1:1 H2o:AcOH, rt, 6h, 98% iv) **6,** α -tert-butyl N-BOC-l-aspartic acid , DCC, DMAP, DCM, rt 12h, 35% v) TFA, DCM, 3h, 98%

7.3 Results and Discussion

7.3.1 Polymerization Method. To create a chemically flexible hydrogel, we based our design on ketone-oxyamine chemistry. Oxime bond formation reactions offer several advantages for this application. Oxyamine chemistry is chemoselective, bio-orthogonal, and does not require a catalyst.[36,37] These features allow for the gels to be functionalized post-polymerization, even in the presence of cells. The hydrogel was composed of two different monomers. The first monomer, PEG-diacrylate (PEGDA), provided a biologically passive and inert gel scaffold and was readily synthesized following a previously reported procedure.[22] The second monomer was terminated with a ketone group (KPEGMA) (supporting information). Thus, the monomer contained three different components: a methacrylate group, PEG chain that provided space to reduce steric hinderance, and ketone that served as a handle for the oxyamine-ketone reaction. The two components were co-polymerized with ammonium

147

persulphate (APS) and tetramethylethylenediamine (TEMED) to prepare the gels and were then functionalized with oxyamine ligands (figure 7.1).
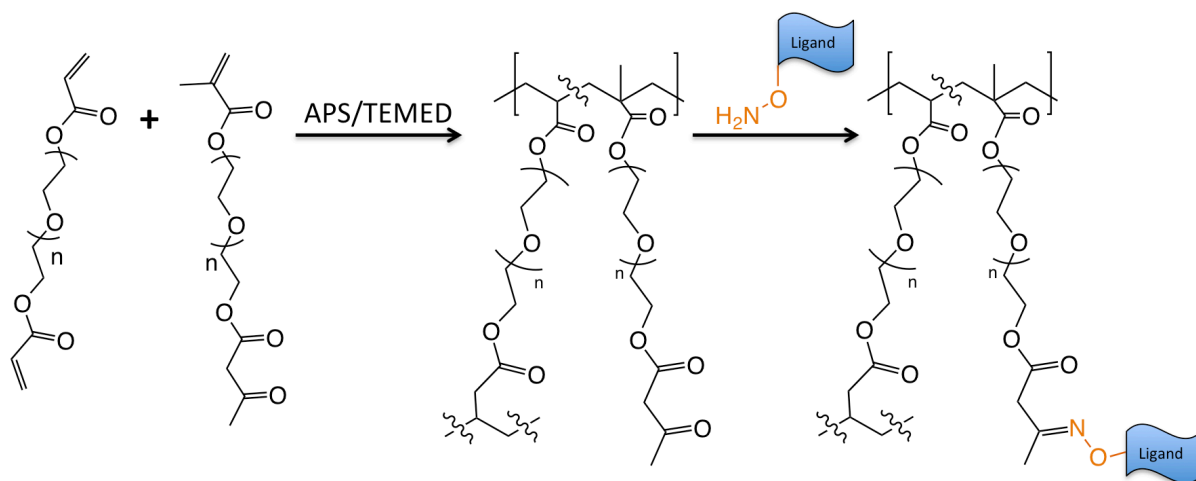

Figure 7.1. Polymerization of the ketone containing hydrogels. A mixture of the diacrylate and ketone containing monomer were mixed and then polymerized with APS and TEMED. The gel could then be functionalized with the introduction of a oxyamine containing ligand.

7.3.2 Fluorescence Characterization. Once the gels were synthesized, the ketone functionality was verified with fluorescence microscopy (figure 7.2). Two gels were synthesized; one with a molar ratio of 9:1 PEGDA : KPEGMA and the other with only PEGDA. The ratios were dissolved in 50 µL of water at 1:2 w/w and cured with 1 µL of 1% w/w APS and TEMED for 15 minutes under vacuum. The gels were functionalized with a 50-µL solution of 10 mM fluorescein-hydrazide overnight and remained in methanol overnight to remove any unreacted reagent. After functionalization, the gels were imaged under a fluorescence microscope. As expected, little to no fluorescence was observed in the PEGDA gel and a significant amount was observed in the gel containing KPEGMA. A linescan of both gels confirmed the visual results and demonstrated only the ketone gel was fluorescent.

7.3.3 Hydrogel Cell Culture Once the monomers were synthesized and gels tested, substrates were prepared for cell culture (figure 7.3). First, 100 µL of a pre-polymer solution

containing a molar ratio of 1:9 KPEGMA : PEGDA was added to a glass coverslip that was functionalized with methacrylate groups. The methacrylate SAM that was immobilized to the glass allowed the gel to covalently couple into surface, which prevented gel detachment during cell culture. Next, the gel was cured with the addition of 1 µL of 1% w/w APS and TEMED and placed under vacuum for 45 min. The hydrogels were then functionalized with the cell adhesive ligand RGD-oxyamine by adding 50 µL of a 10 mM solution overnight. The gels were rinsed and allowed to soak in water for 2 h before cell culture. Swiss Albino 3T3 fibroblasts were then seeded by centrifugation using previously established methods and allowed to grow in culture for several days.[38]
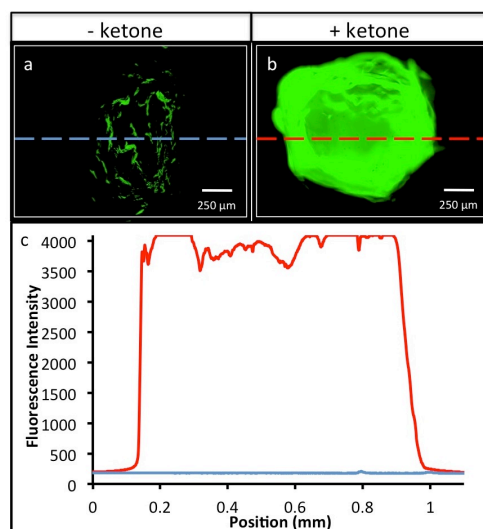
Figure 7.2. Flourescence microscopy of functionalized hydrogels. Two gels were synthesized. A gel with 1:9 molar ratio of PEGDA and KETPEGMA and the other with PEGDA. The monomers were dissolved in 50 µL of water at 1:2 w/w and cured with APS and TEMED. They were then both functionalized with fluorescein hydrazide. a) Image of a hydrogel without ketones present after fluorescein-hydrazide immobilization. b) Hydrogel image after fluorescein-hydrazide immobilization. c) Linescans of both hydrogels.
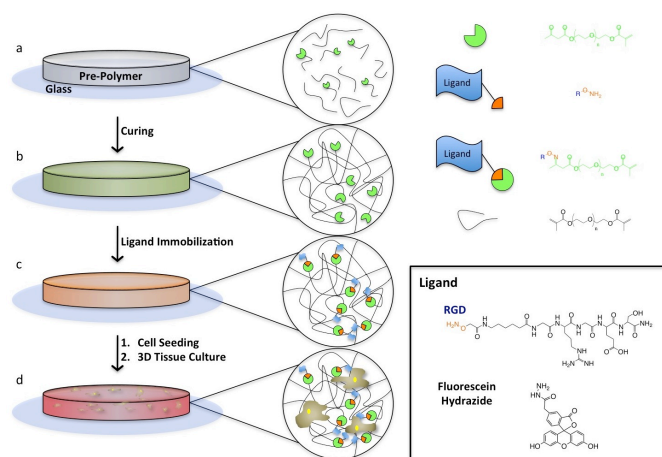
Figure 7.3. Procedural outline of hydrogel formation and functionalization. a) 100 µL of pre-polymer mixture is added to a glass slide functionalized with methacrylate groups. b) The mixture is cured into a gel with APS and TEMED under a vacuum for 45 min. c) An oxyamine or hydrazide ligand is immobilized in the gel by reacting it with a 10 mM solution for 12h. d) Cells are seeded by centrifugation to the gel and allowed to grow and culture.

7.3.4 3D Cell Structures in the Hydrogel. After 3 d of cell culture, the fibroblasts were fixed and stained for actin (red) and nucleus (blue). The cells were then imaged with confocal microscopy, which allowed for the imaging of multilayer cell formations (figure 7.4). Small and large cell assemblies were imaged within the gel. Small cell clusters not only grew within the plane of the gel, but also extended fillopodia out into the gel. Taking advantage of the multiple image planes, these features were imaged in 3D using reconstructive software. The larger cell assemblies were also captured. Here, the observed cells grew 100 µm into the gel, resulting in a multilayer growth up to 8 cells thick. Fibroblasts do not naturally form multilayers in cell culture; these structures were supported by hydrogel and did not form unless the hydrogel was present. Additionally, no cell attachment was observed unless the gels were first reacted with RGD-oxyamine.
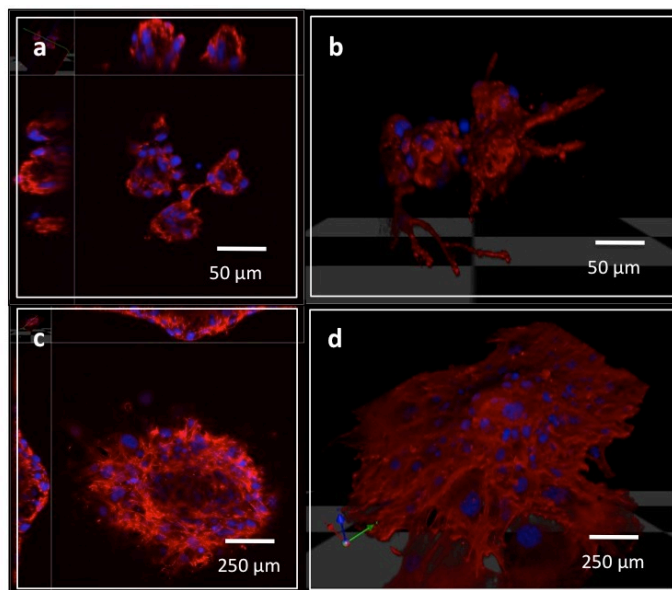
Figure 7.4. 3D cell culture in the hydrogels. Hydrogels were cured on glass slides and functionalized with RGD oxyamine. Cells were then seeded and grew for 3 d before being fixed and stained (red, actin; blue, nucleus). a) Confocal image of a small group cells in the hydrogel. b) A 3D reconstruction of the grouping using confocal microscopy. c) A large multilayer tissue like structure of cells growing in the hydrogel. d) 3D reconstruction of the tissue using confocal microscopy.

7.3.5 Synthesis of Photopeptide. The tripeptide RGD is a useful molecule that is capable of generating cell adhesive materials. However, once reacted, it cannot be patterned further. To overcome this problem, several different photoprotecting groups have been used to mask different amino acids. We chose to photoprotect aspartic acid using 3-(4,5-mimethoxy-2-nitrophenyl)butan-2-ol.[34,35] This group has been used to photoprotect both aspartic and glutamic acids. The photoprotected aspartic acid has been incorporated into cyclic RGD to create a photoactive RGD peptide that cells do not recognize until the molecule is deprotected by UV light.[34] We synthesized a linear RGD peptide by first synthesizing the photoprotecting group (scheme 7.2) and then coupling it to an aspartic acid. This photoprotected aspartic acid was then incorporated into an RGD peptide to create a photoprotected RGD (pRGD).

7.3.6 Photopatterning the Hydrogels. The procedure to photopattern RGD is outlined below (figure 7.5). The pre-polymer was added to the glass slide and cured. pRGD was first

immobilized to the hydrogel and then deprotected by shining UV light through a photomask for 1 h, resulting in cell adhesion patterns within the hydrogel. Fibroblasts were then seeded to the hydrogels, which only adhered to the deprotected regions.

7.3.7 Photopatterned Dynamic Cells. In order to visualize cells responding to dynamic 3D environment, 3 different experiments were carried out. In the first experiment, cells were imaged after forming patterns in the deprotected gels following the above procedure. After seeding, the fibroblasts were cultured for 1 d and then fixed and stained for actin and nucleus (figure 7.6). The cells adhered to the patterns that were generated by the pRGD and even penetrated into the gel. In other experiments, cells were found to maintain these patterns for at least 1 week after seeding demonstrating the ability of the pRGD functionalized hydrogels to resist non-specific adsorption and adhesion. In the second, the cells were imaged migrating out from their initial patterns after global deprotection. The cells were seeded cells in a pattern and then, the pRGD was globally photodeprotected under UV light for 10 min. Cells were then allowed to culture for an additional day to allow the cells to migrate and matriculate into the gel from their initial patterns. They were then fixed and stained to observe their migration using confocal microscopy. In this experiment, the cells had migrated 50 μm into the gel from their initial patterns demonstrating the shift from the inert to adhesive hydrogel after deprotection. Additionally, the cells appeared to penetrate further in the hydrogel once global deprotection had occurred. In the final experiment, cells were allowed more time to migrate into the gel after global deprotection to observe migration and tissue formation. A hydrogel was patterned and the cells were allowed to grow for 1 d, and the pRGD was then globally deprotected for 10 min. After global deprotection, the cells were allowed to migrate for 3d and then fixed and stained. These cells had migrated outside 300 μm their initial patterns once the global deprotection had

occurred. These cells had significantly moved outside the initial pattern not only in the lateral dimension, but in z dimension as well showing enhanced confluency in the larger 3D structures.

Figure 7.5. Hydrogel photopatterning methodology. a) A ketone-containing hydrogel is immobilized on a functionalized glass slide. b) Photoprotected RGD (pRGD) is immobilized within the hydrogel by reacting the gel with 10 mM pRGD solution. c) The peptide is deprotected for 1h under UV light through a photomask to generate cell adhesive patterns. d) Cells are seeded by centrifugation and only bind to the deprotected regions forming 3D cell patterns.

7.4 Conclusions

A chemically dynamic hydrogel was develeoped that are capable of immobilizing a variety of different oxyamine-terminated ligands. By synthesizing a ketone-terminated PEG-methacrylate and combining it with a PEG-diacrylate, the PEG hydrogels were made resistant to nonspecfic cell adsorption and adhesion and synthesized with a small amount of ketone to allow for post-polymerization reactions to occur. After hydrogel synthesis, the ketone content was verified using a fluorescent oxyamine. Tissue culture was then demonstrated with the addition of an RGD ligand. Finally, cells were patterned with a photoprotected RGD ligand. In the future, we hope to explore the combination of other ligands with RGD effects on tissue culture.
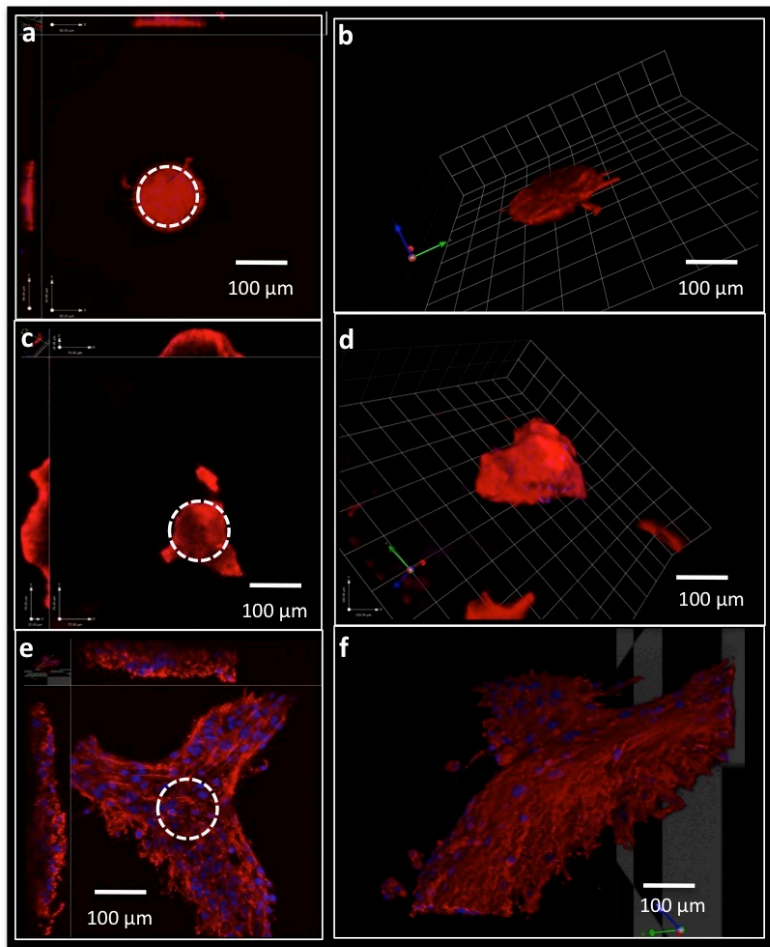
Figure 7.6. Confocal Microscopy of patterned cells within a dynamic hydrogel. All cells were fixed and stained after the described time points for actin (red) and the nuclei (blue). a) After pRGD immobilization and patterned deprotection, cells were seeded to the hydrogels and allowed to grow for 1d. Then, they were imaged using confocal microscopy. b) A 3D reconstruction of these cells in the hydrogel. c) After 1d of patterned growth, the gel was globally deprotected for 10 min under UV light and the cells were allowed to grow for an additional day. d) A 3D reconstruction of the cells migrating out of the pattern. e) After 1d of patterned growth, the hydrogel was globally deprotected for 10 min and the cells were allowed to grow for an additional 3 d. f) A 3D reconstruction of the cells breaking out of the pattern.

7.5 References

1. Aszódi, A.; Legate, K. R.; Nakchbandi, I. & Fässler, R. **2006**, *22*, 591-621.

2. Berrier, A. L.; Yamada, K. M. *J. Cell. Physiol.* **2007**, *213*, 565-573.

3. Luo, B.; Carman, C.V.; Springer, T.A. *Annu. Rev. Immunol.* **2007**, *25*, 619-647.

4. Canavan, H.E.; Cheng, X.; Graham, D.J.; Ratner, B.D.; Castner, D. G. *Langmuir* **2005**, *21*, 1949-1955.

5. Grant, R. P.; Spitzfaden, C.; Altroff, H.; Campbell, I.D.; Mardon, H.J. *J. Biol. Chem.* **1997**, *272*, 6159-6166.

6. Altroff, H. *et al. J. Biol. Chem.* **2004**, **279**, 55995-56003.

7. Humphries, J.D.; Byron, A.; Humphries, M.J. *J. Cell. Sci.* **2006**, **119**, 3901-3903.

8. Feng, Y.; Mrksich, M. *Biochem.* **2004**, *43*, 15811-15821.

9. Ochsenhirt, S.E.; Kokkoli, E.; McCarthy, J.B.; Tirrell, M. *Biomat.* **2006**, *27*, 3863-3874.

10. Arnold, M. *et al. ChemPhysChem* **2004**, *5*, 383-388.

11. Lock, J.G.; Wehrle-Haller, B.; Strömblad, S. *Semin. Cancer Biol.* **2008**, *18*, 65-76.

12. Thery, M. *et al. Nat. Cell Biol.* **2005**, *7*, 947-953.

13. Théry, M.; Pépin, A.; Dressaire, E.; Chen, Y.; Bornens, M. *Cell Motil. Cytoskeleton* **2006**, *63*, 341-355.

14. Théry, M. *et al. Proc. Nat'l Acad. Sci.* **2006**, *103*, 19771-19776.

15. Fukuda, J. *et al. Biomat.* **2006**, *27*, 1479-1486.

16. Love, J. C.; Estroff, L.A.; Kriebel, J.K.; Nuzzo, R.G.; Whitesides, G.M. *Chem. Rev.* **2005**, *105*, 1103-1170.

17. Fraley, S.I. *et al. Nat. Cell Biol.* **2010**, *12*, 598-604.

18. Friedl, P.; Zänker, K.S.; Bröcker, E. *Microsc. Res. Tech.* **1998**, *43*, 369-378 .

19. Guillame-Gentil, O. *et al. Adv. Mater.* **2010**, *22*, 5443-5462.

20. Liu, G.; Amro, N. *Proc. Nat'l Acad. Sci.* **2002**, *99*, 5165-5170.

21. Cukierman, E.; Pankov, R.; Yamada, K. M. *Curr. Opin. Cell Biol.* **2002**, *14*, 633-640.

22. Bott, K. *et al. Biomat.* **2004**, *31*, 8454-8464.

23. Sodek, K.; Brown, T.; Ringuette, M. *BMC Cancer* **2008**, *8*, 223.

24. Yamada, K.M.; Cukierman, E. *Cell* **2007**, *130*, 601-610.

25. Jen, A.C.; Wake, M.C.; Mikos, A.G. *Biotechnol. Bioeng.* **1996**, *50*, 357-364.

26. Bryant, S.J.; Bender, R.J.; Durand, K.L.; Anseth, K.S. *Biotechnol. Bioeng.* **2004**, *86*, 747-755.

27. Raeber, G.P.; Lutolf, M.P.; Hubbell, J. *Biophys. J.* **2005**, *89*, 1374-1388.

28. Herten, M. *et al. Clin. Oral Implants Res.* **2009**, *20*, 116-125.

29. Mann, B.K.; West, J.L. *J. Biomed. Mater. Res.* **2002**, *60*, 86-93.

30. Chan, E.W.L.; Yousaf, M.N. *Molecular BioSystems* **2008**, *4*, 746-753.

31. Andreopoulos, F.M.; Beckman, E.J.; Russell, A.J. *Biomat.* **1998**, *19*, 1343-1352.

32. Bryant, S.J.; Cuy, J.L.; Hauch, K.D.; Ratner, B.D. *Biomat.* **2007**, *28*, 2978-2986.

33. Kloxin, A.M.; Kasko, A.M.; Salinas, C.N.; Anseth, K.S. *Science* **2009**, *324*, 59-63.

34. Ohmuro-Matsuyama, Y.; Tatsu, Y. *Ange. Chem. Internat'l Ed.* **2008**, *47*, 7527-7529.

35. Specht, A. *et al.. ChemBioChem* **2006**, *7*, 1690-1695.

36. Westcott, N.P.; Yousaf, M.N. *Electrophoresis* **2009**, *30*, 3381-3385.

37. Chan, E.W.L.; Yousaf, M.N. *J. Am. Chem. Soc.* **2006**, *128*, 15542-15546.

38. Barrett, D.; Yousaf, M. *Ange. Chem. Internat'l Ed.* **2007**, *46*, 7437-743.

Chapter VIII: Dissertation Conclusions and Future Work

8.1 Dissertation Conclusions.

During the course of this thesis, several tools have been developed to study cell migration and adhesion. In chapter II, microfluidics and electrochemistry were combined to control an electrochemical reaction on the surface. This method was used to pattern cells on a SAM. In chapter III, microfluidic cassettes were used to control a gold etching reaction on the surface. These etched regions were used functionalized with SAMs to control surface chemistry and help observe cell migration around patterned features. In chapter IV, a new surface methodology was developed to functionalize surfaces. Using commercially available starting materials, alcohol terminated SAMs were oxidized to aldehydes and reacted with oxyamines. These substrates were used to pattern cells and fluorescent molecules. This strategy was also extended to phosphonates SAMs on ITO. In chapter V, this methodology was adapted create protein affinity platforms for mass spectrometry. In chapter VI, two methods were used to look at cell migration and adhesion at the nanoscale. Dip pen nanolithography was used to generate substrates for cell division and cell adhesion studies and self-assembly based lithography was used to generate substrates for cell migration studies. In chapter VII, chemically dynamic hydrogels were developed to study cell migration and adhesion in 3D. In sum, these tools represent many different methods to pattern cells and control their adhesive environment in both 2 and 3 dimensions with some preliminary results showing their effect on various cell behaviors.

8.2 Future Work.

In the future, these methods can be applied to study cell biology and look at controlled surface effects on cell migration, polarization, and adhesion. Dynamic substrates have been generated in 3D and in 2D, which will allow for comparisons between the two environments. Cells migrate faster in 3D and form smaller, but more numerous focal adhesions. Using the hydrogels as a 3D platform, several different variables could be tuned including stiffness, pore size, and adhesiveness to see their effect on the cells ability to proliferate and migrate. These results could be compared with cell behavior studies using SAMs as substrates. These studies would help elucidate the differences between cells growing in petri dishes and in tissues providing new insights into cancer metastasis, tissue formation, and development.